universität wien

MASTERARBEIT / MASTER'S THESIS

Titel der Masterarbeit / Title of the Master's Thesis

„On the Migdal effect in Dark Matter direct detection "

verfasst von / submitted by

Lukas Matzi, BSc

angestrebter akademischer Grad / in partial fulfilment of the requirements for the degree of

Master of Science (MSc)

Wien, 2020 / Vienna, 2020

Studienkennzahl lt. Studienblatt / degree programme code as it appears on the student record sheet:	UA 066 876
Studienrichtung lt. Studienblatt / degree programme as it appears on the student record sheet:	Physik
Betreut von / Supervisor:	Mag. Dr. Josef Pradler

Acknowledgements

I would like to thank the High Energy Physics Institute (HEPHY) for the opportunity to be part of the Dark Matter research group with a lot of inspiring Journal Clubs and discussions. I am deeply grateful for the support of my supervisor and head of the research group Josef Pradler, who guided me throughout this work with a lot of feedback, input and discussions. I would also like to thank all my colleagues at the institute for constructive discussions about dark matter and particle physics.

Abstract

The focus in direct detection experiments lies on the detectability of dark matter due to nuclear recoil signatures from dark matter particles. The master thesis will focus on the detectability of dark matter particles, especially the weakly interacting massive particles (WIMPs) with masses below the GeV scale. In standard cosmological models the WIMPs are gravitationally bound to the galaxy with nonrelativistic circular velocities, causing elastic nuclear recoils with atomic nuclei with typical momentum transfers of about $\mathcal{O}(100\text{MeV})$ or less. The recoil signatures can be detected through ionization, scintillation and the production of heat in the detectors. In the thesis, we study the prompt ionization of an electron that follows a dark matter nucleus scattering event. This is the so called *Migdal effect*. The thesis is about the calculation and evaluation of the strength of this ionization signal by using electron wave functions obtained through various methods, such as Hartree-Fock-wave functions, Coulomb wave functions, plane waves etc. The *Migdal effect* will be calculated for various atoms, such as Xe, I, Ge and Ar. The obtained results will be used to calculate dark matter event rates and compare it to the results of conventional liquid xenon detectors, e.g Xenon1T.

Zusammenfassung

Das Ziel direkter Detektionsexperimenten liegt darin atomare Streuungsprozesse dunkler Materie Teilchen zu messen. Diese Masterarbeit beschäftigt sich mit der Nachweisbarkeit von dunkler Materie, mit besonderem Fokus auf "Weakly Interacting Massive Particles" (WIMPs) mit Massen unterhalb der GeV-Skala. Im kosmologischen Standardmodel sind WIMPs gravitativ an Galaxien gebunden und bewegen sich mit nichtrelativistischen Geschwindigkeiten im Orbit, wodurch elastische Streuungsprozessen mit Atomen induziert werden. Für Dunkle Materie Teilchen in der Größenordnung $\mathcal{O}(100)$GeV kommt es zu Impulsübertragungen von etwa $\mathcal{O}(100\text{MeV})$ oder weniger. Die Streuungsprozesse können durch Ionisation, Szintillation und Wärmeerzeugung in den Detektoren nachgewiesen werden. In dieser Arbeit beschreiben wir Ionisatierungsprozesse eines Elektrons durch Streuung von dunklen Materie an isolierten Atomen. Dies ist der sogenannte *Migdal-Effekt*. Die Arbeit befasst sich mit der Berechnung der Stärke dieses Ionisationssignals unter Verwendung von Elektronenwellenfunktionen, die aus verschiedenen numerischen Methoden erhalten wurden, wie Hartree-Fock-Wellenfunktionen, Coulomb-Wellenfunktionen, ebenen Wellen usw. Der *Migdal-Effekt* wird für verschiedene Atome wie Xe, I, Ge und Ar berechnet. Die erhaltenen Ergebnisse werden verwendet, um die Wahrscheinlichkeit solcher Streuungsprozesse zu schätzen und sie mit den Ergebnissen herkömmlicher Flüssig-Xenon-Detektoren, wie beispielsweise Xenon1T, zu vergleichen.

Contents

Chapter 1

Dark Matter

The existence of dark matter is overwhelmingly supported by numerous cosmological and astrophysical observations. Observations of large scale structures emphasize the existence of dark matter through galactic rotation curves, gravitational lensing, baryonic acoustic oscillations for the cosmic microwave background etc. These cosmological phenomena are notoriously difficult to reproduce in the absence of cold dark matter [1].

The direct or indirect detection of Dark Matter is one of the most extensively studied fields in modern particle physics. Direct detection experiments aim to detect Dark Matter through nuclear recoil signatures. However, nuclear scattering processes with dark matter masses below the GeV-scale produce soft nuclear recoils, which are difficult to detect unambiguously. Finite detector thresholds and kinematic limitations on the relative velocity of Dark Matter set a principal limit on the detectability of dark matter [2]. The Migdal effect proposes an inelastic channel of the prompt ionization or excitation of an electron via nuclear recoils, which enhances the detectability of light Dark Matter.

Standard Halo models predict a local dark matter density of $0.3\frac{\mathrm{GeV}}{\mathrm{cm}^3}$.[3] The circular speed of dark matter in the solar system is estimated to be about $239\frac{km}{s}$. For light dark matter with a mass of order $\mathcal{O}(1\mathrm{GeV})$, this would result in an elastic recoil with a typical recoil energy of $\mathcal{O}(1\mathrm{keV})$ for a target with nucleus mass $m_N \approx 100\mathrm{GeV}$.

1.1 Standard cosmological model

The current standard cosmological model describes the evolution of the universe within the Friedmann-Robertson-Walker metric and has it's roots in the discovery of Hubble's law and the observed large-scale isotropy and homogeneity in the distribution of matter. The components of the metric tensor are the degrees of freedom of the gravitational field. The model is able to describe the thermal history, relic background radiation, the abundance of elements as well as many other large-scale properties of the observed universe. The most important building blocks are the Einstein field equations, the metric tensor and the Equation of state[1][4].

The Einstein field equation can be derived by first principles in a Lagrangian field theory and leads to a second order differential equation, which is linear in second derivatives

$$R_{\mu\nu} - \frac{1}{2} g_{\mu\nu} R = \frac{8\pi G}{c^4} T_{\mu\nu} - \Lambda g_{\mu\nu}. \tag{1.1}$$

where $R_{\mu\nu}$ and R are the Ricci tensor and the Ricci scalar, $T_{\mu\nu}$ is the energy momentum tensor, G is Newton's gravitational constant, $g_{\mu\nu}$ is the metric tensor and Λ is the cosmological constant. The geometry of the universe is described by the energy content of the universe, described by the energy momentum tensor. Observation of the cosmological microwave background (CMB) confirm the assumption of homogeneity and isotropy of the universe, often referred as the cosmological principle. The Friedman-Robertson-Walker metric fulfills these requirements

$$ds^2 = -c^2 dt^2 + a(t)^2 \left(\frac{dr^2}{1 - kr^2} + r^2 d\Omega^2 \right), \tag{1.2}$$

where $a(t)$ is the dimensionless scale factor. The constant k depicts the spatial curvature with values $k = \{-1, 0, 1\}$.

The metric is compatible with a perfect fluid energy momentum tensor, which leads to the Friedman equations

$$3\frac{\dot{a}^2 + k}{a^2} = \frac{8\pi G}{c^4} \rho_T + \Lambda, \tag{1.3}$$

$$-2\frac{\ddot{a}}{a} - \frac{\dot{a}^2 + k}{a^2} = \frac{8\pi G}{3c^4} p - \Lambda. \tag{1.4}$$

where ρ_T is the total average density of the universe and $H(t) = \left(\frac{\dot{a}(t)}{a(t)}\right)$ is the Hubble constant, which is actually not a constant but a function of time. There is a controversial discrepancy in the determination of the Hubble constant at current times. The indirect determination of the Hubble constant by the Planck Collaboration based on the ΛCDM yields $H_0 = 67.27 \pm 0.60 \mathrm{km\,s^{-1} Mpc^{-1}}$ [5]. Local measurements currently deduced a value of $H_0 = 73.52 \pm 1.62 \mathrm{km\,s^{-1} Mpc^{-1}}$ [6].

The critical density of the universe is defined as the density, where the universe is flat ($k = 0$), which leads to

$$\rho_c \equiv \frac{3H^2}{8\pi G}. \tag{1.5}$$

The abundance of elements in the universe in terms of the critical density parameter is

$$\Omega_i \equiv \frac{\rho_i}{\rho_c}, \tag{1.6}$$

$$\Omega = \sum_i \Omega_i = \sum_i \frac{\rho_i}{\rho_c}, \tag{1.7}$$

such that we can rewrite the Friedmann equation in terms of

$$\Omega - 1 = \frac{k}{H^2 a^2}. \tag{1.8}$$

The sign of k is determined by the theoretical model under consideration

$\rho < \rho_c$	$\Omega < 1$	k=-1	open
$\rho = \rho_c$	$\Omega = 1$	k=0	flat
$\rho > \rho_c$	$\Omega > 1$	k=1	closed

where ρ_c is the critical density of the universe.

The various Ω_i components evolve different in time, depending on the equation of state of the component. Let there be a apparently small contribution from a hypothetical "X-matter component", which is parametrized by its equation of state $p = \alpha_X \cdot \rho_X$. The expansion rate can be written as

$$\begin{aligned} \frac{H^2(z)}{H_0^2} =& \Big[\Omega_X (1+z)^{3(1+\alpha_X)} + \Omega_K (1+z)^2 \\ & + \Omega_M (1+z)^3 + \Omega_R (1+z)^4 \Big], \end{aligned} \tag{1.9}$$

where M and R denote matter and radiation respectively and X refers to a particle species with equation of state $p = \alpha_X \rho_X$ (in particular for the cosmological constant $\alpha_\Lambda = -1$). $\Omega_M = \Omega_{DM} + \Omega_b$ and Ω_K is the contribution from curvature and is defined as [1]

$$\Omega_K = -\frac{k^2}{a_0^2 H_0^2}, \tag{1.10}$$

$$\Omega_X + \Omega_M + \Omega_K + \Omega_\Lambda = 1. \tag{1.11}$$

The most recent measurements from Planck [5] yield

$$\begin{aligned} \Omega_{DM} h^2 &= 0.1200 \pm 0.0012, && \text{(Cold Dark Matter)} \\ \Omega_b h^2 &= 0.02237 \pm 0.00015, && \text{(Baryonic Matter)} \\ \Omega_\Lambda h^2 &= 0.3107 \pm 0.0082, && \text{(Dark Energy)} \\ \Omega_K h^2 &== 0.0007 \pm 0.0019 && \text{(Curvature)} \end{aligned} \tag{1.12}$$

where $h = 67.8\frac{km}{sMpc}$ [7] is today's value of the Hubble constant.

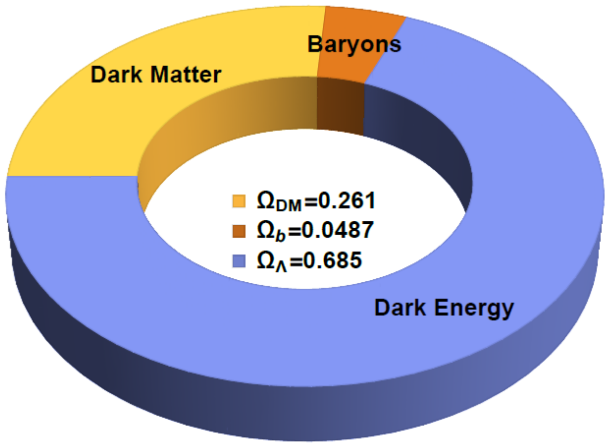

On the left side, the energy budget of the universe is depicted in its three main components. Dark matter accounts for about 26% of the energy budget, Dark energy about 69% and 5% baryonic matter, such that $\sum_i \Omega_i \simeq 1$.

1.1.1 Brief History of the universe

- **Baryogenesis:** Particles and antiparticles annihilate, e.g. $e^+ + e^- \rightarrow \gamma + \gamma$. If the universe would have been filled with the same amount of matter and antimatter, annihilation processes would lead to a radiation dominated universe throughout much of the cosmic history , in conflict with observations. The observed universe has an overabundance of matter (mostly baryons). The general dynamical mechanism, that lead to a baryon asymmetry is called Baryogenesis.The observed baryon-to-photon ratio is approximately [8]

$$\eta \equiv \frac{n_b - n_{\bar{b}}}{n_\gamma} \simeq 10^{-9}. \tag{1.13}$$

- **Electroweak phase transition:** The Standard Model gauge symmetry breaks into $SU(3) \otimes U(1)_{EM}$, which is called electroweak symmetry breaking and enables the Higgs mechanism to take place.

- **QCD phase transition:** Below 150 MeV the strong interaction between quarks and gluons drives the confinement of quarks to form bound states, called *baryons*, and *mesons*. They become the relevant degrees of freedom below the QCD phase transition.

- **Dark matter genesis:** Dark matter is expected to interact very weakly with ordinary matter, and a multitude of generation mechanisms are known. One of the most predictive simple ones is the thermal freeze out of WIMPs.

- **Neutrino decoupling:** Neutrinos interact with the rest of the primordial plasma only through the weak interaction and their decoupling from the SM bath is estimated at 0.8

MeV.

- **Electron-positron annihilation:** After neutrino decoupling electron and positrons begin to annihilate.
- **Nucleosynthesis:** At about 100 keV protons and neutrons fuse into light elements $(\mathrm{D}, {}^3\mathrm{He}, {}^4\mathrm{He}, \mathrm{Li})$ [1].
- **Formation of structure:** At 0.75 eV the matter density becomes equal the radiation density, allowing the formation of structure to begin.
- **Photon decoupling:** At 0.23-0.28 eV Photon decoupling produces the cosmic background radiation [8].
- **Present:** 14 meV, $T \approx 2.7$ K[1]

Event	**time t**	**redshift z**	**temperature T**
Inflation	10^{-34}s	-	-
Baryogenesis	?	?	?
EW phase transition	20 ps	10^{15}	100 GeV
QCD phase transtion	20μs	10^{12}	150 MeV
Dark matter freeze-out	?	?	?
Neurtrino Decoupling	1 s	6×10^9	1 MeV
Electron-positron annihilation	6 s	2×10^9	500 keV
Big Bang nucleosynthesis	3 min	4×10^8	100 keV
Matter radiation equality	60 kyr	3400	0.75 eV
Recombination	$260 - 380$ kyr	$1100 - 1400$	$0.26 - 0.33$ eV
Photon decoupling	380 kyr	$1000 - 1200$	$0.23 - 0.28$ eV
Reionization	$100 - 400$ Myr	$11 - 30$	$2.6 - 7.0$ meV
Dark energy - matter equality	9 Gyr	0.4	0.33 meV
Present	13.8 Gyr	0	0.24 meV

Table 1.1: The table describes key events in the thermal history of the universe [8].

1.2 Evidence for Dark matter

Dark matter has not yet been detected directly and its properties remain largely unknown. In 1933 Fritz Zwicky was the first one, who operated on the virial theorem for galaxy clusters such as the Coma cluster and postulated the existence of dark Matter [9].

One strong piece of evidence comes from the observation of galactic rotation curves of spiral galaxies. The dynamical measurement of the mass in the galaxy follows from the analysis of its gravitational effects. Assuming a spherical distribution of matter in the bulge leads according to Newtonian dynamics to the relation

$$v = \sqrt{\frac{GM(r)}{r}}, \tag{1.14}$$

where v is the orbital velocity at a distance r from the center of the galaxy and $M(r)$ is the mass distribution inside the radius r. If we take r to be the radius, where most of the light from the galaxy is emitted, we would expect the orbital velocity in the outskirt of the galaxy to decrease $\propto r^{-1/2}$, but the observed rotation curves behave as $v \simeq$ constant for increasing r, such that one can conclude that $M(r) \propto r$. The first *flat* rotation curves of spiral galaxies were discovered by Rubin and Ford in the 1970's [10].

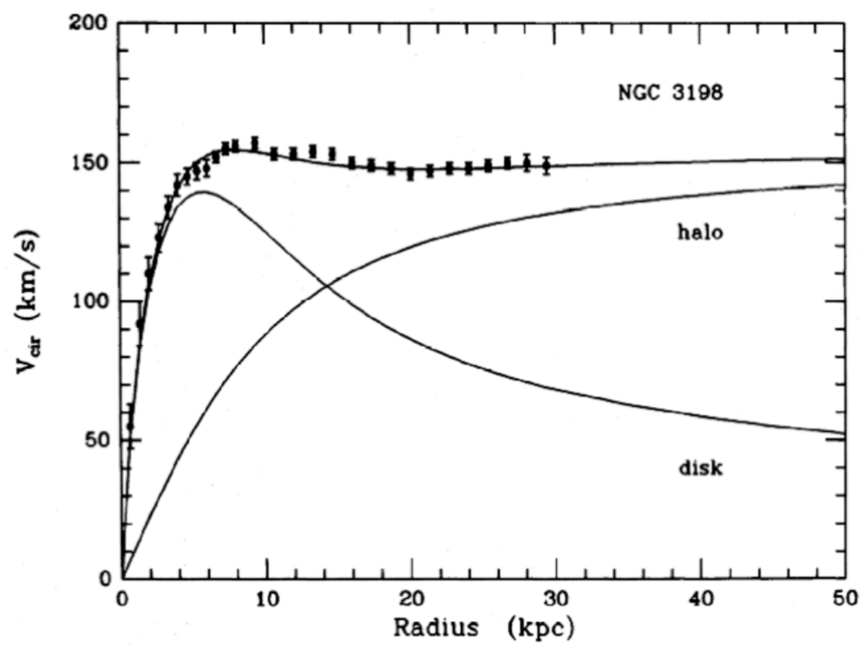

Figure 1.1: The rotation curve of a spiral galaxy, where the luminous disk and the dark matter halo is also depicted [10].

The main contribution of the mass is *dark*, in the sense that it has no detectable radiation associated with it. The non luminous components of matter have to provide a mass distribution $M(r) \propto r$. This mass distribution is believed to be related to new particles that are, except for their gravitational interaction, weakly interacting [11]. This is one of the clearest hints for physics beyond the standard model on galactic scales.

The structure of the cosmic microwave background (CMB) provides the most powerful insights on the parameters of the ΛCDM model. CMB originates from background radiation of decoupled photons in the early universe and has an almost perfect blackbody spectrum with a today's temperature of T=2.728K [12]. The temperature fluctuations of the CMB originate from baryonic acoustic oscillations and can be expanded in terms of spherical harmonics with multipole expansion in l. The peaks in the spectrum provide information of the dark matter abundance in the universe [13]. The latest results from the (TT) power spectrum from Planck Collaboration [5] can be seen in figure 1.2

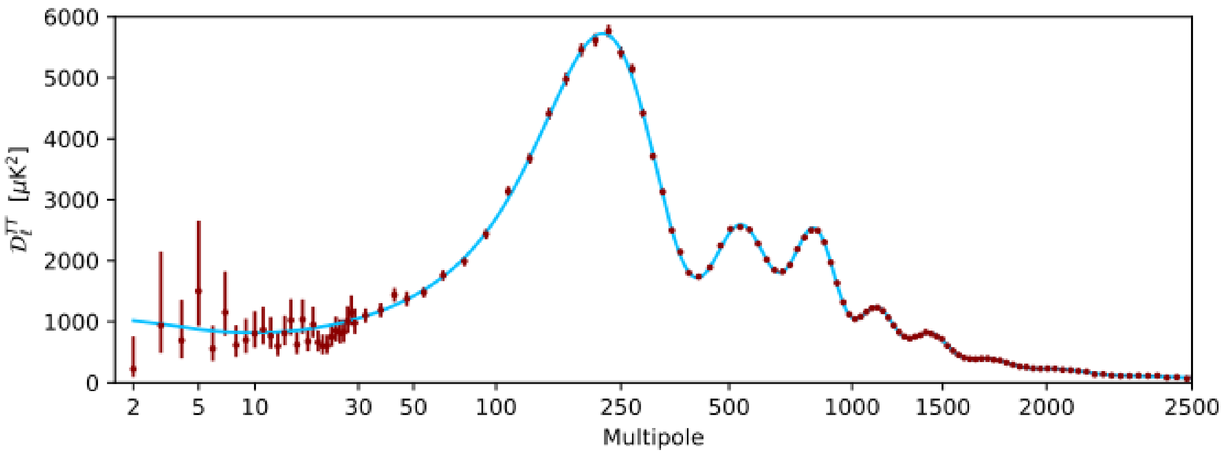

Figure 1.2: The blue lines in the TT power spectrum from Planck show the best fit base-ΛCDM model. The spectrum is foreground-subtracted and frequency averaged [5].

The overwhelming agreement between the minimal 6 parameter ΛCDM-model and the Planck data makes the it one of the most successful phenomenological models supporting that dark matter exists.

1.3 Thermal freeze out

One of the most promising non-baryonic candidates for cold dark matter are WIMPs, which comes from the fact that WIMPs would have been in chemical equilibrium with the SM in the early universe naturally yielding the right abundance for cold dark matter in the universe. For non-relativistic particles in the early universe, the particle density per comoving volume decreases exponentially with decreasing temperature, because of the Boltzmann factor. The relic WIMP density is set before Big Bang Nucleosynthesis (BBN), an epoch were no direct observation is available. It is necessary to make assumptions about the pre-BBN era to compute the relic WIMP density. One of the standard approaches is the assumption, that the entropy of matter and radiation was conserved and the WIMPs were produced thermally via interactions with particles in the plasma. In the radiation dominated universe, where the temperature was higher than the mass of the WIMP $T \gg m_\chi$, the colliding particle/antiparticle pairs had enough energy to produce WIMP pairs efficiently, e.g.

$$\chi\bar{\chi} \leftrightarrow e^+e^-, \mu^+\mu^-, q\bar{q}, W^+W^-, ZZ, HH, \ldots. \tag{1.15}$$

For decreasing temperature, when the $\chi\bar{\chi}$ annihilation rate becomes smaller than the Hubble expansion rate, the WIMP number per comoving volume freezes out [14] [15].

The microscopic evolution of the particle's phase space distribution $f(p^\mu, x^\mu)$ is described by the Boltzmann equation

$$\hat{\mathbf{L}}[f] = C[f], \tag{1.16}$$

where C is the collision operator and $\hat{\mathbf{L}}$ is the Liouville operator, which is a nonrelativistic operator for the phase space density $f(\mathbf{v}, \mathbf{r})$ of a particle species of mass m subject $\mathbf{F} = \frac{d\mathbf{p}}{dt}$ is

$$\hat{\mathbf{L}} = \frac{d}{dt} + \frac{d\mathbf{r}}{dt} \cdot \boldsymbol{\nabla}_x + \frac{d\mathbf{v}}{dt} \cdot \boldsymbol{\nabla}_v = \frac{d}{dt} + \mathbf{v} \cdot \boldsymbol{\nabla}_x + \frac{\mathbf{F}}{m} \cdot \boldsymbol{\nabla}_v \tag{1.17}$$

The covariant, relativistic generalization of the Liouville operator is

$$\hat{\mathbf{L}} = p^\alpha \frac{\partial}{\partial x^\alpha} - \Gamma^\alpha_{\beta\gamma} p^\beta p^\gamma \frac{\partial}{\partial p^\alpha}, \tag{1.18}$$

where $\Gamma^\alpha_{\beta\gamma}$ is the affine connection due to gravitational effects. In the Friedmann Robertson Walker (FRW) model the phase space density is homogenous and isotropic $f = f(|\mathbf{p}|, t) = f(E, t)$ and the Liouville operator becomes

$$\hat{\mathbf{L}}[f(E,t)] = E\frac{\partial f}{\partial t} - \frac{\dot{R}}{R}|\mathbf{p}|^2 \frac{\partial f}{\partial E}. \tag{1.19}$$

The number density in terms of the phase space density is

$$n(t) = \frac{g}{(2\pi)^3} \int d^3p \, f(E,t), \tag{1.20}$$

where g counts the integral degrees of freedom. Using integration by parts, the Boltzmann equation yields

$$\frac{dn}{dt} + 3\frac{\dot{R}}{R}n = \frac{g}{(2\pi)^3} \int C[f] \frac{d^3p}{E}. \tag{1.21}$$

The right hand side describing the collision for the proxess $\chi + a + b + \dots \to i + j + \dots$ is given by

$$
\begin{aligned}
\frac{g}{(2\pi)^3}\int C[f]\frac{d^3p_\chi}{E_\chi} =& -\int d\Pi_\chi d\Pi_a d\Pi_b \dots d\Pi_i d\Pi_j \dots \\
& \times (2\pi)^4\delta^{(4)}(p_\chi + p_a + p_b + \dots - p_i - p_j - \dots) \\
& \times \Big(|\mathcal{M}|^2_{\chi+a+b+\dots\to i+j+\dots} f_a f_b \dots f_\chi (1 \pm f_i)(1 \pm f_j)\dots \\
& \quad - |\mathcal{M}|^2_{i+j+\dots\to\chi+a+b+\dots} f_i f_j \dots (1 \pm f_a)(1 \pm f_b)\dots(1 \pm f_\chi)\Big), \\
d\Pi =& \frac{g}{(2\pi)^3}\frac{d^3p}{2E},
\end{aligned} \tag{1.22}
$$

where f_k are the phase space densities of the particle species k and the $(+)$ sign corresponds to bosons and the $(-)$ sign corresponds to fermions. The invariant matrix element squared $|\mathcal{M}|$ is averaged over initial and final spins and includes also the symmetry factor for identical particles. In general the Boltzmann equation consists of a coupled set of partial differential equations, but some of the particle species under consideration can be approximated to be in equilibrium, such that the problem reduces to a single integral-partial differential equation for the one species of interest.

Assuming the particle interactions to be T invariant implies that

$$
|\mathcal{M}|^2_{\chi+a+b+\dots\to i+j+\dots} = |\mathcal{M}|^2_{i+j+\dots\to\chi+a+b+\dots} = |\mathcal{M}|^2 \tag{1.23}
$$

For further simplification, one may assume Maxwell-Boltzmann statistics instead of Fermi-Dirac for fermions and Bose-Einstein for bosons. To be more explicit, the Boltzmann statistics for any non-relativistic species becomes exact in the limit $(m_i - \mu_i)/T \gg 1$. Without Bose condensation or Fermi degeneracy, the blocking and stimulated emission factors can be ignored, such that $1 + f \simeq 1$ and $f_i(E_i) = \exp[-(E_i - \mu_i)/T]$ for all particle species in thermal equilibrium.

With $H = \frac{\dot{R}}{R}$, which is the Hubble constant, the Boltzmann equation reduces to

$$
\begin{aligned}
\dot{n}_\chi + 3Hn_\chi = & -\int d\Pi_\chi d\Pi_a d\Pi_b \dots d\Pi_i d\Pi_j \dots (2\pi)^4 |\mathcal{M}|^2 \\
& \times \delta^{(4)}(p_i + p_j + \dots - p_\chi - p_a - p_b - \dots)[f_a f_b \dots f_\chi - f_i f_j \dots].
\end{aligned} \tag{1.24}
$$

The term with the Hubble constant provides dilution effects due to the expansion of the universe and the right hand side of Eq. (1.24) accounts for interactions that change the number of $\chi' s$ [15]. The Hubble parameter in terms of the mass-energy density is determined by the Friedmann equation

$$
H^2 = \frac{8\pi}{3m_{pl}^2}\rho, \tag{1.25}
$$

where m_{pl} is the Planck mass. There is also a relation between the energy/entropy density and the photon temperature by

$$\rho = \frac{\pi^2}{30} g_{\text{eff}}(T) T^4, \tag{1.26}$$

$$s = \frac{2\pi^2}{45} h_{\text{eff}}(T) T^3, \tag{1.27}$$

where g_{eff} and h_{eff} are effective degrees of freedom for the energy density and the entropy density [14]. The effective degrees of freedom for $g_{\text{eff}}(T)$ and $h_{\text{eff}}(T)$ were computed for example in [16], where also QCD effects are taken into account. Then the degrees of freedom parameter $g_*^{1/2}$ is defined as

$$g_*^{1/2} = \frac{h_{\text{eff}}}{g_{\text{eff}}^{1/2}} \left(1 + \frac{1}{3} \frac{T}{h_{\text{eff}}} \frac{dh_{\text{eff}}}{dT}\right). \tag{1.28}$$

It is useful to scale out the effect of the expansion of the universe, which is possible by considering the evolution of the number of particles in a comoving volume. This is usually done by using the entropy density s to define the variable

$$Y \equiv \frac{n_\chi}{s}. \tag{1.29}$$

From the conservation of entropy per comoving volume ($sR^3 = \text{constant}$), we get

$$\dot{n}_\chi + 3Hn_\chi = s\dot{Y}. \tag{1.30}$$

Since the interaction term is in strong relation to temperature, we can introduce the independent variable

$$x \equiv \frac{m}{T}, \tag{1.31}$$

where m is the mass of the particle under consideration. During the radiation dominated era of the universe x and t are related by

$$t = 0.301 g_{\text{eff}}^{-1/2} \frac{m_{Pl}}{T^2} = 0.301 g_{\text{eff}}^{-1/2} \frac{m_{Pl}}{m^2} x^2. \tag{1.32}$$

The Boltzmann equation (1.24) is now rewritten by

$$\begin{aligned} \frac{dY}{dx} = &- \frac{x}{H(m)s} \int d\Pi_\chi d\Pi_a d\Pi_b \dots d\Pi_i d\Pi_j \dots (2\pi)^4 |\mathcal{M}|^2 \\ &\times \delta^{(4)}(p_i + p_j + \dots - p_\chi - p_a - p_b - \dots)[f_a f_b \dots f_\chi - f_i f_j \dots], \end{aligned} \tag{1.33}$$

where $H(m) = 1.67 g_{\text{eff}}^{1/2} \frac{m^2}{m_{pl}}$. Considering a massive particle remaining in thermal equilibrium until today, it's abundance , $\frac{n}{s} \approx \left(\frac{m}{T}\right)^{3/2} \exp\left(-\frac{m}{T}\right)$, would be suppressed by the exponential factor. For $\Gamma < H$, the species freezes out at a temperature, such that $\frac{m}{T} \approx 1$ and the species then can have a significant relic abundance today [15].

In case of the WIMP χ, we assume a stable particle with respect to the age of the universe and assume that only annihilation processes of the form $\chi\bar{\chi} \to \psi\bar{\psi}$ change the number of $\chi's$ and $\bar{\chi}'s$ in the comoving volume. The ψ's denote all the species into which χ,$\bar{\chi}$ can annihilate (e.g. Eq.(1.15)), where we assume no asymmetry in χ and $\bar{\chi}$. Assuming the chemical potential of the particle species χ to be zero induces distribution functions of the form

$$\begin{aligned} f_{\psi} &= \exp\left(-E_{\psi}/T\right), \\ f_{\bar{\psi}} &= \exp\left(-E_{\bar{\psi}}/T\right). \end{aligned} \tag{1.34}$$

Conservation of energy leads to

$$f_{\psi} f_{\bar{\psi}} = \exp\left[(E_{\psi} + E_{\bar{\psi}})/T\right] = \exp\left[(E_{\chi} + E_{\bar{\chi}})/T\right] = f_{\chi}^{\mathrm{EQ}} f_{\bar{\chi}}^{\mathrm{EQ}} \tag{1.35}$$

Therefore we can rewrite the factor of the phase space distribution function in the collision term

$$\left(f_{\chi} f_{\bar{\chi}} - f_{\psi} f_{\bar{\psi}}\right) = \left(f_{\chi} f_{\bar{\chi}} - f_{\chi}^{\mathrm{EQ}} f_{\bar{\chi}}^{\mathrm{EQ}}\right). \tag{1.36}$$

The defining equations of the current density of WIMPs are now

$$\frac{dn_{\chi}}{dt} + 3Hn_{\chi} = -\left\langle \sigma_{\chi\bar{\chi}\to\psi\bar{\psi}} v_{M\o l}\right\rangle \left[n_{\chi}^2 - (n_{\chi}^{\mathrm{EQ}})^2\right], \tag{1.37}$$

$$\frac{ds}{dt} = -\,3Hs, \tag{1.38}$$

where $v_{\mathrm{M\o l}}$ is the Møller velocity and the second equation arises from the entropy conservation law. The thermally averaged annihilation cross section times Møller velocity is

$$\begin{aligned} \left\langle \sigma_{\chi\bar{\chi}\to\psi\bar{\psi}} v_{\mathrm{M\o l}}\right\rangle =& \frac{\int \sigma v_{\mathrm{M\o l}} e^{-E_{\chi}/T} e^{-E_{\bar{\chi}}/T} d^3p_{\chi} d^3p_{\bar{\chi}}}{\int e^{-E_{\chi}/T} e^{-E_{\bar{\chi}}/T} d^3p_{\chi} d^3p_{\bar{\chi}}} \\ =& (n_{\chi}^{\mathrm{EQ}})^{-2} \int d\Pi_{\chi} d\Pi_{\bar{\chi}} d\Pi_{\psi} d\Pi_{\bar{\psi}} (2\pi)^4 \delta^{(4)}\left(p_{\chi} + p_{\bar{\chi}} - p_{\psi} - p_{\bar{\psi}}\right) \\ & \times |\mathcal{M}|^2 \exp\left(-\frac{E_{\chi}}{T}\right) \exp\left(-\frac{E_{\bar{\chi}}}{T}\right). \end{aligned} \tag{1.39}$$

Combining Eq. (1.37) and (1.38), we can write

$$\frac{dY}{dx} = -\frac{1}{3H}\frac{ds}{dx}\left\langle \sigma_{\chi\bar{\chi}\to\psi\bar{\psi}} v_{\mathrm{M\o l}}\right\rangle (Y^2 - Y_{\mathrm{EQ}}^2), \tag{1.40}$$

where $Y = \frac{n_{\chi}}{s} = \frac{n_{\bar{\chi}}}{s}$ is the number of χ,$\bar{\chi}$'s per comoving volume and $Y_{\mathrm{EQ}} = \frac{n_{\chi}^{\mathrm{EQ}}}{s} = \frac{n_{\bar{\chi}}^{\mathrm{EQ}}}{s}$ is the equilibrium number of the χ's and $\bar{\chi}$'s per comoving volume. Combining equ (1.28) and (1.40), we can write

$$\frac{dY}{dx} = -\left(\frac{45}{\pi m_{pl}^2}\right)^{-1/2} \frac{g_*^{1/2} m}{x^2} \left\langle \sigma_{\chi\bar{\chi}\to\psi\bar{\psi}} v_{\mathrm{M\o l}} \right\rangle (Y^2 - Y_{\mathrm{EQ}}^2). \tag{1.41}$$

This equation can be solved numerically with the initial condition $Y = Y_{EQ}$ at $x \simeq 1$ to calculate the present WIMP abundance Y_0. The relic WIMP density is then

$$\Omega_\chi h^2 = \frac{\rho_\chi^0 h^2}{\rho_c^0} = \frac{m_\chi s_0 Y_0 h^2}{\rho_c^0} = 2.755 \times 10^8 Y_0 m_\chi/\mathrm{GeV}, \tag{1.42}$$

where ρ_c^0 and s_0 are the present critical density and the entropy density respectively. In figure (1.3), we can see that at high temperatures Y is in accordance with it's equilibrium value Y_{EQ}, but when the temperature decreases Y_{EQ} experiences an exponential suppression, such that Y deviates from the equilibrium value. When the WIMP annihilation rate is of the order of the Hubble expansion rate, the WIMP production becomes negligibly small and the WIMP abundance per comoving volume freezes out. The freeze out temperature of relic WIMP's is about $T_{fo} \simeq m_\chi/20$, which corresponds to a typical velocity of $v_{fo} \simeq 0.27c$ [14].

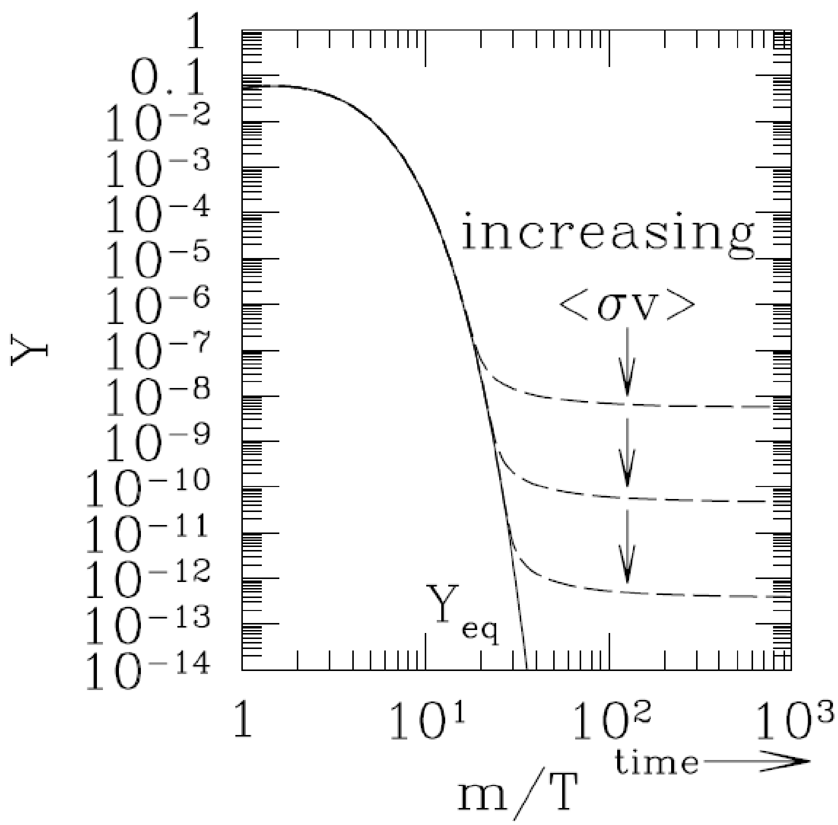

Figure 1.3: Evolution of the WIMP number density in the freeze out scenario of the early universe [14].

Figure (1.3) also shows that smaller annihilation cross sections induce larger relic densities, because WIMP's with stronger interactions are able to remain for a longer time in chemical equilibrium.

In general the final state is not a two body final state, but the result can easily be generalized to an arbitrary physically allowed final state, which is found by replacing $\left\langle \sigma_{\chi\bar{\chi}\to\psi\bar{\psi}} v_{\text{Møl}} \right\rangle \to \langle \sigma_{\chi\bar{\chi}\to F} v_{\text{Møl}} \rangle$. The final result is then obtained by summing over all possible annihilation channels in terms of the total annihilation cross section $\langle \sigma_T v_{\text{Møl}} \rangle$.

Chapter 2

Dark Matter direct detection

In dark matter direct detection, experiments aim to detect scattering events of DM particles in the Milky way halo with underground detectors, e.g. LUX, DAMA, XENON1T etc. The nuclear recoil in the detector results in ionization, scintillation or the production of heat (phonons) in the detectors or a combination of these. The probability of the prompt ionization of one electron with respect to soft nuclear recoil events is the quantity of interest we wish to calculate.

2.1 Dark Matter-nucleon interactions

We consider an effective Dark Matter-nucleon interaction, in which we focus on spin independent (SI) interactions between Dark Matter and nucleons. The non relativistic theory of dark matter nucleon scattering induces an effective Lagrangian of the form

$$\mathcal{L}_{eff} = g^2 \bar{\psi}_N \mathcal{O}_N \psi_N \bar{\psi}_\chi \mathcal{O}_\chi \psi_\chi, \tag{2.1}$$

where $\mathcal{O}_i$ are interactions differentiated by their Lorentz structure. In general, the operators fall into a set of scalar (S), pseudoscalar(P), vector(V), axial vector (A), tensor (T) and axial tensor (AT) interactions with respect to their transformation properties,

$$\text{Scalar type:} \qquad \mathcal{O} = \mathbb{1}, i\gamma^5 \tag{2.2}$$

$$\text{Vector type:} \qquad \mathcal{O}^\mu = \gamma^\mu, \gamma^5\gamma^\mu \tag{2.3}$$

$$\text{Tensor type:} \qquad \mathcal{O}^{\mu\nu} = \sigma^{\mu\nu}, i\gamma^5\sigma^{\mu\nu}, \tag{2.4}$$

where $\sigma^{\mu\nu} = \frac{i}{2}[\gamma^\mu, \gamma^\nu]$. The simplest case is the scalar operator $\mathbb{1}$, which is CPT conserving and induces spin independent interaction. In the non-relativistic limit, also γ^μ induces spin independent interaction [17].

2.2 The nuclear form factor

Spin independent interactions lead to coherence in the first place. The nuclear form factor is a quantity that describes the loss of coherence in the DM-nucleon cross section. If the momentum transfer $q \simeq \sqrt{2mE_R}$ implies a de Broglie wavelength of $\lambda = \frac{h}{q} \lesssim r_n$, where r_n is the effective nuclear radius, E_R is the recoil energy and m is the momentum of the particle, then the effective cross section decreases for scattering processes with increasing q, for spin independent as well as for spin dependent processes [18][19]. The form factor is a function of the dimensionless quantity qr_n. and is defined as the Fourier transformation of the nuclear density

$$F(qr) = \frac{1}{Ze} \int \rho(r) e^{-i\mathbf{qr}} d^3r. \tag{2.5}$$

Assuming a spherically symmetric charge distribution yields

$$\begin{aligned} F(qr) &= \frac{1}{Ze} \int_0^{2\pi} d\varphi \int_0^{\pi} d\vartheta \sin\vartheta \int_0^{\infty} dr\, r^2 \rho(r) e^{-iqr\cos\vartheta} \\ &= \frac{2\pi}{Ze} \int_0^{\pi} d\vartheta \sin\vartheta \int_0^{\infty} dr\, r^2 \rho(r) e^{-iqr\cos\vartheta} \end{aligned} \tag{2.6}$$

Since $\frac{\partial}{\partial\vartheta} e^{-iqrcos\vartheta} = iqr \sin\vartheta e^{-iqrcos\vartheta}$, the integral reduces to

$$\begin{aligned} F(qr) &= \frac{2\pi}{Ze} \int_0^{\infty} dr \left[\frac{-ir}{q} \rho(r) e^{-iqr\cos\vartheta} \right]_0^{\pi} \\ &= \frac{4\pi}{Zeq} \int_0^{\infty} dr\, r\, \rho(r) \left[\frac{e^{iqr} - e^{-iqr}}{2i} \right] \\ &= \frac{4\pi}{Zeq} \int_0^{\infty} dr\, r\, \rho(r) \sin(qr). \end{aligned} \tag{2.7}$$

There are several approaches to determine the nuclear form factor by determining the function $\rho(r)$. Cross sections get then corrected by[18]

$$\sigma(qr_n) = \sigma_0 F^2(qr_n), \tag{2.8}$$

where σ_0 is the total coherent DM-nucleon cross section.

1956 R.H. Helm introduced a "folded" charge distribution to fit the nuclear form factor to experimental data in electron nucleus scattering experiments [20]

$$\rho(r) = \int d^3r' \rho_0(r') \rho_1(r - r'). \tag{2.9}$$

The nuclear charge density can be approximated by

$$\rho(r) = \rho_0 = \frac{3Ze}{4\pi R^3}, \qquad \text{for } r \leq R, \tag{2.10}$$

which is an approximately uniform charge distribution inside a cutoff radius R and zero outside. The distribution $\rho_1(r)$ is set to take care of the soft edge and is defined as

$$\rho_1(r) = \frac{1}{(2\pi s^2)^{\frac{3}{2}}} \exp\left(-\frac{r^2}{2s^2}\right), \tag{2.11}$$

where s is a measure of the nuclear skin thickness. The convolution of $\rho(r)$ with $\rho_1(r)$ yields the Helm form factor

$$F(qr) = \frac{3j_1(qR)}{qR} \exp\left(-\frac{q^2s^2}{2}\right) = 3\frac{\sin(qR) - qR\cos(qR)}{(qR)^3} \exp\left(-\frac{q^2s^2}{2}\right), \tag{2.12}$$

where $j_1(qR)$ is the first order spherical Bessel function. The Helm form factor is the most commonly used form factor in the description of spin independent DM-nucleon scattering. The nuclear radius r_n can be obtained by Fricke et al [21].

$$r_n^2 = c^2 + \frac{7}{3}\pi^2 a^2 - 5s^2, \tag{2.13}$$

where $s \simeq 0.52\,\mathrm{fm}$ is the nuclear skin thickness, c and a are parameters, which are fitted according to Fricke et al. [21]

$$\begin{aligned} c \simeq 1.23\,\mathrm{fm} A^{\frac{1}{3}} - 0.6\,\mathrm{fm}, \\ a \simeq 0.52\,\mathrm{fm}. \end{aligned} \tag{2.14}$$

2.3 Dark matter velocity distribution

The velocity of DM inside the Milky Way is determined from the circular speed curve data of our Galaxy under the assumption of an isotropic spherically symmetric velocity distribution function. Since DM moves with nonrelativistic velocities, the local velocity distribution function is well approximated by a Maxwellian [22]

$$f(\mathbf{v}) = \frac{1}{N_{esc}} e^{-v^2/v_0^2}. \tag{2.15}$$

We have to truncate the velocity distribution function at the local escape velocity v_{esc}. Hence, the normalization factor N_{esc} is defined as

$$\begin{aligned} N_{esc} =& \int_0^{2\pi} d\varphi \int_0^{\pi} \sin\vartheta d\vartheta \int_0^{v_{esc}} v^2 e^{-v^2/v_0^2} dv \\ =& 4\pi v_0^3 \int_0^{\frac{v_{esc}}{v_0}} du\, u^2 e^{-u^2} \\ =& \left(\pi v_0^2\right)^{3/2} \left[\mathrm{erf}\left(\frac{v_{esc}}{v_0}\right) - \frac{2}{\sqrt{\pi}} \frac{v_{esc}}{v_0} e^{-v_{esc}^2/v_0^2}\right] \end{aligned} \tag{2.16}$$

Since the velocity distribution from Eq. (2.15) is defined in the rest frame of the DM halo, we have to consider the motion of the earth with respect to the galactic centre. Applying a Galilean boost to the velocity distribution we get

$$f(\mathbf{v}, t) = f(\mathbf{v} + \mathbf{v}_E), \tag{2.17}$$

where $\mathbf{v}_E$ is the Earth's velocity in the galactic rest frame. The Boltzmann velocity distribution now yields

$$f(\mathbf{v} + \mathbf{v}_E) = \begin{cases} \frac{1}{N_{esc}} \exp\left(-\frac{(\mathbf{v}+\mathbf{v}_E)^2}{v_0^2}\right) & v \leq v_{esc} \\ 0 & v > v_{esc} \end{cases} \tag{2.18}$$

The velocity distribution is bounded by the escape velocity v_{esc}, such that the maximum velocity is

$$\begin{aligned} |\mathbf{v} + \mathbf{v}_E| &\leq v_{esc} \\ v &= \sqrt{v_{esc}^2 - v_E^2(1 - \cos^2\theta)} - v_E \cos\theta, \end{aligned} \tag{2.19}$$

where θ is the scattering angle in the galactic rest frame. The maximum escape velocity is achieved, when $\cos\theta = -1$. The maximum velocity is bounded $v - v_E \leq v_{max}(\theta) \leq v + v_E$ and is a function of the angle θ. The scattering angle of the maximum velocity is defined by

$$\cos\theta = \frac{v_{esc}^2 - v_E^2 - v^2}{2vv_E} \tag{2.20}$$

Hence, the maximum value $\cos\theta = -1$ is related to the velocity $v = v_{esc} + v_E$ and the value $\cos\theta = 1$ is related to the velocity $v_{esc} - v_E$. Now we have the integration boundaries for the velocity distribution fixed. The calculation of the dark matter event rate for the Migdal effect includes the velocity average of a general function $h(v)$ of the form

$$\begin{aligned} \eta(v_{min}) =& \int d^3v \frac{f(v, v_E)}{v} h(v) = \\ =& 2\pi \left\{ \int\limits_{v_{min}}^{v_{esc}-v_E} v dv \int\limits_{-1}^{1} d\cos\theta + \int\limits_{v_{esc}-v_E}^{v_{esc}+v_E} v dv \int\limits_{-1}^{\cos\theta_{max}} d\cos\theta \right\} f(v, v_E) h(v) \end{aligned} \tag{2.21}$$

The integral gets splitted into two regions of integration. The first integration region yields

$$\begin{aligned} \eta_1(v_{min}) =& 2\pi \int\limits_{v_{min}}^{v_{esc}-v_E} v dv \int\limits_{-1}^{1} d\cos\theta f(v, v_E) h(v) \\ =& \frac{\pi v_0^2}{N_{esc} v_E} \int\limits_{v_{min}}^{v_{esc}-v_E} dv \left(e^{-\frac{v^2+v_E^2-2vv_E}{v_0^2}} - e^{-\frac{v^2+v_E^2+2vv_E}{v_0^2}} \right) h(v), \end{aligned} \tag{2.22}$$

whereas the second part of the integration reads

$$\eta_2(v_{min}) = \frac{\pi v_0^2}{N_{esc} v_E} \int_{v_{esc}-v_E}^{v_{esc}+v_E} dv \left(e^{-\frac{v^2+v_E^2-2vv_E}{v_0^2}} - e^{-\frac{v_{esc}^2}{v_0^2}} \right) h(v). \tag{2.23}$$

The velocity average of a general function $h(v)$ takes the form

$$\eta(v_{min}) = \eta_1(v_{min})\Theta(v_{esc} - v_E - v_{min}) + \eta_2(v_{min})\Theta(v_{min} - v_{esc} + v_E)\Theta(v_{esc} + v_E - v_{min}). \tag{2.24}$$

2.3.1 Annual Modulation and Directionality

There is an annual modulation of the velocity distribution due to the Earths motion around the sun [23][22]. The count rate in dark matter direct detection experiences an annual modulation. Let $\tilde{f}(\mathbf{v})$ be the velocity distribution in the rest frame of the dark matter population, which is often referred as the galactic frame. Then, the velocity distribution $f(\mathbf{v}, \mathbf{v}_{obs}(t))$ in the laboratory frame of the earth is obtained by a galilean boost by

$$\begin{aligned} f(\mathbf{v}, \mathbf{v}_E(t)) &= \tilde{f}(\mathbf{v}_{obs}(t) + \mathbf{v}), \\ \mathbf{v}_{obs}(t) &= \mathbf{v}_\odot + \mathbf{v}_\oplus(t) \end{aligned} \tag{2.25}$$

where $\mathbf{v}_{obs}(t)$ is the relative motion between the laboratory frame to the galactic frame and $\mathbf{v}_\odot$ is the relative motion of the sun to that frame and $\mathbf{v}_\oplus(t)$ is the relative velocity of the earth with respect to the sun. The SHM can be described as a smooth non-rotating background halo component, for which

$$\mathbf{v}_\odot = \mathbf{v}_{LSR} + \mathbf{v}_{pec} \tag{2.26}$$

where $\mathbf{v}_{LSR} = (0, v_{rot}, 0)$ is the motion of the Local Standard of Rest in galactic coordinates and $\mathbf{v}_{pec} = (11, 12, 7)\frac{\text{km}}{\text{s}}$ is the sun's peculiar velocity [24] [25] and $\mathbf{v}_\oplus(t)$ is the relative velocity of the earth with respect to the sun [22]. The time dependent term $v_\oplus(t)$ leads to an annual modulation with

$$\mathbf{v}_\oplus(t) = v_\oplus \left[\boldsymbol{\epsilon}_1 \cos(\omega(t - t_1) + \boldsymbol{\epsilon}_2 \sin(\omega(t - t_1))\right], \tag{2.27}$$

where $\omega = \frac{2\pi}{\text{year}}, v_\oplus = 29.8\frac{\text{km}}{\text{s}}$ is the orbital speed of the earth and the $\boldsymbol{\epsilon}_1$,$\boldsymbol{\epsilon}_1$ are unit vectors describing the direction of the earth's velocity at Spring equinox (21 March or $t_1 = 79\text{days}$) and summer solstice ($t_1 + 0.25\text{years} = 171\text{days}$). Eq. (2.27) ignores the elliptic nature of the earth's orbit and approximates it to be round, because the ellipticity only gives negligible small changes to velocity distributions [26] . The unit vectors are defined as

$$\begin{aligned}\boldsymbol{\epsilon}_1 &= (0.9931, 0.1170, -0.01032),\\ \boldsymbol{\epsilon}_2 &= (-0.0670, 0.4927, -0.8676).\end{aligned} \tag{2.28}$$

The time $t_0 = 153$ (2 June) is characterized as the time of the year at which $\mathbf{v}(t)$ is maximized, when the earth's speed is a maximum with respect to the dark matter rest frame. Therefore we can approximate $\mathbf{v}(t)$ in the following way

$$\begin{aligned}v_{obs}(t) &\simeq v_\odot + bv_\oplus \cos(\omega(t-153))\\ &\simeq 232 + 15\cos\left(2\pi\frac{t-153}{365}\right)\frac{\mathrm{km}}{\mathrm{s}}\end{aligned} \tag{2.29}$$

where $b \equiv \sqrt{b_1^2 + b_2^2}$ for $b_i \equiv \boldsymbol{\epsilon} \cdot \mathbf{v}_\odot$ is a geometrical factor [22].

2.4 Dark matter event rate

Dark matter direct detection experiments aim to detect the collision with Dark matter with target nuclei or electrons. A Majority of experiments are based on ionization, scintillation, low temperature phonon techniques and so on.

Owing to the Maxwellian nature of the DM velocity distribution, the differential event rate with respect to the nuclear recoil energy is expected to be smoothly decreasing with the nuclear recoil energy E_R

$$\frac{dR}{dE_R} = \frac{R_0}{E_0 r}\exp\left(-\frac{E_R}{E_0}r\right), \tag{2.30}$$

where R is the event rate per unit mass, R_0 is the total event rate, $r = \frac{4m_\chi m_N}{(m_\chi+m_N)^2}$ is a kinematical factor and E_0 is the typical energy of an incoming DM particle with mass m_χ [18].

In direct detection the required quantity to measure is the scattering rate of a dark matter particle scattering off a nuclear target. The differential event rate with respect to the recoil energy is defined by

$$\frac{dR}{dE_R} = N_T\frac{\rho_\chi}{m_\chi}\left\langle\frac{d\sigma}{dE_R}v\right\rangle, \tag{2.31}$$

where the brackets imply a velocity average over incoming dark matter particles. N_T is the number of target nuclei per kg detector mass

$$N_T = \frac{N_A}{M_u A_r} \simeq \frac{6.02\cdot 10^{26}}{A_r}\mathrm{kg}^{-1}, \tag{2.32}$$

where N_A is the *Avogadro* constant, $M_u \equiv 10^{-3}\text{kg}\,\text{mol}^{-1}$ is the molar mass constant and A_r is the relative atomic mass. The differential event rate is in general expressed in terms of counts $\text{kg}^{-1}\text{day}^{-1}\text{keV}^{-1}$ for a DM particle with mass m_χ and a nucleus of mass m_N.

Hence, the differential event rate reads

$$\frac{dR}{dE_R} = N_T \frac{\rho_\chi}{m_\chi} \int\limits_{v_{min}}^{v_{esc}} d^3v\, f(\mathbf{v}, \mathbf{v}_{obs}) \frac{d\sigma}{dE_R} v, \tag{2.33}$$

where ρ_χ is the local DM density, v_{esc} is the escape velocity of the galaxy and $\frac{d\sigma}{dE_R}$ is the differential cross-section for the DM scattering and $f(\mathbf{v}, \mathbf{v}_{obs})$ is the DM velocity distribution in the galactic rest frame. The total event rate is defined by integrating the differential event rate over all possible recoil energies

$$R = \int_{E_T}^{E_R^{max}} dE_R N_T \frac{\rho_\chi}{m_\chi} \int_{v_{min}}^{v_{esc}} v f(\mathbf{v}, \mathbf{v}_{obs}) \frac{d\sigma}{dE_R} dv, \tag{2.34}$$

where E_T is the threshold energy, which is the smallest possible recoil energy to detect.

The observed number of events in an experiment running for a time T is obtained by integrating equation (2.31) from the threshold energy E_T to the upper boundary E_R^{max}

$$N = T \int\limits_{E_T}^{E_R^{max}} dE_R\, \epsilon(E_R) \frac{dR}{dE_R}, \tag{2.35}$$

where ϵ is the detector efficiency [27].

The DM nucleus cross section depends on the effective Lagrangian under consideration. It can be separated in a spin-independent (SI) and spin-dependent (SD) contribution

$$\begin{aligned} \frac{d\sigma}{dE_R} &= \left(\frac{d\sigma}{dE_R}\right)_{SI} + \left(\frac{d\sigma}{dE_R}\right)_{SD} \\ &= \frac{m_N}{2\mu_N v^2} \left(\sigma_0^{SI} F_{SI}^2(E_R) + \sigma_0^{SD} F_{SD}^2(E_R)\right), \end{aligned} \tag{2.36}$$

where $\sigma_0^{SI,SD}$ are the spin-independent and spin-dependent cross sections at zero momentum transfer. They are defined by the effective Lagrangian of the dark matter theory [28].

2.5 Detection channels

The detection of dark matter is categorized into three different techniques as it can be seen in Fig. 2.1. For simplicity the main focus in this work lies on the interaction with a scalar mediator and contact interaction, but the results can easily be generalized.

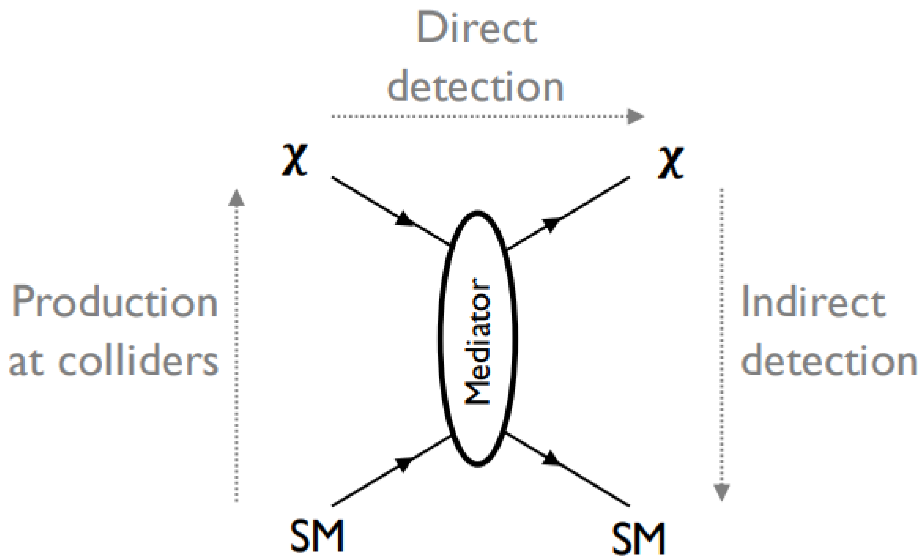

Figure 2.1: Schematic illustration of dark matter detection channels [29].

In this work, we are interested in direct detection experiments and the recoil signatures produced by dark matter particles. Several experiments, such as LUX, PANDAX-II and XENON1T, aim to detect Dark Matter with the use of large liquid xenon detectors in underground direct detection experiments.

2.5.1 Liquid Xenon detectors

Liquid Xenon (LXe) detectors are currently the most sensitives in direct detection experiments in the traditional WIMP mass window $m_\chi \geq 10\,\mathrm{GeV}$. Experiments. LXe is used as a detector medium with the important feature, that it produces both charge carriers and scintillation photons in response to energy deposition. The scintillation yield depends on the density of electron-ion pairs, which are produced on the track of the particle, which is referred as the linear energy transfer (LET). The two signals of scintillation and ionization are anticorrelated in the (LET) and highly complementary, which serves a very precise measurement by simultaneous detection [30]. The liquid xenon detector experiment XENON1T currently holds the most stringent limits on the DM nucleon cross section [31].XENON1T is a dual phase time projection chamber (TPC) filled with LXe located at the Laboratori Nazionali del Gran Sasso laboratory. The working principle can be seen in Figure (2.2).

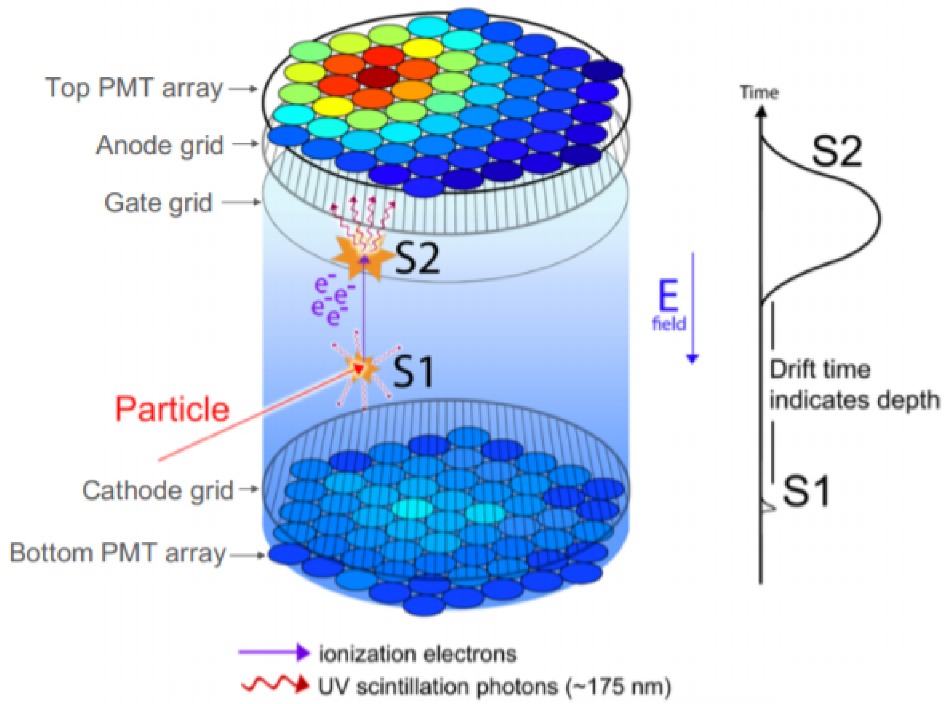

Figure 2.2: Schematic illustration of the dual phase time projection chamber from [29]. The TPC measures a scintillation signal in S1 and the ionization charge within another scintillation signal in S2.

The DM induced nuclear recoils in LXe are generating scintillation light (S1) and can also ionize electrons from the noble gas. An electric field in the LXe volume drifts the ionized electrons upwards and extracts them into the xenon gas phase (GXe), where electroluminescence produces a second scintillation signal (S2). The event vertex is reconstructed from the pattern of the photomultiplier tubes (PMT) on top and the time difference between the signals S1 and S2. The ratio of these signals $S2/S1$ gives information to distinguish between electron recoils caused by β particles and γ rays and nuclear recoils caused by neutrons and DM particles and is also used for background discrimination [32] [31]. However, the S1 signal is only sensitive to events of dark matter masses ($m_\chi \gtrsim$ few GeV) with recoil energies of $\gtrsim 1\,\mathrm{keV}$. The S2 signal is able to detect events with energies as low as 0.7 keV for nuclear recoils and energies of 0.186 keV for electron recoils. The nuclear recoil events lose the biggest amount of their energy through low energy collisions with other nuclei, such that they produce only about one fourth of the electronic excitation of an electron recoil event with the same energy, which was first discovered by Lindhard [33][34].

The energy E_0 deposited in the detector by recoil events can be expanded by the Platzman equation

$$E_0 = N_i E_i + N_{ex} E_{ex} + N_i \epsilon, \tag{2.37}$$

where N_i is the number of electron-ion pairs at an average energy of E_i, N_{ex} is the number of excited atoms at an average energy of E_{ex} and ϵ is the average kinetic energy of sub-excitation electrons. From this equation it is possible to deduce the so called W-value, which is defined as the average energy required to produce one electron-ion pair

$$W = \frac{E_0}{E_i} = E_i + E_{ex}\left(\frac{N_{ex}}{N_i}\right) + \epsilon. \tag{2.38}$$

Assuming E to be the energy of the ionizing radiation, the maximum scintillation yield is defined by $\frac{E}{W_{ph}}$, where W_{ph} is the average energy needed for the production of one single electron and is defined as

$$W_{ph} = \frac{W}{1 + \frac{N_{ex}}{N_i}}. \tag{2.39}$$

The experimental value for LXe is $W_{ph} = 13.8 \pm 0.9 eV$.

Chapter 3

Migdal Effect: Theoretical description

The fundamental scattering process for the Migdal effect is elastic nuclear scattering $\chi + N \rightarrow \chi + N$. The scattered nucleus receives a boost into the direction of the recoil. The electrons around the nucleus need some time to catch up, which can result in the prompt ionization of an electron and excitation processes. The probabilities of excitation processes are much smaller compared to the ionization probabilities [35], such that the transition amplitude is dominated by ionization processes. The nuclear scattering process and possible transitions are depicted in Fig. (3.1). The contributions of photon Bremsstrahlung [2] are about 3-4 orders of magnitude smaller than the contributions from the ionization processes [36]. Of course there are also Auger transitions possible, which result from excitation of inner shell electrons and subsequent photoionization of an electron, but the contribution is small, since the probabilities of excitation are subdominant.

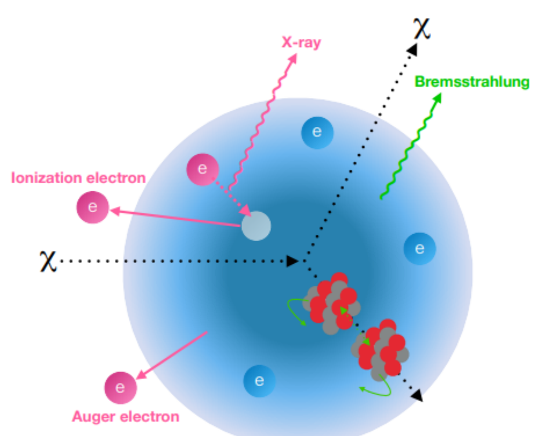

Figure 3.1: Schematic picture of elastic nuclear scattering and possible resulting signals in direct detection [36].

The main focus in this work lies in the calculation of the Migdal effect with respect to ionization processes, because these contribution are the most dominant ones. The overall size of the prompt ionization can be estimated by noting that the state of the electron cloud after the nuclear recoil (in the rest frame of the nucleus) is approximated by

$$|\Phi_{ec}^{F}\rangle = e^{-im_e \sum_i \mathbf{v}\cdot\mathbf{r_i}} |\Phi_{ec}^{I}\rangle , \tag{3.1}$$

where $\mathbf{v}$ is the velocity of the nucleus after the recoil and $\mathbf{r}_i$ is the position operator of the i-th electron and $|\Phi_{ec}^{I}\rangle$ is the inital state of the electron cloud. The probability of the ionization/excitation is then estimated as

$$\mathcal{P} = |\, \langle \Phi_{ec}^{*} | \Phi_{ec}^{F} \rangle \,|^2, \tag{3.2}$$

where $|\Phi_{ec}^{*}\rangle$ is the final state of the electron cloud, where one or multiple electrons are ionized. In the following analysis the ionization processes are treated seperately from the nuclear recoil.

3.1 Atomic recoil

We consider an isolated atom with mass m_A and N_e electrons with mass m_e. The energy scale of the recoil is about $\mathcal{O}(\text{keV})$, such that we can approximate the atomic system by a non relativistic Hamiltonian. Following the steps in [35], we split the atomic Hamiltonian into one part describing the nucleus and one describing the electron cloud, such that we can treat the nuclear recoil separately from final state ionization processes. The Hamiltonian reads

$$H_A(\mathbf{r},\mathbf{p}) = \frac{\mathbf{p}_N^2}{2m_N} + H_{ec}(\mathbf{r},\mathbf{p}), \tag{3.3}$$

$$H_{ec}(\mathbf{r},\mathbf{p}) = \sum_{i=1}^{N_e} \frac{\mathbf{p}_i^2}{2m_e} + V(\mathbf{r}_i,\mathbf{r}_j,\mathbf{r}_N), \tag{3.4}$$

$$V(\mathbf{r}) = \frac{1}{2}\sum_{i\neq j} \frac{e^2}{|\mathbf{r}_i - \mathbf{r}_j|} - \sum_{i=1}^{N} \frac{Ze}{|\mathbf{r}_i - \mathbf{r}_N|}, \tag{3.5}$$

where $\mathbf{r}$ and $\mathbf{p}$ are the position and momentum operators and H_{ec} is the Hamiltonian of the electron cloud, which contains the nucleon-electron interaction as well as the electron-electron interaction.

The eigenequation in the coordinate representation is

$$\left(\frac{\mathbf{p}_N^2}{2m_N} + \sum_{i=1}^{N_e} \frac{\mathbf{p}_i^2}{2m_e} + V(\mathbf{r}_i,\mathbf{r}_j,\mathbf{r}_N)\right)\psi_E(\mathbf{r},\mathbf{r}_N) = E_A\psi_E(\mathbf{r},\mathbf{r}_N). \tag{3.6}$$

3.1.1 Born Oppenheimer Approximation

For the Hamiltonian of (3.3), we can first solve the eigenequation for the eigenstates of $H_{ec}(\mathbf{r}_N)$ and obtain

$$H_{ec}(\mathbf{r}_N)\Phi_{ec}(\mathbf{r},\mathbf{r}_N) = E_{ec}(\mathbf{r}_N)\Phi_{ec}(\mathbf{r},\mathbf{r}_N). \tag{3.7}$$

Translation invariance of the Hamiltonian induces $E_{ec}(\mathbf{r}_N) \equiv E_{ec}$, such that the wave functions $\Phi_{ec}(\mathbf{r},\mathbf{r}_N)$ only depend on $\mathbf{r}_N$ through $\mathbf{r}-\mathbf{r}_N$:

$$\Phi_{ec}(\mathbf{r},\mathbf{r}_N) \equiv \Phi_{ec}(\mathbf{r}-\mathbf{r}_N). \tag{3.8}$$

The eigenstates $\Phi_{ec}(\mathbf{r}-\mathbf{r}_N)$ form a complete orthogonal basis of the electron cloud for a given $\mathbf{r}_N$.

Now we can use equation (3.6) to get the eigenequation of the nucleus in the rest frame

$$\frac{\mathbf{p}_N^2}{2m_N}\psi_{E_A}^{\text{rest}}(\mathbf{r},\mathbf{r}_N) = (E_A - E_{ec})\psi_{E_A}^{\text{rest}}(\mathbf{r},\mathbf{r}_N). \tag{3.9}$$

Due to momentum conservation, we have

$$\mathbf{p}_N\psi_{E_A}^{\text{rest}}(\mathbf{r},\mathbf{r}_N) = -\sum_i^{N_e}\mathbf{p}_i\psi_{E_A}^{\text{rest}}(\mathbf{r},\mathbf{r}_N). \tag{3.10}$$

The kinetic energy of the electron cloud can be estimated to be

$$\left\langle\frac{\mathbf{p}_i^2}{2m_e}\right\rangle \simeq \frac{E_{ec}}{N_e}. \tag{3.11}$$

The left hand side of Eq. (3.9) is highly suppressed

$$\left\langle\frac{\mathbf{p}_N^2}{2m_N}\right\rangle \simeq \frac{2m_e}{2m_N}N_e\left\langle\frac{\mathbf{p}_i^2}{2m_e}\right\rangle \simeq \frac{m_e}{m_N}E_{ec}, \tag{3.12}$$

because the motion of the nucleus is very slow compared to the speed at which electrons move [37]. The eigenequation is well approximated by

$$H_A\psi_{E_A}^{\text{rest}}(\mathbf{r},\mathbf{r}_N) = E_{ec}\psi_{E_A}^{\text{rest}}(\mathbf{r},\mathbf{r}_N). \tag{3.13}$$

We conclude that the energy eigenfunction of the whole atomic system at rest are well approximated by Φ_{ec}.

3.1.2 Galilean boost of an atom at rest

Since the Hamiltonian is invariant under galilean transformations, the wave functions after the atomic recoil are obtained by a galilean boost of the energy eigenstates of an atom at rest. The boosted energy eigenstates of a certain velocity $\mathbf{v}$ are

$$\psi_{E_A}(\mathbf{r}, \mathbf{r}_N) = U(\mathbf{v})\psi^{\text{rest}}_{E_A}(\mathbf{r}, \mathbf{r}_N). \tag{3.14}$$

The unitary operator of the Galilean boost is defined as

$$U(\mathbf{v}) = \exp\left(im_N \mathbf{v}\cdot\mathbf{r}_N + im_e \sum_{i=1}^{N_e} \mathbf{v}\cdot\mathbf{r}_i \right), \tag{3.15}$$

so that the momentum operators follow the transformation law

$$U(\mathbf{v})^\dagger \mathbf{p}_N U(\mathbf{v}) = \mathbf{p}_N + m_N\mathbf{v}, \tag{3.16}$$

$$U(\mathbf{v})^\dagger \mathbf{p}_i U(\mathbf{v}) = \mathbf{p}_i + m_e\mathbf{v}. \tag{3.17}$$

The Hamiltonian of the atom transformes as

$$U(\mathbf{v})^\dagger H_A(\mathbf{r},\mathbf{p})U(\mathbf{v}) = H_A(\mathbf{r},\mathbf{p}) + \mathbf{v}\left(\mathbf{p}_N + \sum_{i=1}^{N_e}\mathbf{p}_i\right) + \frac{1}{2}\bar{m}_A\mathbf{v}^2 + V(\mathbf{r}_i,\mathbf{r}_j,\mathbf{r}_N), \tag{3.18}$$

where $\bar{m} = m_A + N_e m_e$. Combining equation (3.13),(3.10) and (3.18), we obtain

$$U(\mathbf{v})^\dagger H_A(\mathbf{r},\mathbf{p})U(\mathbf{v})U^\dagger(\mathbf{v})\psi^{\text{rest}}_{E_A} = \left(E_{ec} + \frac{1}{2}\bar{m}\mathbf{v}^2\right)\psi_{E_A} \tag{3.19}$$

Hence, the boosted wave function ψ_{E_A} can be approximated by

$$\psi_{E_A}(\mathbf{r},\mathbf{r}_N) \simeq e^{i\mathbf{p}_N\cdot\mathbf{r}_N + i\sum_{i=1}^{N_e}\mathbf{p}_e\cdot\mathbf{r}_i}\psi^{\text{rest}}_{E_A}(\mathbf{r},\mathbf{r}_N) \tag{3.20}$$

with eigenvalue of $E_A \simeq E_{ec} + \frac{1}{2}\bar{m}\mathbf{v}^2$ and $\mathbf{p}_e = m_e\mathbf{v}, \mathbf{p}_N = m_N\mathbf{v}$.

Now, $\psi_{E_A}(\mathbf{r},\mathbf{r}_N)$ is not an eigenstate of the nucleus momentum $\mathbf{p}_N$, but an eigenstate of the momentum of the whole atom, such that

$$\left(\mathbf{p}_N + \sum_{i=1}^{N_e}\mathbf{p}_i\right)\psi_{E_A}(\mathbf{r},\mathbf{r}_N) = (\bar{m}\mathbf{v})\,\psi_{E_A}(\mathbf{r},\mathbf{r}_N). \tag{3.21}$$

3.1.3 Inelastic scattering and kinematical constraints

The prompt ionization or excitation of electrons is an inelastic scattering process due to the energy loss ΔE of the atom under consideration. Assuming non relativistic scattering, the momentum transfer q_A in the center of mass (COM) after the recoil is given by

$$\begin{aligned} q_A^2 &\simeq \left(|\mathbf{p}_\chi^F| - |\mathbf{p}_\chi^I|\right)^2 + 2|\mathbf{p}_\chi^F||\mathbf{p}_\chi^I|(1-\cos\vartheta_{CM}) \\ &\simeq -(\Delta E)^2 + 2m_A E_R \simeq 2m_A E_R, \end{aligned} \tag{3.22}$$

where $\Delta E = E_{ec}^F - E_{ec}^I$ is the energy loss due to ionization/excitation processes. Since the deposited electron energy ΔE is of order $\mathcal{O}(1\text{keV})$, the recoil energy is well approximated by

$$E_R = \frac{\left(|\mathbf{p}_\chi^F| - |\mathbf{p}_\chi^I|\right)^2 + 2|\mathbf{p}_\chi^F||\mathbf{p}_\chi^I|(1-\cos\vartheta_{CM})}{2m_A} \simeq \frac{\mathbf{q}_A^2}{2m_A}. \tag{3.23}$$

The initial momentum $\mathbf{p}_\chi^I$ in the COM frame is related to the DM velocity $\mathbf{v}$ in the LAB frame by

$$\mathbf{p}_\chi^I = -\mathbf{q}_A^I = \mathbf{p}^I \simeq \mu_N v. \tag{3.24}$$

In the center of mass frame, the final state momentum $\mathbf{p}_\chi^F$ is related to the initial momentum $\mathbf{p}_\chi^I$ by

$$|\mathbf{p}_\chi^F|^2 = |\mathbf{p}_\chi^I|^2 - 2\mu_N \Delta E, \tag{3.25}$$

where $\mu_N = \frac{m_\chi m_N}{m_\chi + m_N}$. Hence, the DM threshold velocity ($|\mathbf{p}_F| > 0$) is given by

$$v^{(th)} = \sqrt{\frac{2\Delta E}{\mu_N}}, \tag{3.26}$$

which also sets a kinematical upper limit for the electron transition energy

$$\Delta E^{MAX} = \frac{1}{2}\mu_N v^2. \tag{3.27}$$

It is notable that for $\Delta E = \Delta E^{MAX}$, the atomic recoil energy E_R is smaller than ΔE^{MAX}

$$E_R = \frac{\mathbf{q}_A^2}{2m_A} = \frac{\mu_N^2 v^2}{2m_A} = \frac{\mu_N}{m_A}\Delta E^{MAX}, \tag{3.28}$$

which is a very important property for direct detection experiments.

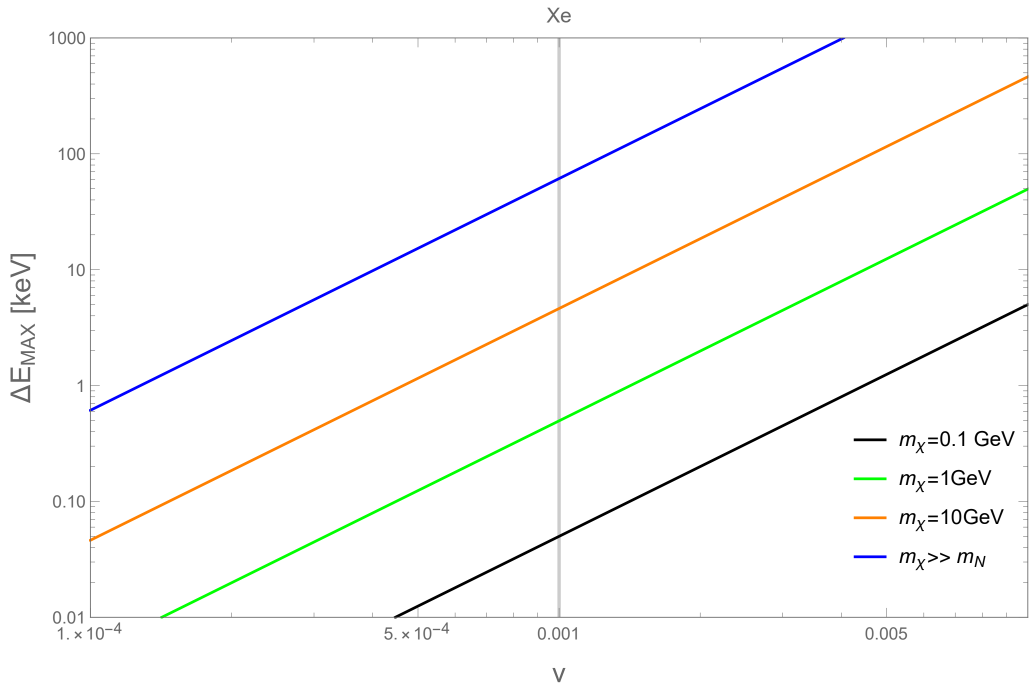

Figure 3.2: The (E_R,v_{min})-plane shows the kinematical constraints with fixed dark matter masses and fixed deposited energy ΔE for an isolated Xenon atom.

Combining equation (3.23) and (3.25), we are able to express the recoil energy with respect to the inelastic scattering process

$$E_R = \frac{\mu_N^2 v^2}{2m_A}\left(\left(1-\sqrt{1-\frac{2\Delta E}{\mu_N v^2}}\right)^2 + 2(1-\cos(\theta))\sqrt{1-\frac{2\Delta E}{\mu_N v^2}}\right). \tag{3.29}$$

In case of ionization, $\Delta E = E_{nl} + \epsilon$, where E_{nl} is the binding energy and ϵ the energy of the electron in the continuum. By maximizing Eq. (3.29), by setting $\theta = \pi$ and expand the root terms up to first order, we find the minimum dark matter velocity to be

$$v_{min} \simeq \frac{m_A E_R + \mu_N \Delta E}{\mu_N \sqrt{2 m_A E_R}}. \tag{3.30}$$

Hence, the maximum and minimum recoil energy of the inelastic process is given by

$$E_R = \frac{\mu_N^2 v^2}{m_A}\left(1-\frac{\Delta E}{\mu_N v^2} \pm \sqrt{1-\frac{2\Delta E}{\mu_N v^2}}\right). \tag{3.31}$$

The kinematical constraints for Xenon for certain dark matter masses are illustrated in Figure (3.3) and Figure (3.4).

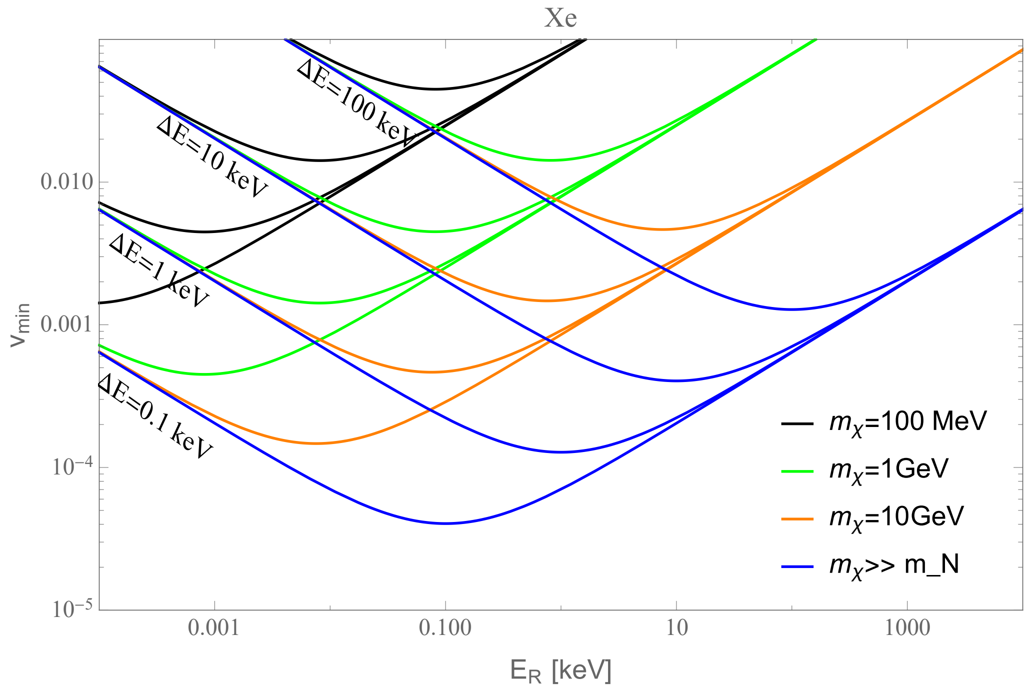

Figure 3.3: The (E_R,v_{min})-plane shows the kinematical constraints with fixed dark matter masses and fixed deposited energy ΔE for an isolated Xenon atom. The kinematical allowed region for the nuclear recoil energy lies above the curves.

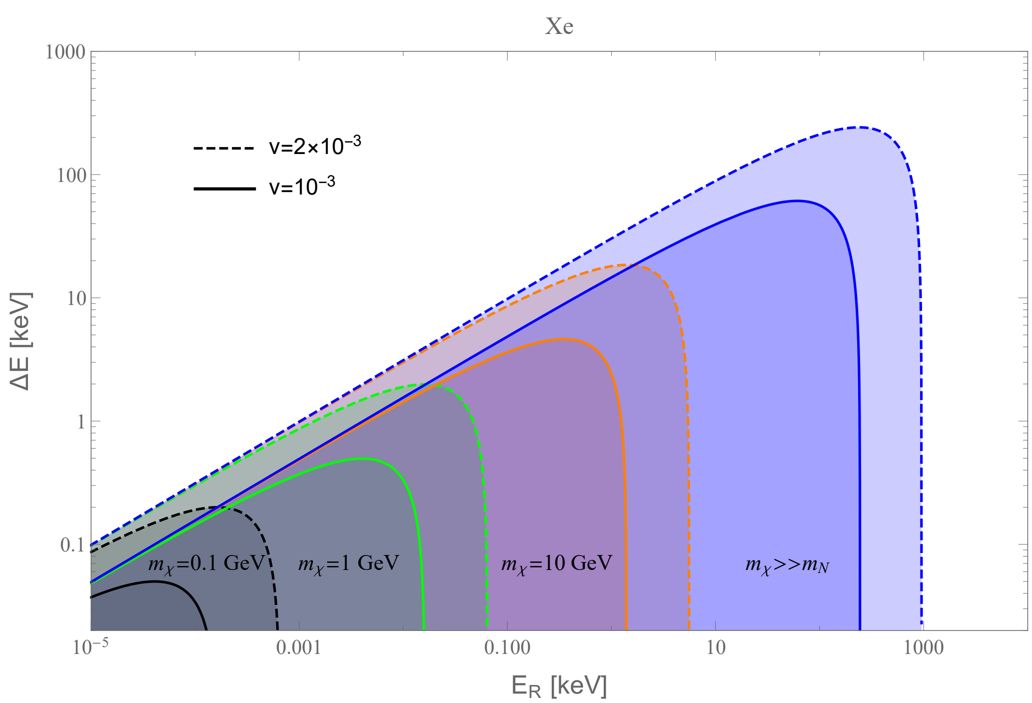

Figure 3.4: The (E_R,ΔE)-plane shows the kinematical bound of the deposit energy as a function of the recoil energy with fixed DM masses m_χ for an isolated Xenon atom.

3.1.4 Isolated nuclear recoil

In this formulation the nuclear recoil is treated seperately from the final state ionization/excitation. The main focus in this thesis lies on spin independent interactions. The S-Matrix is of the form $S_{fi} = \mathbb{1} + iT_{fi}$ and we have a relation to the invariant matrix element by

$$iT_{FI} = \langle p_N^f p_\chi^f | k_N^i k_\chi^i \rangle = i\mathcal{M} \times (2\pi)^4 \delta^{(4)}(p_N^I + p_\chi^I - k_N^F - k_\chi^F) \tag{3.32}$$

The normalization of the plane waves of dark matter and the nucleus is

$$\langle p|p' \rangle = (2\pi)^3 2p^0 \delta^{(3)}(p' - p). \tag{3.33}$$

Light DM particles are expected to have non relativistic velocities, such that we assume coherent nuclear scattering ($q \cdot r \lesssim 1$). One possibility is to realize the interaction by the spin-independent Lagrangian

$$\mathcal{L}_{int} = \sum_{i=p,n} \frac{f_i}{M_*^2} \bar{\psi}_i \psi_i \bar{\psi}_\chi \psi_\chi, \tag{3.34}$$

which induces contact interaction. The Lagrangian has to be of mass dimension four, such that it is necessary to introduce mass parameter M_* to achieve the right mass dimension. The coupling constants $f_{p,n}$ are dimensionless. Therefore, the invariant amplitude squared for the scattering process is

$$|\mathcal{M}|^2 = 16 \frac{m_N^2 m_\chi^2}{M_*^4} \left(g_p Z + g_n (A - Z) \right)^2. \tag{3.35}$$

where A is the atomic number and Z is the mass number.

The energy in the center of mass frame for the scattering process is $E_{CM} \simeq m_\chi + m_N$. Hence the cross section σ yields

$$\begin{aligned} \sigma &\simeq \frac{|\mathcal{M}|^2}{16\pi (m_\chi + m_N)^2} \\ &\simeq \frac{\mu_N^2}{\pi M_*^4} (g_p Z + g_n (A - Z))^2, \end{aligned} \tag{3.36}$$

where $\mu_N = \frac{m_N m_\chi}{m_N + m_\chi}$ is the reduced mass. The invariant matrix element is related to the interaction potential in the coordinate representation by

$$\begin{aligned} H &= H_0 + V_{\text{int}}, \\ H_0 &= \frac{\mathbf{p}_N^2}{2m_N} + \frac{\mathbf{p}_\chi^2}{2m_\chi}, \\ V_{\text{int}} &= \frac{-\mathcal{M}}{4 m_\chi m_N} \delta^{(3)}(\mathbf{r}_N - \mathbf{r}_\chi). \end{aligned} \tag{3.37}$$

The initial and final states of the isolated nuclear recoil are respectively

$$\psi_{I,F}(\mathbf{r}, \mathbf{r}_N) = \sqrt{4m_\chi m_N} e^{i\mathbf{p}_N^{I,F}\cdot\mathbf{r}_N + i\mathbf{p}_\chi^{\mathbf{I,F}}\cdot\mathbf{r}_\chi}. \tag{3.38}$$

Another possibility would be to describe the interaction by the exchange of a light scalar particle ϕ with mass m_ϕ. Therefore the interaction can be realized by an effective Yukawa interaction Lagrangian

$$\mathcal{L}_Y = -\sum_{i=p,n} y_i \phi\bar{\psi}\psi - y_\chi \phi \bar{\psi}_\chi \psi_\chi, \tag{3.39}$$

where y_i and y_χ are Yukawa coupling constants. The invariant matrix element is then of the form

$$\mathcal{M}_Y = \bar{u}_N(y_p Z + y_n(A-Z))u_N \frac{i}{q^2 - m_\phi^2} \bar{u}_\chi g_\chi u_\chi. \tag{3.40}$$

Since $\bar{u}_N u_N = 2m$ and $\bar{u}_\chi u_\chi = 2m_\chi$, we arrive at the result

$$|\mathcal{M}_\mathrm{Y}|^2 \simeq \frac{16 m_N^2 m_\chi^2}{(m_\phi^2 - t)^2}(y_p Z + y_n(A-Z))y_\chi,$$

$$t \simeq -\mathbf{q}_N^2 = -(\mathbf{p}_N^F - \mathbf{p}_N^I)^2, \tag{3.41}$$

which is very similar to the matrix element 3.35. Assuming $t \ll m_\Phi$, we find the relation $\mathcal{M} = \mathcal{M}_Y$ with $M_* = m_\Phi$. The invariant matrix element is reproduced in nonrelativistic quantum mechanics by the interaction potential

$$V_{int}(\mathbf{r}_N - \mathbf{r}_\chi) = -\int \frac{d^3\mathbf{q}}{(2\pi)^3} e^{i\mathbf{q}(\mathbf{r}_N - \mathbf{r}_\chi)} \frac{\mathcal{M}(q^2)}{4m_\chi m_N}. \tag{3.42}$$

3.2 Perturbation of the electron cloud

Now, we want to take further investigation on the inelastic process with respect to the electron cloud. The interaction is described by the Hamiltonian

$$H = H_A + \frac{\mathbf{p}_\chi^2}{2m_\chi} + V_{int} \tag{3.43}$$

in the coordinate representation of NRQM. Considering the initial atom at rest in the lab frame, we have the total energies

$$E_I = E_{ec}^I + \frac{\mathbf{p}_\chi^{I\,2}}{2m_\chi^2},$$

$$E_F = E_{ec}^F + \frac{\bar{m}_A \mathbf{v}_F^2}{m_A} + \frac{\mathbf{p}_\chi^{F\,2}}{2m_\chi^2}. \tag{3.44}$$

The final state wave function is now obtained by a galilean boost of the wave function at rest. Hence, the T-matrix of the scattering process is given by

$$\begin{aligned} iT_{FI} =& - i(2\pi)\delta(E_F - E_I) \int d^3r_N d^3r_\chi \prod_i d^3r_i 4m_\chi m_N V_{\text{int}}(\mathbf{r}_N - \mathbf{r}_\chi) \\ & \times \Phi^*_{E^F_{ec}}(\mathbf{r} - \mathbf{r}_N) e^{-i\sum_i \mathbf{q}_e\cdot\mathbf{r}_i} e^{-i\mathbf{p}^F_N\cdot\mathbf{r}_N} \Phi_{E^I_{ec}}(\mathbf{r} - \mathbf{r}_N) e^{-i(\mathbf{p}^F_\chi - \mathbf{p}^I_\chi)\cdot\mathbf{r}_\chi}. \end{aligned} \tag{3.45}$$

Now shifting the variables $\mathbf{r}_i$ and $\mathbf{r}_\chi$ by $\mathbf{r}_N$, we obtain

$$\begin{aligned} iT_{FI} =& - i(2\pi)^4\delta(E_F - E_I)\delta^{(3)}(\bar{m}\mathbf{v}_F + \mathbf{p}^F_\chi - \mathbf{p}^I_\chi)\mathcal{F}(q_A^2)\mathcal{M}(q_A^2) \\ & \times \int \prod d^3r_i \Phi^*_{E^F_{ec}}(\mathbf{r}) e^{-i\sum_i \mathbf{q}_e\cdot\mathbf{r}_i} \Phi^*_{E^I_{ec}}(\mathbf{r}), \end{aligned} \tag{3.46}$$

where $\mathbf{q}_A^2 = (\mathbf{p}^F_\chi - \mathbf{p}^I_\chi)^2$. The delta function can now be rewritten in the form $\delta^{(4)}(p_F - p_I) = \delta(E_F - E_I) \times \delta^{(3)}(\bar{m}\mathbf{v}_F + \mathbf{p}^F_\chi - \mathbf{p}^I_\chi)$, such that the T-matrix element reduces to

$$iT_{FI} = i(2\pi)^4\delta(p_F - p_I)\mathcal{F}(q_A^2)\mathcal{M}(q_A^2) Z_{FI}(\mathbf{q}_e), \tag{3.47}$$

and we identify the electron transition amplitude to be

$$Z_{FI}(q_e) = \int \prod d^3r_i \Phi^*_{E^F_{ec}}(\mathbf{r}) e^{-i\sum_i \mathbf{q}_e\cdot\mathbf{r}_i} \Phi_{E^I_{ec}}(\mathbf{r}). \tag{3.48}$$

3.3 The electron transition amplitude

Now we make further investigation on the electron transition amplitude defined by Eq. (3.48)

$$Z_{FI}(\mathbf{q}_e) = \langle \psi^F | e^{i\sum_i \mathbf{q}_e\cdot\mathbf{r}_i} | \psi^I \rangle = \int \prod_i d^3r_i \Phi^*_{E^F_{ec}}(\mathbf{r}) e^{-i\sum_i \mathbf{q}_e\cdot\mathbf{r}_i} \Phi_{E^I_{ec}}(\mathbf{r}). \tag{3.49}$$

Now any feasible calculation of these matrix elements involves the application of self consistent field theory methods, such as the Hartree Fock method, which is explained in Appendix B. In SCF theory, the total electron wave function is realized as a Slater determinant of one-electron wave functions and therefore an antisymmetric product of single electron wave functions

$$\Phi^I_{o_1,o_2,\ldots,o_{N_e}}(\mathbf{r}_i) = \frac{1}{\sqrt{N_e!}} \sum_{\sigma\in S_{N_e}} \text{sgn}(\sigma) \prod_{i=1}^{N_e} \phi_{o_{\sigma(i)}}(\mathbf{r}_i), \tag{3.50}$$

$$\int d^3r_i \phi^*_{o_j}(\mathbf{r}_i)\phi_{o_i}(\mathbf{r}_i) = \delta_{o_j,o_i}, \tag{3.51}$$

where o_i contains the quantum numbers that define the state of the electron under consideration. The one-electron wave functions $\phi_o(x)$ contain a radial part, which is usually obtained by SCF methods and an angular part, which is in the nonrelativistic treatment described by spherical harmonics $Y_{lm}(\vartheta,\varphi)$ and in the relativistic approach by spherical spinors $\Omega_{\kappa m}(\vartheta,\varphi)$, see Appendix C for more details. The Galilean boost operator $e^{-i\mathbf{q}_e\cdot\sum_i \mathbf{r_i}}$ is identified with the interaction operator, which induces atomic transitions and can be expanded in the form

$$\begin{aligned} e^{-i\sum_i \mathbf{q}_e\cdot\mathbf{r}_i} &= 1 - i\mathbf{q}_e\cdot(\mathbf{r}_1+\dots+\mathbf{r}_{N_e}) + \frac{(-i\mathbf{q}_e\cdot(\mathbf{r}_1+\dots+\mathbf{r}_{N_e}))^2}{2!} + \dots \\ &= \sum_{L=0}^{\infty}\frac{(-i)^L(\mathbf{q}_e\cdot\sum_{i=1}^{N_e}\mathbf{r}_i)^L}{L!} = \sum_{L=0}^{\infty}\frac{(-i)^L q_e^L}{L!}\left(\sum_{i=1}^{N_e} r_i\cos\vartheta_i\right)^L, \end{aligned} \tag{3.52}$$

where $\cos\vartheta_i = \angle(\mathbf{q_e},\mathbf{r}_i)$. Since the one-electron wave functions form an orthonormal basis set, the order $(L=0)$ vanishes. Hence, we can split the matrix elements into different orders of L. The electron transition amplitude is then rewritten as

$$\begin{aligned} \langle\psi^F|e^{i\sum_i \mathbf{q}_e\cdot\mathbf{r}_i}|\psi^I\rangle = &\sum_{\sigma,\tilde{\sigma}\in S_{N_e}}\frac{\mathrm{sgn}(\sigma)\mathrm{sgn}(\tilde{\sigma})}{N_e!}\int d^3r_i\sum_{L=1}^{\infty}\frac{(-i)^L q_e^L}{L!} \\ &\times\prod_{i,j=1}^{N_e}\phi^*_{o^F_{\sigma(j)}}(\mathbf{r}_j)\left(\sum_{i=1}^{N_e} r_i\cos\vartheta_i\right)^L\phi_{o^I_{\tilde{\sigma}(i)}}(\mathbf{r}_i). \end{aligned} \tag{3.53}$$

From now on, I will use the Einstein sum convention to omit exuberant notation. The summation over the antisymmetric products can be simplified by using the totally antisymmetric Levi-Civita symbol $\epsilon_{i_1\dots i_n}$ with the usual convention $\epsilon_{123\dots N_e}=1$ to rewrite the matrix element in the form

$$\begin{aligned} \langle\psi^F|e^{i\sum_i \mathbf{q}_e\cdot\mathbf{r}_i}|\psi^I\rangle = &\int\frac{\epsilon^{k_1,k_2,\dots,k_{N_e}}\epsilon_{m_1,m_2,\dots,m_{N_e}}}{N_e!}\frac{(-i)^L q_e^L}{L!} \\ &\times\prod_{i=1}^{N_e} d^3r_i\phi^*_{o^F_{m_i}}(\mathbf{r}_i)\left(r_1\cos\vartheta_1+\dots+r_{N_e}\cos\vartheta_{N_e}\right)^L\phi_{o^I_{k_i}}(\mathbf{r}_i). \end{aligned} \tag{3.54}$$

The final state is of the same form as Eq. (3.50), but the operator $\exp(-i\mathbf{q}_e\cdot\sum_i\mathbf{r}_i)$ now allows transitions to continuum or excited states. The angular part of the the matrix elements defines the allowed final states, which we will examine later on.

3.3.1 The dipole transition

The first order $(L=1)$ of Eq.(3.66) for an atom with N_e electrons leads to

$$\begin{aligned} \langle\psi^F|e^{i\sum_i \mathbf{q}_e\cdot\mathbf{r}_i}|\psi^I\rangle = &-iq_e\int\frac{\epsilon^{k_1,k_2,\dots,k_{N_e}}\epsilon_{m_1,m_2,\dots,m_{N_e}}}{N_e!} \\ &\times\prod_{i=1}^{N_e} d^3r_i\phi^*_{o^F_{m_i}}(\mathbf{r}_i)\left(r_1\cos\vartheta_1+r_2\cos\vartheta_2+\dots+r_{N_e}\cos\vartheta_{N_e}\right)\phi_{o^I_{k_i}}(\mathbf{r}_i). \end{aligned} \tag{3.55}$$

Using the normalization condition of Eq. (3.51), the transition amplitude reduces to

$$
\begin{aligned}
\langle\psi^F|e^{i\sum_i \mathbf{q}_e\cdot\mathbf{r}_i}|\psi^I\rangle = &- iq_e \int \frac{\epsilon^{k_1,k_2,\ldots,k_{N_e}}\epsilon_{m_1,m_2,\ldots,m_{N_e}}}{N_e!} \\
&\times\Big[d^3r_1\phi^*_{o^F_{m_1}}(\mathbf{r}_1)r_1\cos\vartheta_1\phi_{o^I_{k_1}}(\mathbf{r}_1)\delta_{k_2,m_2}\delta_{k_3,m_3}\ldots\delta_{k_{N_e},m_{N_e}} \\
&+ d^3r_2\phi^*_{o^F_{m_2}}(\mathbf{r}_2)r_2\cos\vartheta_2\phi_{o^I_{k_2}}(\mathbf{r}_2)\delta_{k_1,m_1}\delta_{k_3,m_3}\ldots\delta_{k_{N_e},m_{N_e}} \\
&\ldots \\
&+ d^3r_{N_e}\phi^*_{o^F_{m_{N_e}}}(\mathbf{r}_{N_e})r_{N_e}\cos\vartheta_{N_e}\phi_{o^I_{k_{N_e}}}(\mathbf{r}_{N_e})\delta_{k_1,m_1}\delta_{k_2,m_2}\ldots\delta_{k_{N_e-1},m_{N_e-1}}\Big]
\end{aligned}
\tag{3.56}
$$

The indices of the Levi-civita tensor get now contracted with the Kronecker deltas, such that the Levi-civita tensors of the individual terms only differ in one index, e.g $\epsilon^{k_1,k_2,\ldots,k_{N_e}}\epsilon_{m_1,k_2,\ldots,k_{N_e}}$. The contraction rule for the Levi civita tensor is

$$
\epsilon^{k_1,k_2,\ldots,k_{N_e}}\epsilon_{m_1,k_2,\ldots,k_{N_e}} = \delta^{k_1}_{m_1}(N_e-1)!, \tag{3.57}
$$

which can be used for all expressions by the use of cyclic permutations. Now the matrix element reads

$$
\begin{aligned}
\langle\psi^F|e^{i\sum_i \mathbf{q}_e\cdot\mathbf{r}_i}|\psi^I\rangle = -iq_e \int \frac{1}{N_e}\Big[&\; d^3r_1\,\delta^{k_1}_{m_1}\phi^*_{o^F_{m_1}}(\mathbf{r}_1)r_1\cos\vartheta_1\phi_{o^I_{k_1}}(\mathbf{r}_1) \\
&+d^3r_2\,\delta^{k_2}_{m_2}\phi^*_{o^F_{m_2}}(\mathbf{r}_2)r_2\cos\vartheta_2\phi_{o^I_{k_2}}(\mathbf{r}_2) \\
&+\ldots \\
&+d^3r_{N_e}\,\delta^{k_{N_e}}_{m_{N_e}}\phi^*_{o^F_{m_{N_e}}}(\mathbf{r}_{N_e})r_{N_e}\cos\vartheta_1\phi_{o^I_{k_{N_e}}}(\mathbf{r}_{N_e})\Big]
\end{aligned}
\tag{3.58}
$$

The transition amplitude now still involves a summation over the indices of the Kronecker deltas $\delta^{k_i}_{m_i}$, but since there are only N_e indices of the same kind, we simply get an additional factor of N_e and of course $k_i = m_i$, such that

$$
\begin{aligned}
\langle\psi^F|e^{i\sum_i \mathbf{q}_e\cdot\mathbf{r}_i}|\psi^I\rangle &= - iq_e \int \sum_{i=1}^{N_e} d^3r_i\,\phi^*_{o^F_{k_i}}(\mathbf{r}_i)r_i\cos\vartheta_i\phi_{o^I_{k_i}}(\mathbf{r}_i) \\
&= - i\sum_{i=1}^{N_e}\langle\phi^F_i|\,\mathbf{q}\cdot\mathbf{r}\,|\phi^I_i\rangle
\end{aligned}
\tag{3.59}
$$

The first order of the interaction operator is analogous to a dipole transition matrix element, which is in general of the form $\mathbf{d}_{ij} = -\langle\phi_i|\,e\,\mathbf{r}\,|\phi_j\rangle$. Eq.3.59 shows that the electron transition amplitude in the first order is just the sum of the individual one electron transition amplitudes.

In this master thesis, the transition amplitude will be calculated in the non relativistic as well as in the relativistic regime.

The bound state and continuum one-electron wave functions used for the relativistic treatment are respectively

$$\phi_{n\kappa m}(\mathbf{r}) = \frac{1}{r}\begin{pmatrix} P_{n\kappa}(r)\Omega_{\kappa m}(\vartheta,\varphi) \\ iQ_{n\kappa}(r)\Omega_{-\kappa m}(\vartheta,\varphi)\end{pmatrix}, \qquad \phi_{\epsilon\kappa m}(\mathbf{r}) = \frac{1}{r}\begin{pmatrix} P_{\epsilon\kappa}(r)\Omega_{\kappa m}(\vartheta,\varphi) \\ iQ_{\epsilon\kappa}(r)\Omega_{-\kappa m}(\vartheta,\varphi)\end{pmatrix}, \tag{3.60}$$

where ϵ denotes the energy that the electron in the continuum is carrying and $\Omega_{\kappa m}$ are the spherical spinors described in chapter C and κ is the relativistic angular quantum number. The bound state one-electron wave functions in the nonrelativistic regime are of the form

$$\psi_{nlm}(\mathbf{r}) = R_{nl}(r)Y_{lm}(\vartheta,\varphi), \qquad \psi_{\epsilon lm}(x) = R_{\epsilon l}(\mathbf{r})Y_{lm}(\vartheta,\varphi). \tag{3.61}$$

In Eq. (3.59), we can rewrite $\cos\vartheta = \sqrt{\frac{4\pi}{3}}Y_{10}(\vartheta,\varphi)$. Hence, the electron transition amplitude combining Eq. (3.60) and Eq. (3.59) for single electron ionization is

$$\begin{aligned} Z^{n\kappa m}_{\epsilon\kappa' m'}(\mathbf{q}_e) =& -iq_e \int dr\, r \times [P_{\epsilon\kappa'}(r)P_{n\kappa}(r) + Q_{\epsilon\kappa'}(r)Q_{n\kappa}(r)] \\ & \times \sqrt{\frac{4\pi}{3}} \int dS\, \Omega^{\dagger}_{\kappa' m'}(\vartheta,\varphi)Y_{10}(\vartheta,\varphi)\Omega_{\kappa m}(\vartheta,\varphi), \end{aligned} \tag{3.62}$$

where $dS = d\varphi d\cos\vartheta$ denotes the integrand over the sphere with unit radius. The one electron wave functions of the form (3.61) lead to a transition amplitude for single electron ionization of the form

$$Z^{nlm}_{\epsilon l' m'}(\mathbf{q}_e) = -iq_e \int dr r^3 R^*_{\epsilon l'}(r)R_{nl}(r) \times \sqrt{\frac{4\pi}{3}} \int dS\, Y^*_{l'm'}(\vartheta,\varphi)Y_{10}(\vartheta,\varphi)Y_{lm}(\vartheta,\varphi). \tag{3.63}$$

Now the selection rules arise from the angular integral of the transition amplitudes.

In the dipole approximation, the selection rules of the transition amplitudes arise in the non relativistic as well as in the relativistic case from the angular integral of the form $\int dS\, Y_{l'm'}(\vartheta_i,\varphi_i)\cos\vartheta_i Y_{lm}$. These expressions can be rewritten by the use of

$$\begin{aligned} \cos\vartheta Y_{l,m}(\vartheta,\varphi) =& \sqrt{\frac{(l-m+1)(l+m+1)}{(2l+1)(2l+3)}}Y_{l+1,m}(\vartheta,\varphi) \\ & + \sqrt{\frac{(l-m)(l+m)}{(2l-1)(2l+1)}}Y_{l-1,m}(\vartheta,\varphi). \end{aligned} \tag{3.64}$$

Hence, this expression together with the orthonormality conditions of the spherical harmonics yield

$$\sqrt{\frac{4\pi}{3}}\int dS\,\Omega^{\dagger}_{\kappa' m'}(\vartheta,\varphi)Y_{10}(\vartheta,\varphi)\Omega_{\kappa m}(\vartheta,\varphi) = \sqrt{\frac{(l-m+1)(l+m+1)}{(2l+1)(2l+3)}}\delta_{l',l+1}\delta_{m',m} + \sqrt{\frac{(l-m)(l+m)}{(2l-1)(2l+1)}}\delta_{l',l-1}\delta_{m',m}, \tag{3.65}$$

such that only transitions with $\Delta l = 1$ contribute in the dipole approximation. The formula in Eq. (3.64) can be used several times to obtain all the nonzero transitions to a certain order L.

3.3.2 Higher order transitions

To generalize the formula

$$\langle\psi^F|e^{i\sum_i \mathbf{q}_e\cdot\mathbf{r}_i}|\psi^I\rangle = \int \frac{\epsilon^{k_1,k_2,\ldots,k_{N_e}}\epsilon_{m_1,m_2,\ldots,m_{N_e}}}{N_e!}\frac{(-i)^L q_e^L}{L!} \times \prod_{i=1}^{N_e} d^3r_i\phi^*_{o^F_{m_i}}(\mathbf{r}_i)\left(r_1\cos\vartheta_1+\ldots+r_{N_e}\cos\vartheta_{N_e}\right)^L\phi_{o^I_{k_i}}(\mathbf{r}_i), \tag{3.66}$$

we note that the formula involves a multinomial expansion of the form

$$\left(\sum_{i=1}^{N_e} y_i\right)^L = \sum_{k_1+\ldots+k_{N_e}=L}\frac{L!}{k_1!k_2!\ldots k_{N_e}!}y_1^{k_1}\cdot y_2^{k_2}\cdot\ldots\cdot y_{N_e}^{k_{N_e}}. \tag{3.67}$$

This formula gets quite complicated for higher order transitions. To make further investigations, let's have a look at the next leading order ($L=2$). Therefore, we have

$$(r_1+r_2+\ldots+r_{N_e})^2 = \underbrace{\sum_{i=1}^{N_e} r_i^2\cos^2\vartheta_i}_{\text{(I)}} + \underbrace{\sum_{i,j}^{N_e} r_i\cos\vartheta_i r_j\cos\vartheta_j}_{\text{(II)}} \qquad \text{with}(i\neq j). \tag{3.68}$$

For the terms of the form (I) the mathematical procedure is basically the same as for the dipole transition, such that the terms of the form (I) reduce to the formula

$$\begin{aligned}\langle\psi^F|e^{i\sum_i \mathbf{q}_e\cdot\mathbf{r}_i}|\psi^I\rangle &= \frac{(-iq_e)^2}{2}\int\sum_{i=1}^{N_e} d^3r_i\,\phi^*_{o^F_{k_i}}(\mathbf{r}_i)r_i^2\cos^2\vartheta_i\phi_{o^I_{k_i}}(\mathbf{r}_i)\\ &= \frac{(-iq_e)^2}{2}\sum_{i=1}^{N_e}\langle\phi_i^F|\,r_i^2\cos^2\vartheta_i\,|\phi_i^I\rangle\,. \end{aligned}\tag{3.69}$$

For the mixing terms of the form (II), we have

$$
\begin{aligned}
\langle\psi^F|\sum_{\substack{i,j\\ i\neq j}} r_i\cos\vartheta_i r_j\cos\vartheta_j\,|\psi^I\rangle = &\frac{\epsilon^{k_1,k_2,\ldots,k_{N_e}}\epsilon_{m_1,m_2,\ldots,m_{N_e}}}{N_e!}\\
&\times 2\Bigg[\langle\phi_{o^F_{m_1}}|\,r_1\cos\vartheta_1\,|\phi_{o^I_{k_1}}\rangle\,\langle\phi_{o^F_{m_2}}|\,r_2\cos\vartheta_2\,|\phi_{o^I_{k_2}}\rangle\,\delta_{k_3,m_3}\ldots\delta_{k_{N_e},m_{N_e}}\\
&+\langle\phi_{o^F_{m_1}}|\,r_1\cos\vartheta_1\,|\phi_{o^I_{k_1}}\rangle\,\langle\phi_{o^F_{m_3}}|\,r_3\cos\vartheta_3\,|\phi_{o^I_{k_3}}\rangle\,\delta_{k_2,m_2}\delta_{k_4,m_4}\ldots\delta_{k_{N_e},m_{N_e}}\\
&\ldots\\
&+\langle\phi_{o^F_{m_{N_e}}}|\,r_{N_e}\cos\vartheta_{N_e}\,|\phi_{o^I_{k_{N_e}}}\rangle\,\langle\phi_{o^F_{m_{N_e-1}}}|\,r_{N_e-1}\cos\vartheta_{N_e-1}\,|\phi_{o^I_{k_{N_e-1}}}\rangle\,\delta_{k_1,m_1}\delta_{k_2,m_2}\ldots\delta_{k_{N_e-2},m_{N_e-2}}\Bigg].
\end{aligned}
\tag{3.70}
$$

Since we have N_e electrons, we have a summation over $\frac{N_e(N_e-1)}{2}$ terms of that kind. We note that every term has two epsilon tensors, which differ only in two indices. Through cyclic permutations these epsilon tensors are all of the form

$$
\epsilon^{a_1,a_2,\ldots,a_{N_e}}\epsilon_{b_1,b_2,a_3,\ldots,a_{N_e}} = (N_e-2)!\delta^{a_1a_2}_{b_1b_2}, \tag{3.71}
$$

where $\delta^{a_1\ldots a_n}_{b_1\ldots b_n}$ is the generalized Kronecker delta and is defined as

$$
\delta^{a_1\ldots a_n}_{b_1\ldots b_n} = \begin{vmatrix} \delta^{a_1}_{b_1} & \ldots & \delta^{a_1}_{b_n}\\ \vdots & \ddots & \vdots\\ \delta^{a_n}_{b_1} & \ldots & \delta^{a_n}_{b_n}\end{vmatrix}, \tag{3.72}
$$

which reduces in our case to the simple form $\delta^{a_1a_2}_{b_1b_2} = \delta^{a_1}_{b_1}\delta^{a_2}_{b_2} - \delta^{a_1}_{b_2}\delta^{a_2}_{b_1}$. Now we can rewrite Eq. (3.70) in the form

$$
\begin{aligned}
\langle\psi^F|\sum_{\substack{i,j\\ i\neq j}} r_i\cos\vartheta_i r_j\cos\vartheta_j\,|\psi^I\rangle = &\frac{1}{N_e(N_e-1)}\\
&\times\Bigg[(\delta^{k_1}_{m_1}\delta^{k_2}_{m_2}-\delta^{k_1}_{m_2}\delta^{k_2}_{m_1})\,\langle\phi_{o^F_{m_1}}|\,r_1\cos\vartheta_1\,|\phi_{o^I_{k_1}}\rangle\,\langle\phi_{o^F_{m_2}}|\,r_2\cos\vartheta_2\,|\phi_{o^I_{k_2}}\rangle\\
&+(\delta^{k_1}_{m_1}\delta^{k_3}_{m_3}-\delta^{k_1}_{m_3}\delta^{k_3}_{m_1})\,\langle\phi_{o^F_{m_1}}|\,r_1\cos\vartheta_1\,|\phi_{o^I_{k_1}}\rangle\,\langle\phi_{o^F_{m_3}}|\,r_3\cos\vartheta_3\,|\phi_{o^I_{k_3}}\rangle\\
&\ldots\\
&+(\delta^{k_{N_e}}_{m_{N_e}}\delta^{k_{N_e-1}}_{m_{N_e-1}}-\delta^{k_{N_e}}_{m_{N_e-1}}\delta^{k_{N_e-1}}_{m_{N_e}})\,\langle\phi_{o^F_{m_{N_e}}}|\,r_{N_e}\cos\vartheta_{N_e}\,|\phi_{o^I_{k_{N_e}}}\rangle\,\langle\phi_{o^F_{m_{N_e-1}}}|\,r_{N_e-1}\cos\vartheta_{N_e-1}\,|\phi_{o^I_{k_{N_e-1}}}\rangle\Bigg].
\end{aligned}
\tag{3.73}
$$

Let's have a closer look on the second line of Eq. (3.73)

$$
\begin{aligned}
&(\delta^{k_1}_{m_1}\delta^{k_2}_{m_2} - \delta^{k_1}_{m_2}\delta^{k_2}_{m_1}) \langle \phi_{o^F_{m_1}} | \, r_1 \cos\vartheta_1 \, | \phi_{o^I_{k_1}} \rangle \langle \phi_{o^F_{m_2}} | \, r_2 \cos\vartheta_2 \, | \phi_{o^I_{k_2}} \rangle = \\
&\qquad \langle \phi_{o^F_{k_1}} | \, r_1 \cos\vartheta_1 \, | \phi_{o^I_{k_1}} \rangle \langle \phi_{o^F_{k_2}} | \, r_2 \cos\vartheta_2 \, | \phi_{o^I_{k_2}} \rangle - \langle \phi_{o^F_{k_2}} | \, r_1 \cos\vartheta_1 \, | \phi_{o^I_{k_1}} \rangle \langle \phi_{o^F_{k_1}} | \, r_2 \cos\vartheta_2 \, | \phi_{o^I_{k_2}} \rangle \, .
\end{aligned}
\tag{3.74}
$$

The phase space of all possible final states o_F is infinitely large, since the spectrum of the final state wave functions is continuous. The selection rules that arise out of the angular part of the transition amplitude only reduces the number of allowed final state quantum numbers. The mixing terms are summations over antisymmetric permutations of products of transition matrix elements between an initial orbital o^I and a final orbital o^F. In section 3.3.3, we will see that the transition matrix element doesn't depend on the magnetic quantum numbers m and m'.

Consider a noble gas atom, then the number of electrons for every pair of principal quantum numbers n and orbital quantum number l or κ is even. Since the transition amplitude doesn't depend on the magnetic quantum numbers, all the mixing terms cancel out in the antisymmetric permutation, such that the only remaining terms are of the form

$$
\begin{aligned}
\langle \psi^F | e^{i\sum_i \mathbf{q}_e\cdot\mathbf{r}_i} | \psi^I \rangle \simeq \int & \frac{\epsilon^{k_1,k_2,\ldots,k_{N_e}} \epsilon_{m_1,m_2,\ldots,m_{N_e}}}{N_e!} \frac{(-iq_e)^L}{L!} \\
& \times \prod_{i=1}^{N_e} d^3 r_i \phi^*_{o^F_{m_i}}(\mathbf{r}_i) \left(r_1^L \cos^L\vartheta_1 + \ldots + r_{N_e}^L \cos^L \vartheta_{N_e} \right) \phi_{o^I_{k_i}}(\mathbf{r}_i),
\end{aligned}
\tag{3.75}
$$

which reduces to the simple formula

$$
\begin{aligned}
\langle \psi^F | e^{i\sum_i \mathbf{q}_e\cdot\mathbf{r}_i} | \psi^I \rangle &\simeq \frac{(-iq_e)^L}{L!} \int \sum_{i=1}^{N_e} d^3 r_i \, \phi^*_{o^F_{k_i}}(\mathbf{r}_i) r_i^L \cos^L \vartheta_i \phi_{o^I_{k_i}}(\mathbf{r}_i) \\
&= \frac{(-iq_e)^L}{L!} \sum_{i=1}^{N_e} \langle \phi^F_i | \, r_i^L \cos^L \vartheta_i \, | \phi^I_i \rangle \, .
\end{aligned}
\tag{3.76}
$$

In general all atoms, for which there exist only even numbers of electrons for a given principal quantum number n and angular momentum quantum number l or κ, the formula holds. In the next section, we will find a more comprehensive approach to calculate the matrix elements via the Wigner-Eckhart theorem.

3.3.3 The Wigner Eckhart theorem

In this section, we will make use of the Wigner Eckhart theorem to simplify the calculation of the electron transition amplitude. The interaction operator in the transition matrix element

$e^{-i\mathbf{q}_e\cdot\mathbf{r}}$ can be expanded in the form [38]

$$e^{-i\mathbf{q_e}\cdot\mathbf{r}} = \sum_{L=0}^{\infty}(-i)^L j_L(q_e r)(2L+1)P_L(\cos\vartheta), \tag{3.77}$$

where $P_L(\cos\vartheta)$ are the Legendre polynomials. The form of the transition operator makes it possible to apply the Wigner Eckhart theorem and will be formulated for non relativistic and relativistic descriptions respectively.

Non relativistic transition

According to the Wigner-Eckhart theorem, we consider matrix elements of the irreducible tensor operator

$$C_{LM} = \sqrt{\frac{4\pi}{2L+1}}Y_{LM}(\vartheta,\varphi) \tag{3.78}$$

to calculate the transition matrix elements. The Legendre polynomial of Eq. (3.77) can now be rewritten in terms of $P_L(\cos\vartheta) = \sqrt{\frac{4\pi}{2L+1}}Y_{L0}(\vartheta,\varphi) = C_{L0}$. Now the transition amplitude involves matrix elements of the form

$$\begin{aligned}\langle\epsilon l'm'|\, e^{-i\mathbf{q}_e\cdot\mathbf{r}}\,|nlm\rangle &= \sum_{L=0}^{\infty}\langle\epsilon l'm'|\,(2L+1)(-i)^L j_L(q_e r)C_{L0}\,|nlm\rangle \\ &= \sum_{L=0}^{\infty}(-i)^L(2L+1)\int drr^2 R^*_{\epsilon l}(r)j_L(q_e r)R_{nl}(r)\,\langle l'm'|\,C_{L0}\,|lm\rangle\,, \end{aligned} \tag{3.79}$$

which can be evaluated by the use of the Wigner Eckhart theorem

$$\langle l'm'|\,C_{L0}\,|lm\rangle = (-1)^{l'-m'}\begin{pmatrix} l' & L & l \\ -m' & 0 & m\end{pmatrix}\langle l'|\,|C_L|\,|l\rangle\,, \tag{3.80}$$

where $\langle l'|\,|C_L|\,|l\rangle$ is the reduced matrix element and $\begin{pmatrix} l_1 & l_2 & l_3 \\ m_1 & m_2 & m_3\end{pmatrix}$ is the Wigner 3j-symbol. To determine the reduced matrix element, we expand the product of the two spherical harmonics into

$$Y_{L0}(\vartheta,\varphi)Y_{lm}(\vartheta,\varphi) = \sum_{kq}A_{kq}Y_{kq}(\vartheta,\varphi). \tag{3.81}$$

The expansion coefficient A_{kq} is deduced from Eq. (3.80)

$$A_{kq} = \sqrt{\frac{2L+1}{4\pi}}(-1)^{k-q}\begin{pmatrix} k' & L & l \\ -q' & 0 & m\end{pmatrix}\langle k|\,|C_L|\,|l\rangle\,. \tag{3.82}$$

The Wigner 3j-symbols follow the orthogonality relation

$$\sum_{m_1,m_2} \begin{pmatrix} l_1 & l_2 & l_3 \\ m_1 & m_2 & m_3 \end{pmatrix} \begin{pmatrix} l_1 & l_2 & l_3' \\ m_1 & m_2 & m_3' \end{pmatrix} = \frac{1}{2l_3+1}\delta_{l_3 l_3'}\delta_{m_3 m_3'}, \tag{3.83}$$

such that we can invert Eq. (3.82)

$$\begin{aligned} &\sum_m \begin{pmatrix} l' & L & l \\ -m' & 0 & m \end{pmatrix} Y_{LM}(\vartheta,\varphi)Y_{lm}(\vartheta,\varphi) = \\ &\quad = \sum_m \begin{pmatrix} l' & L & l \\ -m' & 0 & m \end{pmatrix} \begin{pmatrix} k & L & l \\ q & 0 & m \end{pmatrix} \sqrt{\frac{2L+1}{4\pi}}(-1)^{k-q}\langle k| \, |C_L| \, |l\rangle \, Y_{kq}(\vartheta,\varphi) \\ &\quad = \frac{(-1)^{l-m}}{2l+1}\sqrt{\frac{2L+1}{4\pi}} \langle l| \, |C_L| \, |l\rangle \, Y_{lm}(\vartheta,\varphi). \end{aligned} \tag{3.84}$$

For $\vartheta = 0$ the spherical harmonics are $Y_{lm}(\vartheta=0,\varphi) = \sqrt{\frac{2l+1}{4\pi}}\delta_{m0}$. Now we can calculate the reduced matrix element by evaluating both sides of Eq. (3.84) for $\vartheta = 0$ to obtain

$$\langle l'| \, |C_L| \, |l\rangle = (-1)^{l'}\sqrt{(2l'+1)(2l+1)} \begin{pmatrix} l' & L & l \\ 0 & 0 & 0 \end{pmatrix}. \tag{3.85}$$

The matrix element of Eq. (D.5) becomes

$$\langle l'm'| \, C_{L0} \, |lm\rangle = (-1)^{-m'}\sqrt{(2l'+1)(2l+1)} \begin{pmatrix} l' & L & l \\ -m' & 0 & m \end{pmatrix} \begin{pmatrix} l' & L & l \\ 0 & 0 & 0 \end{pmatrix} \tag{3.86}$$

The quantity of interest is now Eq. (3.79) squared, such that we arrive at the result

$$\begin{aligned} \sum_{mm'} \left| Z^{nlm}_{\epsilon l'm'}(\mathbf{q}_e) \right|^2 &= \sum_{mm'} | \langle \epsilon l'm' | \, e^{-i\mathbf{q}_e\cdot\mathbf{r}} \, |nlm\rangle \, |^2 \\ &= \sum_{L=0}^{\infty} (2L+1)^2 \left| \int drr^2 R^*_{\epsilon l}(r) j_L(q_e r) R_{nl}(r) \right|^2 (2l+1)(2l'+1) \\ &\quad \times \sum_{m,m'} \begin{pmatrix} l' & L & l \\ -m' & 0 & m \end{pmatrix}^2 \begin{pmatrix} l' & L & l \\ 0 & 0 & 0 \end{pmatrix}^2 \\ &= \sum_{L=0}^{\infty} \left| \int drr^2 R^*_{\epsilon l}(r) j_L(q_e r) R_{nl}(r) \right|^2 \\ &\quad \times (2L+1)(2l+1)(2l'+1) \begin{pmatrix} l' & L & l \\ 0 & 0 & 0 \end{pmatrix}^2. \end{aligned} \tag{3.87}$$

Relativistic transition

In the case of spherical spinors with relativistic angular momentum quantum number κ, we make use of the irreducible spherical tensor operator

$$T_{LM} = 4\pi(-i)^L j_L(q_e r) Y_{LM}(\vartheta_q, \varphi_q) Y_{LM}(\vartheta_r, \varphi_r), \tag{3.88}$$

such that we can rewrite the exponential operator in terms of (3.88) by

$$e^{-i\mathbf{q}_e\cdot\mathbf{r}} = \sum_{L=0}^{\infty} \sum_{M=-L}^{L} T_{LM}. \tag{3.89}$$

We apply the Wigner Eckhart theorem and get

$$\langle \epsilon\kappa' m'| T_{LM} |n\kappa m\rangle = (-1)^{j'-m'} \begin{pmatrix} j' & L & j \\ -m' & M & m \end{pmatrix} \langle \epsilon\kappa'| |T_L| |n\kappa\rangle , \tag{3.90}$$

where $\langle \epsilon\kappa'| T_{LM} |n\kappa\rangle$ is the reduced matrix element. The transition element is reduced to a summation over reduced matrix elements, which are independent of the magnetic quantum numbers. Evaluating both sides of (3.90) for $m' = m = \frac{1}{2}$ and $M = 0$ determines the reduced matrix element $\langle \epsilon\kappa'| |T_L| |n\kappa\rangle$. Making use of the orthogonality relation of the Wigner-3j symbols gives

$$\begin{aligned}
&\sum_{m,m'} |Z^{n\kappa m}_{\epsilon\kappa' m'}(\mathbf{q}_e)|^2 = \sum_{m,m'} \sum_{L,M} | \langle \epsilon\kappa' m'| T_{LM} |n\kappa m\rangle |^2 = \\
&\quad \sum_{L=0}^{\infty} (2L+1)(-1)^{j'+j-l'-l} \left| \int dr j_L(q_e r) \left[P^*_{\epsilon\kappa'} P_{n\kappa'}(r) + Q^*_{\epsilon\kappa'} Q_{n\kappa'}(r)\right] \right|^2 \begin{pmatrix} j' & L & j \\ -\frac{1}{2} & 0 & \frac{1}{2} \end{pmatrix}^{-2} \begin{pmatrix} l' & L & l \\ 0 & 0 & 0 \end{pmatrix}^2 \\
&\quad \times \left[\frac{1}{4}(-1)^{j'+j-l'-l}(2j'+1)(2j+1) \begin{pmatrix} l' & L & l \\ 0 & 0 & 0 \end{pmatrix}^2 + 2\sqrt{l'(l'+1)l(l+1)} \begin{pmatrix} l' & L & l \\ 0 & 0 & 0 \end{pmatrix} \begin{pmatrix} l' & L & l \\ -1 & 0 & 1 \end{pmatrix} \right. \\
&\quad \left. - (\kappa'+1)(\kappa+1) \begin{pmatrix} l' & L & l \\ -1 & 0 & 1 \end{pmatrix}^2 \right].
\end{aligned} \tag{3.91}$$

3.4 Migdal effect - Dark Matter event rate

The basic quantity of interest for the Migdal effect is the DM differential event rate with respect to the energy of the ionized electron ϵ

$$\frac{dR}{d\epsilon} = N_T \frac{d\sigma}{d\epsilon} \frac{\rho_\chi}{m_\chi} v, \tag{3.92}$$

where ρ_χ is the local dark matter density, which can only be estimated by different models [39] and v is the dark matter velocity. The differential cross section with respect to the ionized electron is

$$\frac{d\sigma}{d\epsilon} = \int_{E_{R_{\min}}}^{E_{R_{\max}}} dE_R \frac{d\sigma}{dE_R d\epsilon}. \tag{3.93}$$

The differential cross section can be estimated $\frac{d\sigma}{dE_R d\epsilon} \simeq \frac{d\sigma}{dE_R}\frac{2}{\pi}\frac{dp}{d\epsilon}(nl \to \epsilon)$ in the first order of inelastic scattering, such that

$$\frac{d\sigma}{d\epsilon} = \int_{E_{R_{\min}}}^{E_{R_{\max}}} dE_R \frac{d\sigma}{dE_R}\frac{2}{\pi}\frac{dp}{d\epsilon}(nl \to \epsilon). \tag{3.94}$$

From nonrelativistic kinematics, we get the cross section with respect to the nuclear recoil energy $\frac{d\sigma}{dE_R}$ as

$$\frac{d\sigma}{dE_R} = \frac{1}{2}\frac{m_A}{\mu_N^2 v^2}\sigma(q_A)\left|\mathcal{F}(q_A)\right|^2, \tag{3.95}$$

such that the differential event rate with respect to the ionized electron energy is

$$\frac{dR}{d\epsilon} = N_T \frac{\rho_\chi m_A}{\pi m_\chi \mu_N^2 v}\int_{E_{R_{\min}}}^{E_{R_{\max}}} dE_R\, \sigma(q_A)\left|\mathcal{F}(q_A)\right|^2 |Z_{FI}(\mathbf{q}_e)|^2. \tag{3.96}$$

The relation between the momenta q_e and q_A is well approximated by

$$q_e \simeq \frac{m_e}{m_A} q_A. \tag{3.97}$$

Now we approximate the cross section to be constant in the sense of $\sigma(q_A) \simeq \sigma$ and assume $g_p = g_n$, such that we can express the cross section in terms of the nucleon-dark matter cross section, which is defined by $\sigma = A^2\frac{\mu_N^2}{\mu_n^2}\sigma_n$. Because of the non relativistic kinematics of dark matter, the recoil energy is defined by $E_R = \frac{q_A^2}{2m_A}$, such that we can write

$$\frac{dR}{d\epsilon} = N_T \frac{\rho_\chi m_A}{\pi m_\chi \mu_N^2 v} A^2 \frac{\mu_N^2}{\mu_n^2}\sigma_n \int_{E_{R_{\min}}}^{E_{R_{\max}}} dE_R\, \left|\mathcal{F}(E_R)\right|^2 |Z_{FI}(E_R)|^2. \tag{3.98}$$

Because of the dynamics of the dark matter particles in the galactic halo, we have to take an additional velocity average such that the differential event rate becomes

$$\left\langle \frac{dR}{d\epsilon} \right\rangle = N_T \frac{\rho_\chi m_A}{m_\chi \mu_N^2 \pi} A^2 \frac{\mu_N^2}{\mu_n^2}\sigma_n \int_{v_{\min}}^{v_{\max}} d^3v \frac{f(v, v_{obs})}{v}\int_{E_R^{\min}}^{E_R^{\max}} dE_R \left|\mathcal{F}(E_R)\right|^2 |Z_{FI}(E_R)|^2 \tag{3.99}$$

The maximum and minimum recoil energy of the inelastic process is given by Eq. (3.31) where $\Delta E = \epsilon + E_{nl}$ and ϵ is the energy of the ionized electron and E_{nl} is the binding energy of the ionized/excited electron. After performing the integral over the recoil energies, we have to take further investigation on the integral over the dark matter velocities. The minimum velocity of dark matter is constrained by

$$v_\chi^{(\mathrm{min})} \simeq \frac{m_A E_R + \mu_N \Delta E}{\mu_N \sqrt{2 m_A E_R}}, \tag{3.100}$$

such that it is necessary to find it's minimum with respect to the recoil energy to find the integration area over the dark matter velocities. The minimum is given by $E_R = \frac{\mu_N \Delta E}{m_N}$, which gives a dark matter minimum velocity of $v_{min} = \sqrt{\frac{2\Delta E}{\mu_N}}$.

Chapter 4

Migdal effect: Atomic physics code evaluation

4.1 Flexible Atomic Code

For the calculation of the Migdal effect, we adopt the radial and continuum wave functions from the flexible atomic code (FAC), which is an open source software package for the calculation of various atomic processes [40]. The program uses a fully relativistic Hartree Fock approach in self consistent field theory, which is more detailed in Appendix B.1. The atomic state wave functions are given by the so called configuration state functions Φ_ν

$$\psi = \sum_\nu b_\nu \Phi_\nu, \tag{4.1}$$

where b_ν are the mixing coefficients, which are calculated in the diagonalization process of the Hamiltonian [40]. The basis sets Φ_ν are an antisymmetric sum of products of N_e one electron Dirac spinors $\phi_{n\kappa m}$

$$\phi_{n\kappa m}(\mathbf{r}) = \frac{1}{r}\begin{pmatrix} P_{n\kappa}(r)\Omega_{\kappa m}(\theta,\varphi) \\ iQ_{n\kappa}(r)\Omega_{-\kappa m}(\theta,\varphi) \end{pmatrix}, \tag{4.2}$$

where $\Omega_{\kappa m}$ are spherical spinors, described in Appendix C. The bound one electron wave functions are characterized by the the orbital quantum numbers $o = \{n, \kappa, m\}$, where n is the principle quantum number, κ is the relativistic angular momentum and m the magnetic quantum number. The continuum wave functions are determined by the quantum numbers $o = \{\epsilon, \kappa, m\}$, where ϵ is the energy of the electron.

The one electron Dirac orbitals are normalized as

$$\sum_{\alpha=1}^{4} \int d^3r \, \phi_o(\mathbf{r})^{\alpha *} \phi_{o'}(\mathbf{r})^{\alpha} = \begin{cases} \left(\frac{\pi}{2}\right) \delta(\epsilon - \epsilon')\delta_{\kappa\kappa'}\delta_{mm'} & \text{(continuum states)} \\ \delta_{nn'}\delta_{\kappa\kappa'}\delta_{mm'} & \text{(bound states)} \end{cases} \tag{4.3}$$

Hence, the probabilities for the ionization processes are defined by

$$\frac{2}{\pi}\frac{dP}{d\epsilon}(\text{n,l} \to \epsilon) = \frac{2}{\pi}\frac{\omega_{nl}}{\omega_{\max}} \sum_{\kappa,\kappa',m,m'} |Z^{n\kappa m}_{\epsilon\kappa' m'}(\mathbf{q}_e)|^2 \,, \tag{4.4}$$

where ω_{nl} is the occupation number and $\omega_{\max}$ is the maximum occupation number and the electron transition amplitude squared is given by Eq. 3.91.

4.2 Dipole transition

First, we want to calculate the ionization probabilities in the dipole approximation of the transition operator, where the transition matrix elements are of the form

$$\langle\phi^F_j|\, e^{-i\mathbf{q}_e\cdot\mathbf{r}} \,|\phi^I_i\rangle \simeq -i \,\langle\phi^F_j|\, \mathbf{q}_e \cdot \mathbf{r} \,|\phi^I_i\rangle = \frac{i}{e}\mathbf{q}_e \cdot \mathbf{d}_{ij}, \tag{4.5}$$

where $\mathbf{d}_{ij} = -e\,\langle\phi^F_j|\,\mathbf{r}\,|\phi^I_i\rangle$ is the dipole transition moment. This corresponds to Eq. 3.91, where $L = 1$ is fixed. For a momentum transfer smaller than $\mathcal{O}(100\text{MeV})$, the factor $|\mathbf{q}_e \cdot \mathbf{r}| \ll 1$, such that the dipole approximation serves as a very comprehensive approach. In the dipole approximation only transitions with $\Delta l = 1$ and $\Delta m = 0$ are allowed. In Fig. 4.1 the probabilities in the dipole approximation are calculated for Xe,I,Ge and Ar with fixed momentum transfer q_e.

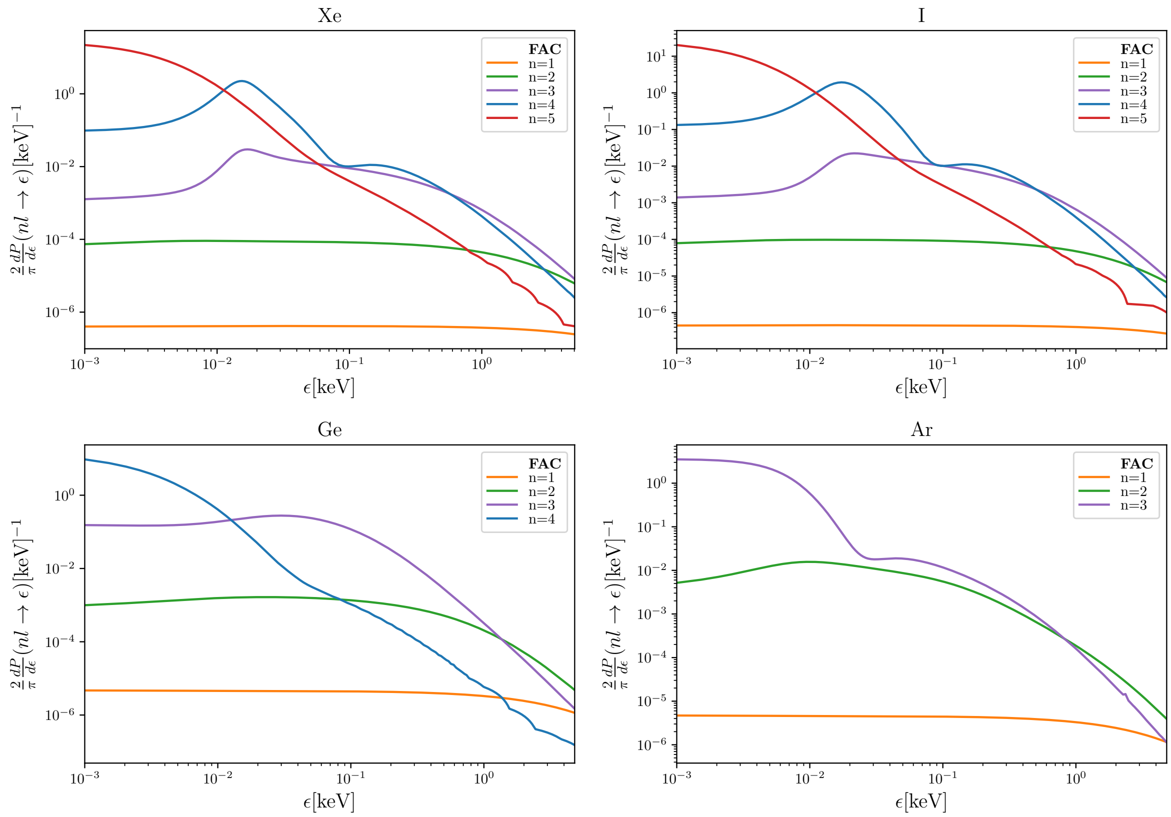

Figure 4.1: The curves show the ionization probabilities $\frac{dP}{d\epsilon}(nl \to \epsilon)$ in the dipole approximation for the shells of the isolated atoms Xe,I,Ge and Ar with respect to an electron momentum of $q_e = m_e \times 10^{-3}$. The results are in perfect agreement with Ibe et al. [35].

4.2.1 Higher order calculations

For higher order transitions, we make again use of Eq. 3.91. Now we want to further investigate the contributions from higher orders. Therefore we calculate the transition amplitude up to order $L = 5$ for Xenon and compare it to the results of the dipole approximation. The ionization probabilities are defined by Eq. 4.4. The ratio between the dipole approximation and the higher order calculation can be seen in Fig. 4.2.

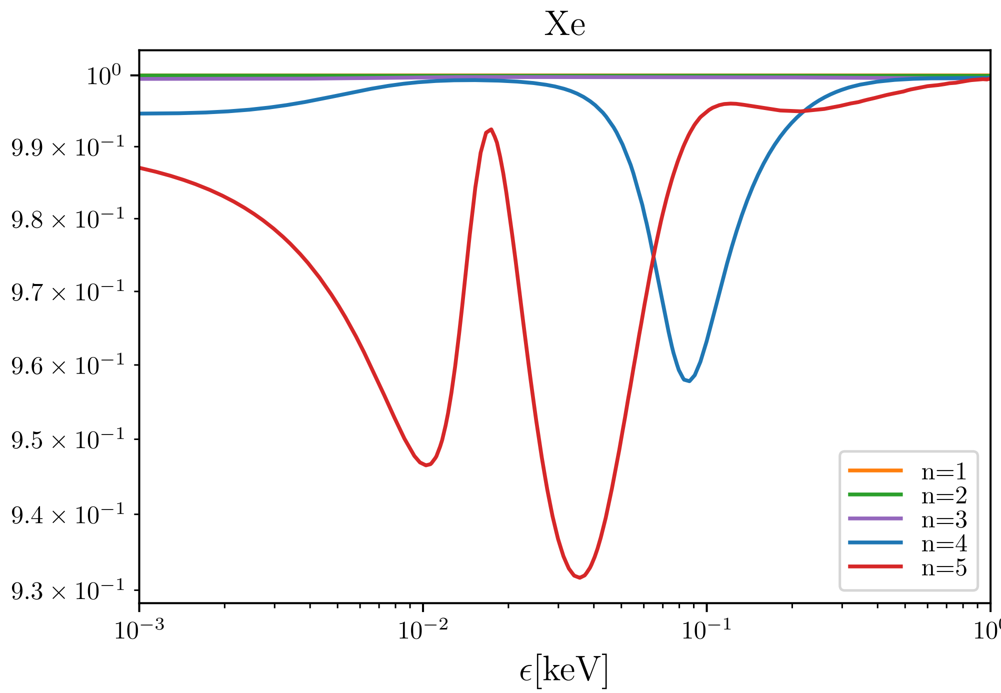

Figure 4.2: The plot shows the ratio between the dipole approximation and the higher order transition amplitude for $q_e = m_e \times 10^{-3}$.

We conclude, that the ionization probabilities in the dipole approximation are completely sufficient.

Chapter 5

Migdal effect: simplified descriptions

5.1 Choice of continuum wave functions

Calculating the Migdal effect with certain accuracy for isolated atoms depends on the choice of appropriate radial wave functions of bound and free electrons. There are numerous theoretical frameworks in self consistent field theory for the calculation of bound state wave functions. Now we want to try to simplify the result by approximating the continuum wave functions by analytic expressions and use tabulated bound state wave functions, such that it is possible to calculate probabilities within an analytic formula. The bound state wave functions were taken from Bunge et al. [41]. For the continuum wave functions, we will investigate three different types of continuum wave functions

- Spherical waves as solutions of the free Schrödinger equation
- Coulomb wave functions
- Plane waves

The Normalization for continuum wave functions can be found in Appendix D.

5.1.1 Radial solution of the Schrödinger equation - free particle

The wave function describing continuum states of a freely moving particle in the non relativistic scheme is defined by

$$\psi_{\mathbf{p}} = \mathcal{N} e^{i\mathbf{p}\cdot\mathbf{r}}, \tag{5.1}$$

where $\mathcal{N}$ is an appropriately chosen normalization and the momentum $\mathbf{p}$ and the kinetic energy ϵ of the free particle in the non-relativistic limit are related through $p = \sqrt{2m\epsilon}$. Since $\mathbf{p} = \hbar\mathbf{k}$, the wave number k and the momentum p are formally identical. The wave function of a free (continuum state) of a particle is in general of the form

$$\psi_{klm} = R_{kl} Y_{lm}(\vartheta, \varphi), \tag{5.2}$$

where the spherical harmonics arise as solution of the radial part of the Schrödinger equation [42]. The radial function is determined by solving the differential equation

$$\frac{\partial^2 R_{kl}}{\partial r^2} + \frac{2}{r}\frac{\partial R_{kl}}{\partial r} + \left[k^2 - \frac{l(l+1)}{r^2}\right] R_{kl} = 0. \tag{5.3}$$

Since wave functions with a continuous spectrum require certain normalization conditions we can choose a normalization. Usually one chooses a normalization with respect to the wavenumber k or the energy ϵ. We impose a normalization condition of the form

$$\int dV \;\psi_{\epsilon' l' m'} \psi_{\epsilon l m} = \delta_{mm'} \delta_{ll'} \left(\frac{\pi}{2}\right) \delta(\epsilon - \epsilon'), \tag{5.4}$$

where the radial wave functions $R_{\epsilon l}$ and R_{kl} are related by

$$R_{\epsilon l} = R_{kl} \sqrt{\frac{dk}{d\epsilon}} = \sqrt{\frac{m}{k}} R_{kl}. \tag{5.5}$$

Since the equation depends on the angular quantum number l, we can start to solve the differential equation for $l = 0$

$$\frac{\partial^2 r R_{k0}}{\partial r^2} + k^2 r R_{k0} = 0. \tag{5.6}$$

The solution that is finite at r=0 and normalized according to (5.4) is

$$R_{\epsilon 0} = \sqrt{\frac{m}{k}} \frac{\sin(kr)}{r}. \tag{5.7}$$

For a solution with $l \neq 0$, it is convenient to make a substitution of the form

$$R_{kl} = r^l \chi_{kl}, \tag{5.8}$$

such that we have a partial differential equation of the form

$$\chi''_{kl} + 2(l+1)\frac{\chi'_{kl}}{r} + k^2 \chi_{kl} = 0. \tag{5.9}$$

Differentiation with respect to r serves the equation

$$\chi'''_{kl} + \frac{2(l+1)}{r}\chi''_{kl} + \left[k^2 \chi_{kl} - \frac{l(l+1)}{r^2}\right] \chi'_{kl} = 0. \tag{5.10}$$

The ansatz $\chi_{kl} = r\chi_{k,l+1}$ leads to the equation

$$\chi''_{k,l+1} + \frac{2(l+2)}{r}\chi'_{k,l+1} + k^2\chi_{k,l+1} = 0, \tag{5.11}$$

which is the equation satisfied by $\chi_{k,l+1}$. Now we have found a recurrence relation, so that we obtain the result

$$\chi_{k,l} = \left(\frac{1}{r}\frac{\partial}{\partial r}\right)^l \chi_{k,0}, \tag{5.12}$$

where $\chi_{k,0} = R_{k,0}$. Thus the radial functions of a free moving particle are described by

$$\begin{aligned} R_{kl}(r) &= (-1)^l \frac{r^l}{k^l}\left(\frac{1}{r}\frac{d}{dr}\right)^l \frac{\sin(kr)}{r}, \\ R_{\epsilon l}(r) &= (-1)^l \sqrt{\frac{m}{k}}\frac{r^l}{k^l}\left(\frac{1}{r}\frac{d}{dr}\right)^l \frac{\sin(kr)}{r}, \end{aligned} \tag{5.13}$$

where the factor $(-1)^l$ depends comes from analyzing the differential of $sinc(x)$ function

$$\frac{d}{dr}\frac{\sin kr}{r} = -k\sin\left(kr - \frac{1}{2}\pi\right), \ldots, \frac{d}{dr}\frac{\sin kr}{r} = (-1)^l k\sin\left(kr - \frac{l}{2}\pi\right). \tag{5.14}$$

The radial wave functions can now be simplified by using the definition of the Bessel functions of half integral order

$$J_{l+1/2}(kr) = \frac{1}{\sqrt{\pi}}(-1)^l(2kr)^{l+1/2}\frac{d^l}{d(k^2r^2)^l}\frac{\sin(kr)}{kr}. \tag{5.15}$$

The radial wave functions can now be approximated in the form

$$\begin{aligned} R_{kl}(r) &= \sqrt{\frac{\pi k}{2r}}J_{l+1/2}(kr) = kj_l(kr), \\ R_{\epsilon l}(r) &= \sqrt{\frac{\pi m}{2r}}J_{l+1/2}(kr) = \sqrt{mk}j_l(kr). \end{aligned} \tag{5.16}$$

The solutions describe a free spherical wave with definite angular momentum l [42][43]. To make contact with the atomic code evaluation, we want to compare the solution of the free Schrödinger equation with the continuum wave functions from the Flexible Atomic code. In fig. (5.1) we can see that these wave functions coincide with the continuum wave functions from FAC.

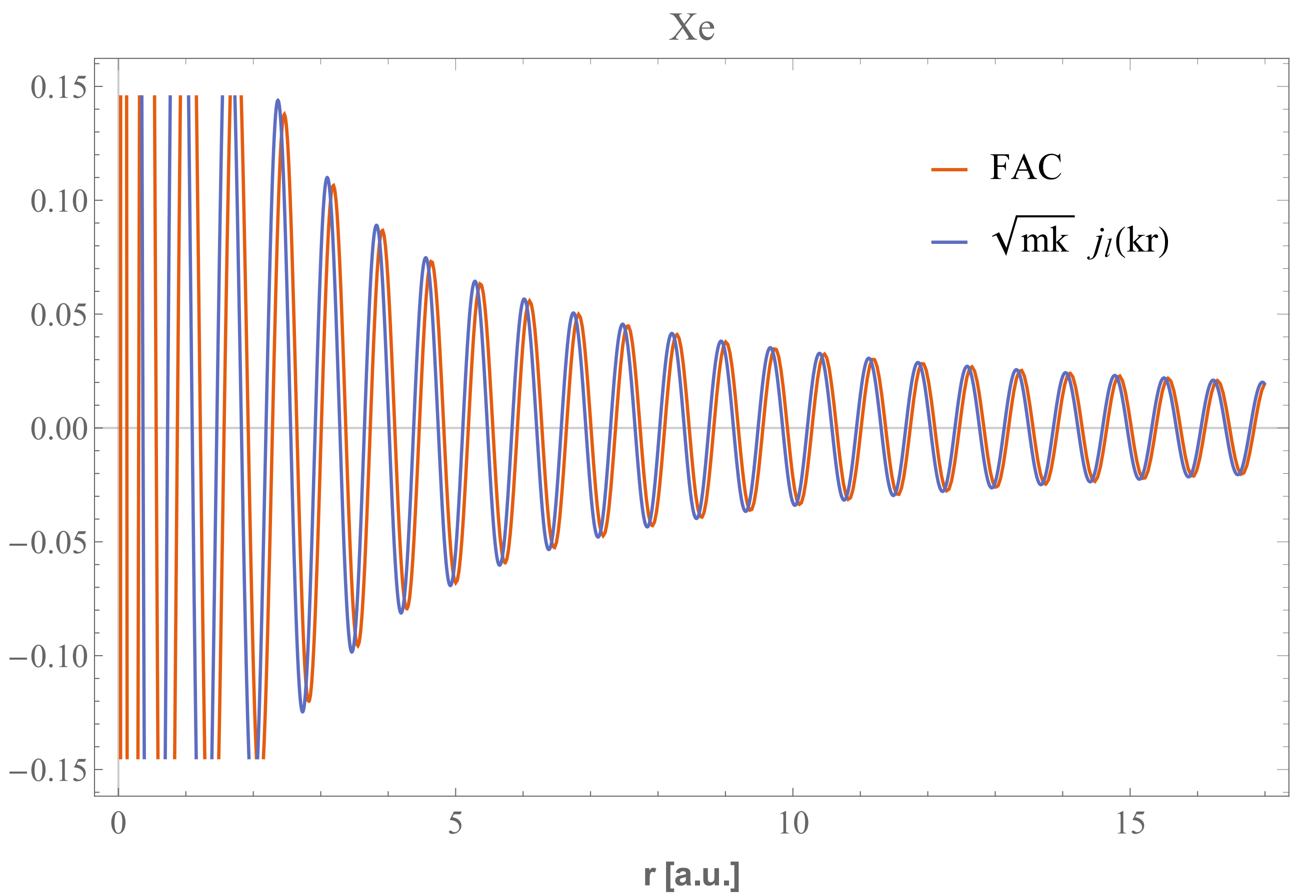

Figure 5.1: The plot shows the amplitude of a free spherical wave with angular momentum $l = 0$ and the corresponding numerical wave function from FAC with $\epsilon = 0.1\text{keV}$ in atomic units.

5.1.2 Coulomb wave functions

We have seen that the solution of the Schrödinger equation of a free particle can be solved to estimate the continuum wave functions of the final state. Now, a more sophisticated choice of the continuum wave functions can be done by calculating the Schrödinger equation with a Coulomb potential of the form

$$V(r) = -\frac{Z_{\text{eff}}}{r}. \tag{5.17}$$

The computation of the radial part of the continuum wave functions can be found in [44], where the radial part of the continuum wave functions is normalized on the "k-scale" in a way such that the radial part of the wave function has mass dimension zero. For our purpose I change the normalization condition to a normalization condition on the "ϵ-scale" and choose the normalization condition to be

$$\int drr^2 \tilde{R}^*_{\epsilon' l'}(r)\tilde{R}_{\epsilon l}(r) = \left(\frac{\pi}{2}\right)\delta(\epsilon - \epsilon')\delta_{ll'}. \tag{5.18}$$

The continuum wave functions on the "ϵ-scale" are then of the form

$$\begin{aligned}\tilde{R}_{\epsilon l}(r) =& \sqrt{km}(2kr)^l \frac{\left|\Gamma\left(l+1-\frac{iZ_{\text{eff}}}{ka_0}\right)\right| e^{\frac{\pi Z_{\text{eff}}}{2ka_0}}}{(2l+1)!} \\ &\times e^{-ikr}{}_1F_1\left(l+1+\frac{iZ_{\text{eff}}}{ka_0}, 2l+2, 2ikr\right).\end{aligned} \tag{5.19}$$

The effective charge is usually approximated by the following the steps in [45] or by Slater's rule. The effective charge is therefore given by

$$E_{nl} = 13.6\text{eV}\frac{Z^2_{\text{eff}}}{n^2}, \tag{5.20}$$

where E_{nl} is the binding energy of the bound state electron that gets ionized or excited. The binding energies for several atoms are tabulated in [46]. This approximation is a quite conservative approach for valence electrons, e.g. the effective charge for the valence electrons for Xenon yield respectively $Z^{\text{eff}}_{5s} = 6.21$ and $Z^{\text{eff}}_{5p} = 4.24$. For the calculation of the probability curves we assume for single electron ionization of a noble gas atoms, such as Xenon and Argon $Z_{\text{eff}} = 1$ for the valence electrons. For Sodium the effective charge for the valence electrons will be estimated by $Z_{\text{eff}} = 2$.

5.1.3 Plane wave ansatz

In general, a free particle moving in the $\mathbf{r}$-direction is described by a plane wave of the form $\phi = e^{i\mathbf{k}\cdot\mathbf{r}}$. The simplest approach of a free particle would therefore be a plane wave ansatz, where the normalization constant $\mathcal{N}$ is determined by the normalization condition

$$\int d^3r \phi^*_{\mathbf{k}'}(\mathbf{r})\phi_{\mathbf{k}}(\mathbf{r}) = \frac{\pi}{2}\delta(\epsilon - \epsilon'). \tag{5.21}$$

The direct calculation of the normalization constant can be seen in Appendix D.1 and leads to

$$\phi_\epsilon(\mathbf{r}) = \frac{\sqrt{km_e}}{4\pi}e^{i\mathbf{k}\cdot\mathbf{r}}. \tag{5.22}$$

This enables us to treat the Migdal effect like a Fourier transformation of the form

$$\tilde{\phi}_{nlm}(\mathbf{p}) = \int \phi_{nlm}(x)e^{-i\mathbf{p}\cdot\mathbf{r}}d^3r = \chi_{nl}(p)Y_{lm}(\vartheta_p, \varphi_p). \tag{5.23}$$

Strictly speaking the exponential operator of the plane wave ansatz is just a summation over all possible angular momenta of the spherical waves in the form

$$e^{i\mathbf{k}\cdot\mathbf{r}} = \frac{1}{\sqrt{km}} \sum_{L=0}^{\infty} i^L (2L+1) R_{\epsilon l}(r) P_L(\cos\vartheta) = \sqrt{\frac{4\pi}{km}} \sum_{L=0}^{\infty} i^L \sqrt{(2L+1)} R_{\epsilon l}(r) Y_{L0}(\vartheta, \varphi). \quad (5.24)$$

Therefore the sum over all possible angular momenta of the spherical waves leads exactly to the plane wave ansatz, such that we conclude that the the plane wave ansatz coincides with the solutions of the free Schrödinger equation by the summation over all angular momenta l. We expect that the calculation of the Migdal effects with plane waves should coincide with the multipole expansion of the calculation of the Migdal effects with spherical waves in higher orders.

5.2 Hartree Fock orbitals in self consistent field theory

For our simplified approach we take a set of non relativistic bound state orbitals from Bunge et al [41]. The wavefunction set consists out of a Slater-type basis set, where the coefficients are fitted. The wavefunctions can be compared to the P-function of the atomic physics code evaluation as it can be seen in Fig. 5.2. The radial wave functions of atomic orbitals R_{nl} are expanded as a superposition of primitive radial functions of the form

$$R_{nl}(r) = \sum_j C_{jnl} S_{jl}(r), \quad (5.25)$$

where the coefficients C_{jnl} and Z_{jl} were fitted and tabulated in [41] and the S_{jl} are a Slater-type orbital defined as

$$S_{jl}(r) = (a_0)^{-3/2} N_{jl} \left(\frac{r}{a_0}\right)^{n_{jl}-1} \exp\left(-Z_{jl}\frac{r}{a_0}\right), \quad (5.26)$$

where $a_0 = 0.268\text{keV}^{-1}$ is the Bohr radius, n_{jl} is the principle quantum number and Z_{jl} the orbital exponent corresponding to the orbital quantum number l. The N_{jl} is a normalization constant defined as

$$N_{jl} = \frac{(2Z_{jl})^{n_{jl}+1/2}}{[(2n_{jl})!]^{1/2}}. \quad (5.27)$$

In this chapter, we want to simplify the calculation of the Migdal effects by approximating continuum wave functions with simple analytic wave functions, with the same asymptotic behavior as the continuum wave functions from FAC. Therefore the difference of the two different approaches has to be examined. The bound state wave functions of the non relativistic and the relativistic approach are respectively of the form

$$\phi^{\mathrm{NR}}_{nlm}(\mathbf{r}) = R_{\epsilon l} Y_{lm}(\vartheta,\varphi), \qquad \phi_{n\kappa m}(\mathbf{r}) = \frac{1}{r}\begin{pmatrix} P_{n\kappa}(r)\Omega_{\kappa m}(\vartheta,\varphi) \\ iQ_{n\kappa}(r)\Omega_{-\kappa m}(\vartheta,\varphi)\end{pmatrix}, \tag{5.28}$$

where the relativistic angular momentum quantum number κ is related to the non relativistic angular momentum quantum number l by

$$l = |\kappa + 1/2| - 1/2. \tag{5.29}$$

In general, the dominant contribution in relativistic calculations of the Migdal effects comes from the "big component" $P(r)$ of the wave function, which makes up $> 99\%$ of the electron transition amplitude. Hence, we are able to compare both approaches by comparing the big radial component $P_{n\kappa}(r)$ from FAC with the radial component $R_{nl}(r)$. For every angular momentum quantum number l, we have two relativistic quantum numbers κ, such that there are two radial wave functions for each l, such that we have to average over the radial wave functions that belong to the same l. Fig. (5.2) compares the amplitudes of the radial wave functions for both approaches for a Xenon atom.

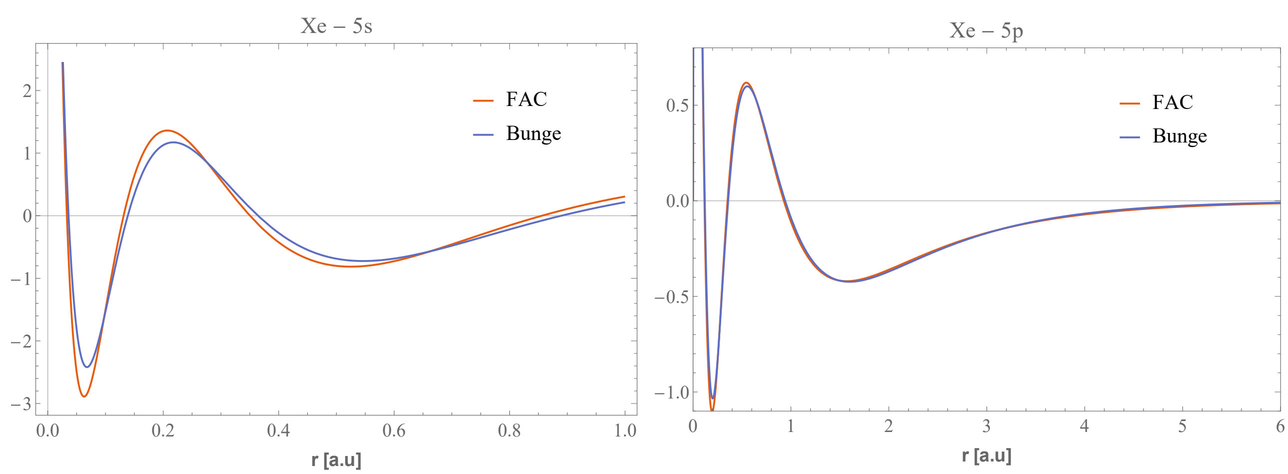

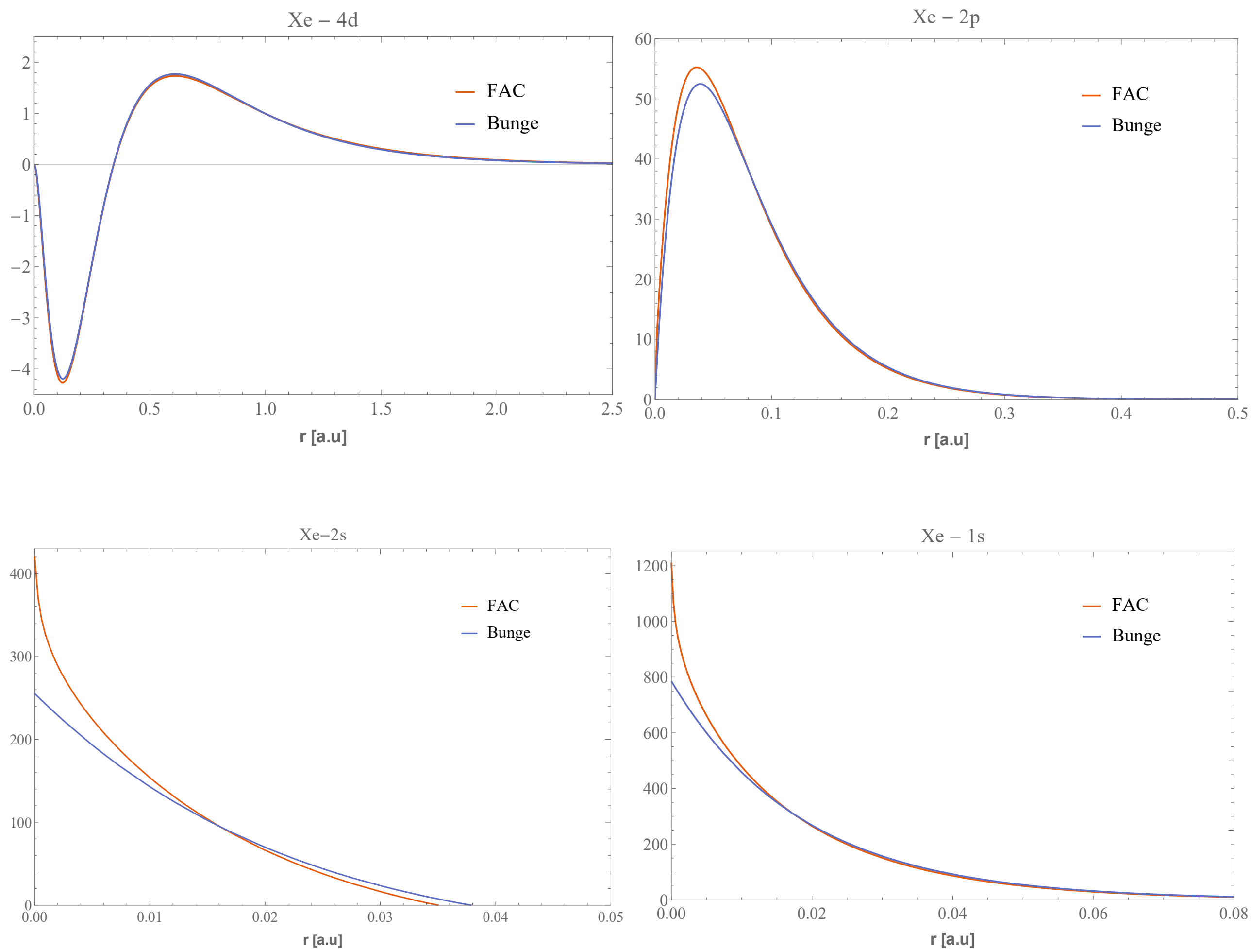

Figure 5.2: The plots show the amplitude of the Bunge bound state wave functions compared to the wave functions obtained from FAC in atomic units.

In fig. (5.2), we can see that the wave functions are in very good accordance, except for the s-orbitals of the principal quantum numbers $n = 1$ and $n = 2$. The amplitude of the $1s$ orbital of the wave functions of Bunge at al. ([41]) is several orders of magnitude smaller than the radial wave function from FAC, such that we expect a discrepancy between the transition amplitudes of the inner shell orbitals for between the two wave functions sets.

5.3 Ionization probabilities

The differential probability with respect to the energy of the ionized electron is given by

$$\frac{2}{\pi}\frac{dP}{d\epsilon}(\mathrm{n,l} \to \epsilon) = \frac{2}{\pi}\frac{\omega_{nl}}{\omega_{\max}} \sum_{l',m,m'} \left| Z^{nlm}_{\epsilon l' m'}(\mathbf{q}_e) \right|^2, \tag{5.30}$$

where the electron transition amplitude squared is given by 3.87 for the spherical waves (SW) and the Coulomb wave functions (CO). We have already shown in chapter 4.1 that the dipole approximation is completely sufficient for the calculation of the Migdal effect.

5.3.1 Spherical waves

In this section, we explicitly work out the Migdal effects for spherical waves with definite angular momentum l from (5.16) with

$$\phi_{\epsilon lm}(\mathbf{r}) = \sqrt{km}\, j_l(kr) Y_{lm}(\vartheta, \varphi), \tag{5.31}$$

$$\int d^3x \phi^*_{\epsilon l' m'}(\mathbf{r}) \phi_{\epsilon lm}(\mathbf{r}) = \left(\frac{\pi}{2}\right) \delta(\epsilon - \epsilon') \delta_{ll'} \delta_{mm'}. \tag{5.32}$$

The ionization probabilities in the dipole approximation are given by Eq. 5.30 and Eq. 3.87, where $L = 1$ is fixed. The curves of figure 5.3 show the differential transition probability with respect to the principal quantum number n in the dipole approximation. We conclude that the spherical waves serve as a good approximation for the continuum wave function for ionized electrons in the outer shell ($n = 3, 4, 5$). For $n = 2$, we see that the probability for electron energies of $\approx$ 1eV is about one order of magnitude smaller than the output from FAC and for energies of $\approx$ 5keV the probabilities are about one order of magnitude larger. For $n = 1$, the transition probability seems to be highly suppressed.

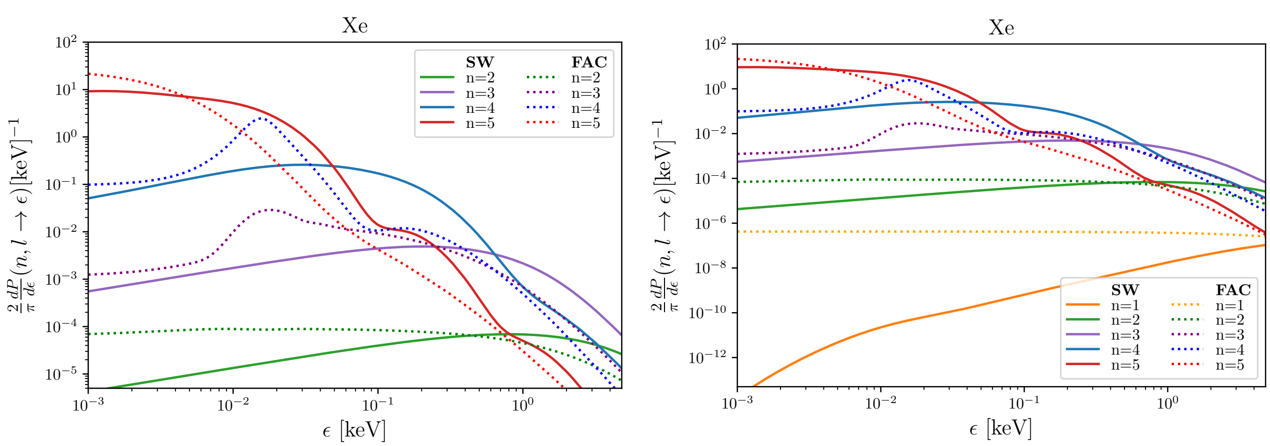

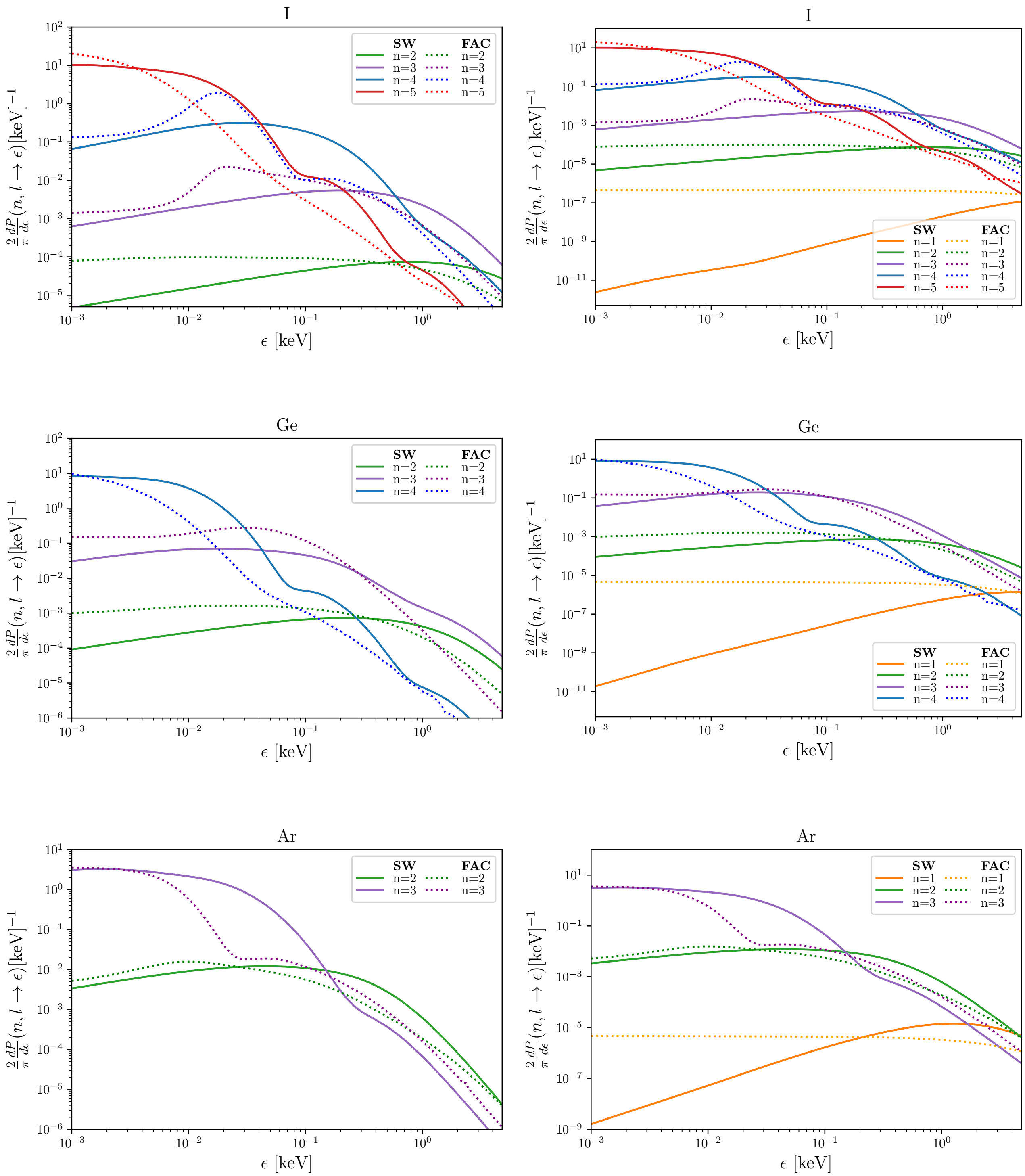

Figure 5.3: The plots show the ionized electron transition probability in the dipole approximation with respect to the energy of the ionized electron ϵ in keV for the isolated atoms Xe, I, Ge and Ar. The dotted lines correspond to the results of the Flexible atomic code (FAC) evaluated in the previous chapter and the solid lines show the approximation with spherical waves (SW). The momentum of the electron is fixed to $q_e = me \times 10^{-}3$.

5.3.2 Coulomb wave functions

Considering the continuum wave functions from chapter 5.1.2. The ionization probabilities in the dipole approximation with respect to the energy of the ionized electron is again given by Eq. 5.30 and Eq. 3.87 with $L = 1$. For the calculation, we assume single electron ionization and therefore estimate the effective charge of for noble gases Ar and Xe to be $Z_{\text{eff}} = 1$. For Sodium the effective charge is estimated by $Z_{\text{eff}} = 2$. For Germanium the effective charge is approximated by Eq. (5.20).

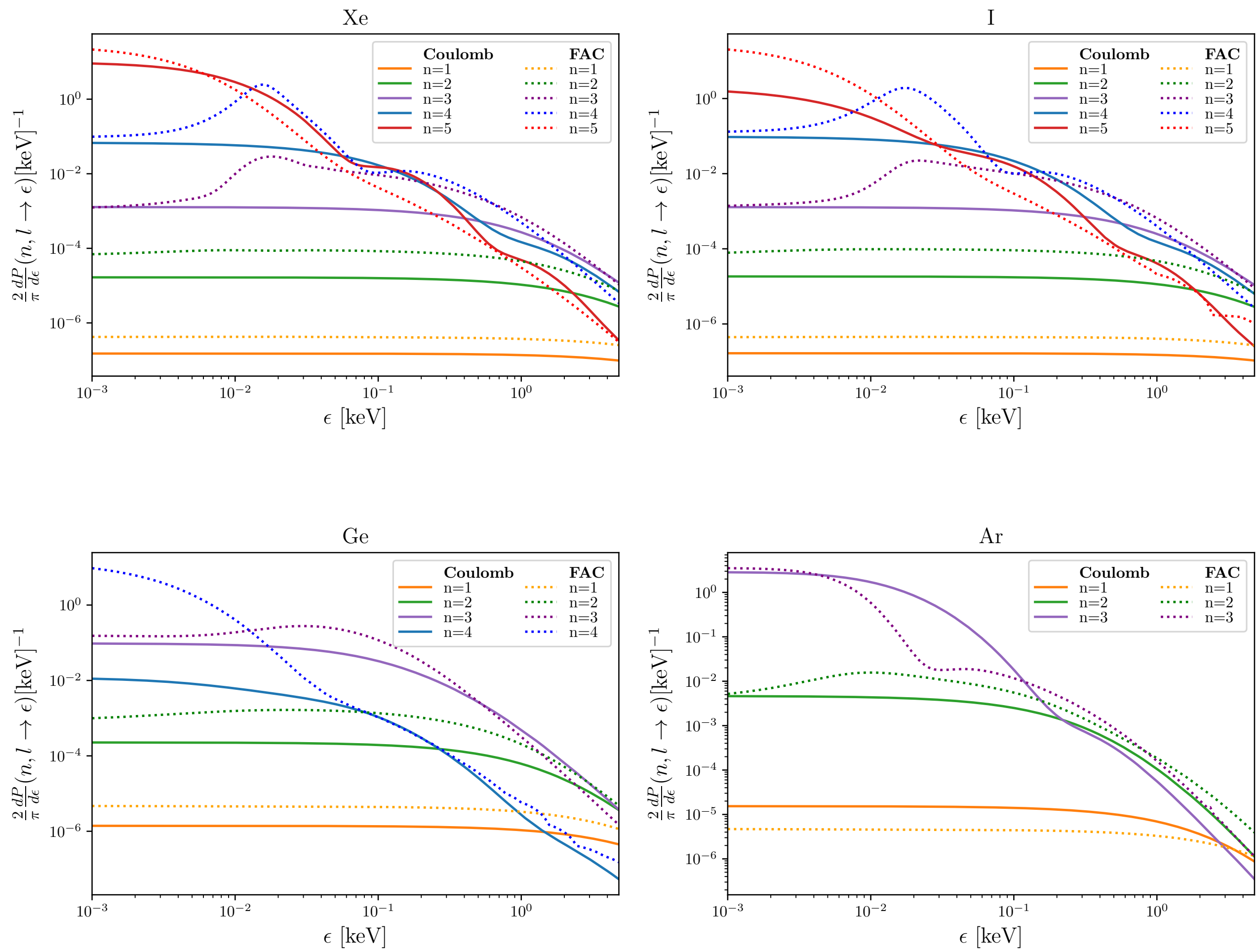

Figure 5.4: The plots show the transition probabilities for ionization for isolated Xe, Ar,Ge and I atoms with respect to the Coulomb wave functions in the dipole approximation. The dotted lines correspond to the results of the Flexible atomic code (FAC) evaluated in the previous chapter and the solid lines show the approximation with Coulomb wave functions (CO). The momentum of the electron is fixed by $q_e = m_\chi \times 10^{-3}$.

The Coulomb wave functions seem to be a more appropriate choice for the calculation of the

Migdal effect, since for very large atoms the distortion of the wave function becomes a non negligible effect and the Coulomb wave functions takes the effective charge "felt" by the escaping electron into account.

5.3.3 Migdal effect as a Fourier transformation

In this section, we want to treat the continuum wave functions as plane waves

$$\psi_\epsilon(\mathbf{r}) = \frac{1}{4\pi}\sqrt{km_e}e^{i\mathbf{k}\cdot\mathbf{r}}, \tag{5.33}$$

such that we can evaluate the probabilities of the Migdal effect in a calculation similiar to a Fourier transformation. Therefore the electron transition amplitude can be brought to the form

$$\tilde{\phi}_{nlm}(\mathbf{q}) = \int \phi_{nlm}(x)e^{-i\mathbf{q}\cdot\mathbf{r}}d^3r = \chi_{nl}(q)Y_{lm}(\vartheta_q, \varphi_q), \tag{5.34}$$

modulo the normalization constant of the plane wave. Now we want to adopt this framework that has been successfully used in the context of dark matter electron scattering e.g. [47][48] and reformulate it in terms of the Migdal effect. A concise derivation of the $\chi_{nl}(p)$ can be seen in Appendix E. The $\chi_{nl}(p)$ are then given by the formula

$$\chi_{nl}(p) = 4\pi(-i)^l \int drr^2 R_{nl}(r), \tag{5.35}$$

and fulfills the normalization condition $\int dp\, p^2 \chi_{nl}(p) = (2\pi)^3$. Therefore, the transition amplitude in terms of the continuum state ψ_ϵ and bound state ϕ_{nlm} is

$$Z^{nlm}_{\epsilon l'm'}(\mathbf{q}_e) = \langle \epsilon l'm' |\, e^{-i\mathbf{q}_e\cdot\mathbf{r}} \,| nlm\rangle\,. \tag{5.36}$$

Identifying the galilean boost operator with the transition operator and expanding it yields

$$e^{-i\mathbf{p}\cdot\mathbf{r}} = \mathbb{1} - i\mathbf{p}\cdot\mathbf{r} + \frac{(-i\mathbf{p}\cdot\mathbf{r})^2}{2!} + \ldots. \tag{5.37}$$

In the case of dark matter electron scattering the electron directly picks up the whole energy of the recoil, but in the case of the Migdal effect, the momentum transfer with respect to the ionized electron is suppressed by $q_e \simeq \frac{m_e}{m_A}q_A$, such that $\mathbf{q}\cdot\mathbf{r} \ll 1$. To avoid spurious contributions in the transition amplitude we have to subtract the case, where no interaction takes place. Therefore the electron transition amplitude squared gets corrected by subtracting the identity operator from the transition operator

$$|\langle \epsilon l'm' |\, e^{-i\mathbf{q}_e\cdot\mathbf{r}} \,| nlm\rangle|^2 \to |\langle \epsilon l'm' |\, e^{-i\mathbf{q}_e\cdot\mathbf{r}} - 1 \,| nlm\rangle|^2. \tag{5.38}$$

The electron transition amplitude squared is then of the form

$$\begin{aligned}\sum_s \sum_{m=-l}^{l} |Z^{nlm}_{\epsilon l'm'}(\mathbf{q}_e)|^2 =& \int \frac{d\Omega_{\mathbf{p}}}{4\pi} \sum_s \sum_{m=-l}^{l} \left|\langle \epsilon l'm'|\, e^{-i\mathbf{q}_e\cdot\mathbf{r}} - 1\,|nlm\rangle\right|^2 \\ =& \int \frac{d\Omega_{\mathbf{p}}}{4\pi} \frac{km_e}{(4\pi)^2} \sum_s \sum_{m=-l}^{l} \left| \int d^3r\, e^{-i(\mathbf{q}_e+\mathbf{k})\cdot\mathbf{r}} \phi_{nlm}(\mathbf{r}) - \int d^3r\, e^{-i\mathbf{k}\cdot\mathbf{r}} \phi_{nlm}(\mathbf{r}) \right|^2 \\ =& \int \frac{d\Omega_{\mathbf{p}}}{4\pi} \frac{km_e}{(4\pi)^2} \sum_s \sum_{m=-l}^{l} |\chi_{nl}(p) Y_{lm}(\vartheta_p, \varphi_p) - \chi_{nl}(k) Y_{lm}(\vartheta_k, \varphi_k)|^2 ,\end{aligned} \tag{5.39}$$

where $\mathbf{p} = \mathbf{q}_e + \mathbf{k}$. Since, the momentum $\mathbf{p}$ depends on the angle between $\mathbf{q}_e$ and $\mathbf{k}$, the momentum p can reach values from $|q_e - k|$ to $q_e + k$. The integral $\int \frac{d\Omega_{\mathbf{p}}}{4\pi}$ averages over all the possible outgoing momenta. Therefore Eq. 5.39 together with Eq. E.3 yields

$$\begin{aligned}\sum_s \sum_{m=-l}^{l} |Z^{nlm}_{\epsilon l'm'}(\mathbf{q}_e)|^2 = \int \frac{d\Omega_{\mathbf{p}}}{4\pi} \frac{km_e}{(4\pi)^2} \sum_s \sum_{m=-l}^{l} \Big[& |\chi_{nl}(p)|^2 |Y_{lm}(\vartheta_p, \varphi_p)|^2 + |\chi_{nl}(k)|^2 |Y_{lm}(\vartheta_k, \varphi_k)|^2 \\ & - 2|\chi_{nl}(k)||\chi_{nl}(p)| Y_{lm}(\vartheta_p, \varphi_p) Y_{lm}(\vartheta_k, \varphi_k) \Big]\end{aligned} \tag{5.40}$$

Making use of Eq. E.3, we arrive at

$$\begin{aligned}\sum_s \sum_{m=-l}^{l} |Z^{nlm}_{\epsilon l'm'}(\mathbf{q}_e)|^2 =& \frac{km_e}{(4\pi)^2} \frac{2(2l+1)}{4\pi} \Bigg[\int \frac{d\Omega_{\mathbf{p}}}{4\pi} |\chi_{nl}(p)|^2 + |\chi_{nl}(k)|^2 \\ & - 2\chi_{nl}(k) \int \frac{d\Omega_{\mathbf{p}\cdot\mathbf{k}}}{4\pi} \chi_{nl}(p) P_l\left(\hat{\mathbf{p}}\cdot\hat{\mathbf{k}}\right) \Bigg] \\ =& \frac{km_e}{(4\pi)^2} \frac{2(2l+1)}{4\pi} \Bigg[\int_{|q_e-k|}^{|q_e+k|} \frac{p\,dp}{2q_e k} |\chi_{nl}(p)|^2 + |\chi_{nl}(k)|^2 \\ & - |\chi_{nl}(k)| \int_{-1}^{1} d\cos\vartheta \left| \chi_{nl}\left(\sqrt{q_e^2 + k^2 + 2q_e k\cos\vartheta}\right) \right| P_l\left(\frac{k + q_e\cos\vartheta}{\sqrt{q_e^2 + k^2 + 2q_e k\cos\vartheta}} \right) \Bigg],\end{aligned} \tag{5.41}$$

where $d\Omega_{\mathbf{p}} = \frac{2\pi\, pdp}{q_e k}$ and $d\Omega_{\mathbf{p}\cdot\mathbf{k}} = 2\pi\, d\cos\vartheta$. The quanitities $\chi_{nl}(q)$ are defined by Eq. 5.35, where the $R_{nl}(r)$ are given by Bunge et al. [41] and are in general of the form

$$\begin{aligned}\chi_{nl}(q) =& a_0^{-3/2} \sum_k \frac{1}{(Z_{lk}\pi)^{\frac{3}{2}}} c_{nlk} 2^{n_{lk}+3/2} \left(\frac{-ia_0 q}{2Z_{lk}}\right)^l \frac{\Gamma(2 + n_{lk} + l)}{\sqrt{(2n_{lk})!}} \\ & \times {}_2F_1 \left[\frac{1}{2}(2 + l + n_{lk}), \frac{1}{2}(3 + l + n_{lk}), \frac{3}{2} + l, -\left(\frac{qa_0}{Z_{lk}}\right)^2 \right].\end{aligned} \tag{5.42}$$

where ${}_2F_1[a, b, c; z]$ is the regularized hypergeometric function.

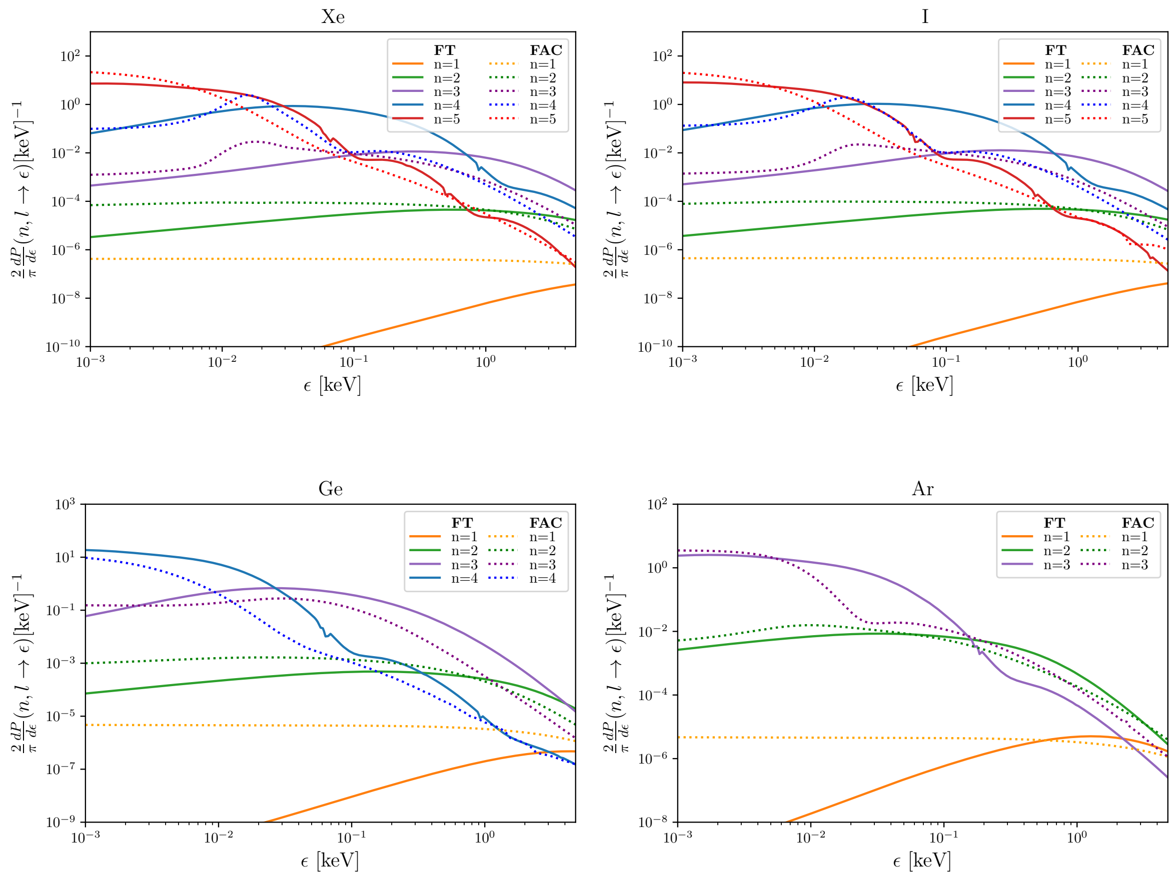

Figure 5.5: The plots show the transition probability $\frac{dp}{d\epsilon}(nl \to \epsilon)$ for the Fourier transformation compared to the FAC result.

In fig. (5.5), we can see that the Fourier transformation in comparison to the FAC serves as a very good approximation especially for outer shell electrons. The inner shell electrons the probability curves show incorrect behaviour for increasing ϵ, since they are monotonously increasing.

5.4 Comparison of the different approaches

Now we want to examine the different approaches, for the calculation of the Migdal effects. In the last chapter, we analyzed three diferent sets of analytic continuum wave functions with the bound state Hartree Fock wave functions from [41]. The three different methods can be characterized by the three kinds of continuum wave functions:

- Fourier transformation (FT)

- Spherical waves with definite l (SW)
- Coulomb wave functions (CO)

which have to be compared to the numeric result of FAC.

The following plots show the different probability curves for single electron ionization with fixed principal quantum number n.

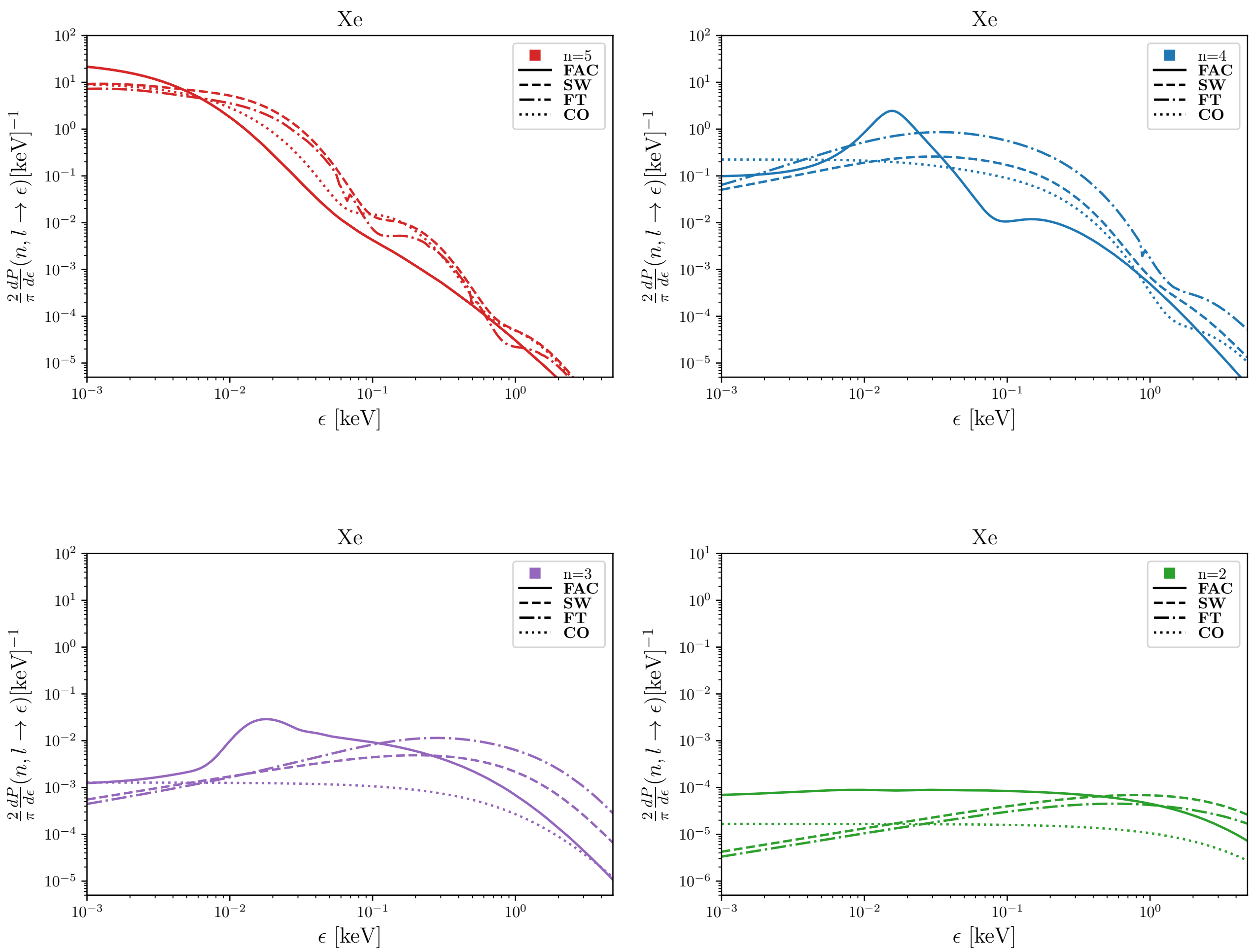

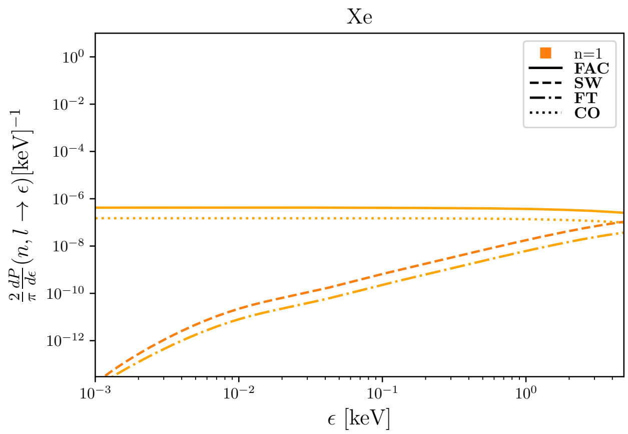

Figure 5.6: The plots show the differential probability curve with respect to the energy of the ionized electron ϵ with fixed momentum transfer $q_e = m_e \times 10^{-3}$ for Xenon.

The Coulomb wave functions yield a good approximation for the continuum wave function. for all principle quantum numbers n. The (SW) as well as the (FT) method agree well with the results of the flexible atomic code for the principle quantum numbers $n = 2, 3, 4, 5$. For $n = 1$ the probability curves show a large discrepancy between the results. The probability curves of the spherical waves have the same behaviour as the curves of the Fourier transform, which we expected from the fact that the use of plane waves is nothing but an infinite summation over spherical waves.

5.4.1 Final Probabilities

The following tables show the total ionization probabilities obtained by different wave functions for Xe, I, Ge and Ar. The obtained ionization probabilities are ordered by the method used. The third line of the table denotes the procedure from which the bound state wave functions are obtained, where the column Bunge refers to the bound state wave functions of Bunge et al. [41] and the FAC column denotes the use of the flexible atomic code [40]. The fourth line denotes the approximation of the continuum wave functions, where (SW) denotes the spherical wave of 5.16, (FT) denotes the Fourier transform and (Coulomb) the Coulomb wave functions from 5.19.

Xenon:	$\int d\epsilon \frac{dp}{d\epsilon}(nl \to \epsilon)$			
Dipole Approximation:				
Method:	Bunge			FAC
(n,l)	SW	FT	Coulomb	FAC
(1,s)	3.97×10^{-7}	8.84×10^{-8}	5.87×10^{-7}	1.64×10^{-6}
(2,s)	1.40×10^{-4}	3.11×10^{-5}	4.11×10^{-6}	2.20×10^{-5}
(2,p)	2.28×10^{-4}	1.14×10^{-4}	3.05×10^{-5}	1.18×10^{-4}
(3,s)	1.12×10^{-3}	2.48×10^{-4}	5.77×10^{-6}	1.07×10^{-4}
(3,p)	3.24×10^{-3}	1.62×10^{-3}	5.34×10^{-5}	6.02×10^{-4}
(3,d)	4.39×10^{-3}	1.37×10^{-2}	8.16×10^{-4}	3.60×10^{-3}
(4,s)	6.12×10^{-3}	1.35×10^{-3}	8.21×10^{-5}	3.53×10^{-4}
(4,p)	1.75×10^{-2}	1.01×10^{-2}	6.65×10^{-4}	1.47×10^{-3}
(4,d)	2.01×10^{-2}	1.35×10^{-1}	4.66×10^{-3}	3.68×10^{-2}
(5,s)	4.23×10^{-2}	9.39×10^{-3}	8.54×10^{-3}	4.70×10^{-4}
(5,p)	2.88×10^{-1}	8.58×10^{-2}	6.74×10^{-2}	8.13×10^{-2}
$\sum_{n,l}$	2.02×10^{-1}	2.58×10^{-1}	8.23×10^{-2}	1.25×10^{-1}

Iod:	$\int d\epsilon \frac{dp}{d\epsilon}(nl \to \epsilon)$			
Dipole Approximation:				
Method:	Bunge			FAC
(n,l)	SW	FT	Coulomb	Dirac HF
(1,s)	4.45×10^{-7}	9.91×10^{-8}	6.42×10^{-7}	1.77×10^{-6}
(2,s)	1.48×10^{-4}	3.30×10^{-5}	4.36×10^{-6}	2.37×10^{-5}
(2,p)	2.43×10^{-4}	1.22×10^{-4}	3.29×10^{-5}	1.26×10^{-4}
(3,s)	1.17×10^{-3}	2.60×10^{-4}	5.10×10^{-6}	1.15×10^{-4}
(3,p)	3.40×10^{-3}	1.70×10^{-3}	5.61×10^{-5}	6.41×10^{-4}
(3,d)	4.65×10^{-3}	1.46×10^{-2}	7.69×10^{-4}	3.81×10^{-3}
(4,s)	6.52×10^{-3}	1.44×10^{-3}	9.45×10^{-5}	3.75×10^{-4}
(4,p)	2.16×10^{-2}	1.08×10^{-2}	7.15×10^{-4}	1.54×10^{-3}
(4,d)	4.74×10^{-2}	1.49×10^{-1}	6.19×10^{-3}	4.09×10^{-2}
(5,s)	4.71×10^{-2}	1.05×10^{-2}	3.35×10^{-3}	4.74×10^{-4}
(5,p)	1.56×10^{-1}	8.09×10^{-2}	8.80×10^{-3}	6.82×10^{-2}
$\sum_{n,l}$	2.89×10^{-1}	2.69×10^{-1}	2.00×10^{-2}	1.16×10^{-1}

Germanium:	$\int d\epsilon \frac{dp}{d\epsilon}(nl \to \epsilon)$			
Dipole Approximation:				
Method:	Bunge			FAC
(n,l)	SW	FT	Coulomb	Dirac HF
(1,s)	7.35×10^{-6}	1.64×10^{-6}	3.91×10^{-6}	1.20×10^{-5}
(2,s)	5.21×10^{-4}	1.16×10^{-4}	1.58×10^{-5}	1.24×10^{-4}
(2,p)	1.15×10^{-3}	1.22×10^{-4}	1.73×10^{-4}	7.25×10^{-4}
(3,s)	4.51×10^{-3}	1.00×10^{-3}	1.47×10^{-4}	5.67×10^{-4}
(3,p)	1.46×10^{-2}	1.70×10^{-3}	3.05×10^{-4}	2.40×10^{-3}
(3,d)	3.21×10^{-2}	1.46×10^{-2}	1.02×10^{-2}	2.90×10^{-2}
(4,s)	5.35×10^{-2}	1.21×10^{-2}	4.23×10^{-5}	6.03×10^{-4}
(4,p)	7.86×10^{-2}	1.24×10^{-1}	3.54×10^{-4}	2.65×10^{-2}
$\sum_{n,l}$	1.85×10^{-1}	1.54×10^{-1}	1.13×10^{-2}	5.99×10^{-2}

Argon:	$\int d\epsilon \frac{dp}{d\epsilon}(nl \to \epsilon)$			
Dipole Approximation:				
Method:	Bunge			FAC
(n,l)	SW	FT	Coulomb	Dirac HF
(1,s)	7.23×10^{-5}	1.61×10^{-5}	2.06×10^{-5}	6.83×10^{-5}
(2,s)	1.97×10^{-3}	4.39×10^{-4}	5.06×10^{-5}	5.40×10^{-4}
(2,p)	5.13×10^{-3}	2.57×10^{-3}	8.98×10^{-4}	4.53×10^{-3}
(3,s)	2.27×10^{-2}	5.07×10^{-3}	7.97×10^{-3}	1.32×10^{-3}
(3,p)	9.18×10^{-2}	4.68×10^{-2}	4.04×10^{-2}	6.66×10^{-2}
$\sum_{n,l}$	1.22×10^{-1}	5.49×10^{-2}	4.94×10^{-2}	7.30×10^{-2}

Chapter 6

Ionization Event rates

6.1 Dark Matter Event Rates

For the calculation of the dark matter event rate, we assume coherent nuclear scattering, such that the atomic form factor can be approximated to be $|\mathcal{F}|^2 = 1$. Therefore, the differential dark matter event rate is

$$\left\langle \frac{dR}{d\epsilon} \right\rangle = N_T \frac{\rho_\chi m_A}{m_\chi \mu_N^2 \pi} A^2 \frac{\mu_N^2}{\mu_n^2} \sigma_n \int_{v_{\min}}^{v_{\max}} d^3v \frac{f(v, v_{obs})}{v} \int_{E_R^{\min}}^{E_R^{\max}} dE_R \, \frac{2}{\pi} \sum_{ec} |Z_{FI}(E_R)|^2, \tag{6.1}$$

where the momentum transfer is related to the recoil energy by $q_e = \frac{m_e}{m_N}\sqrt{2m_N E_R}$. The maximum and minimum recoil energy of the inelastic process is given by Eq. (3.31), where $\Delta E = \epsilon + E_{nl}$ and ϵ is the energy of the ionized electron and E_{nl} is the binding energy of the ionized/excited electron. For the calculation of the dark matter event rates with annual modulation, v_{obs} gets replaced by $v_{\mathrm{obs}}(t)$ given by Eq. 2.29. On the next page the differential event rates with respect to the energy of the ionized electrons ϵ for Xenon are plotted. The momentum is integrated over all possible final momenta constrained by the kinematical constraints of chapter 3.1.3. The local dark matter density is approximated to be $\rho_\chi = 0.3 \frac{\mathrm{GeV}}{\mathrm{cm}^3}$.

6.1.1 Flexible atomic code

Fig.6.1 shows the differential event rates with respect to the energy of the ionized electrons $\Delta E = E_{nl} + \epsilon$ for Xenon are plotted. The momentum is integrated over all possible final momenta constrained by the kinematical constraints of chapter 3.1.3. The local dark matter density is approximated to be $\rho_\chi = 0.3 \frac{\mathrm{GeV}}{\mathrm{cm}^3}$.

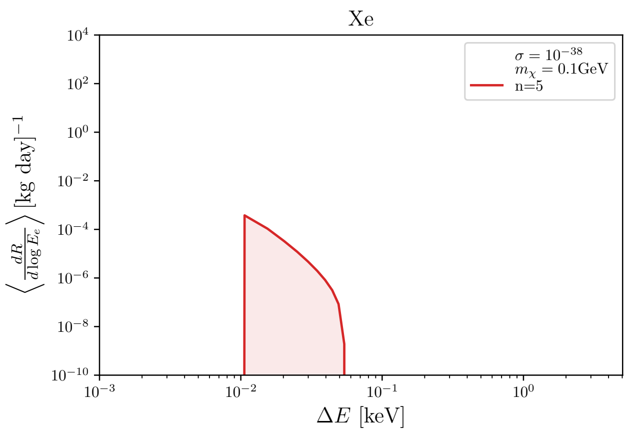
Xe
$\sigma = 10^{-38}$
$m_\chi = 0.1$GeV
n=5
$\left\langle \frac{dR}{d\log E_e} \right\rangle$ [kg day]$^{-1}$
ΔE [keV]

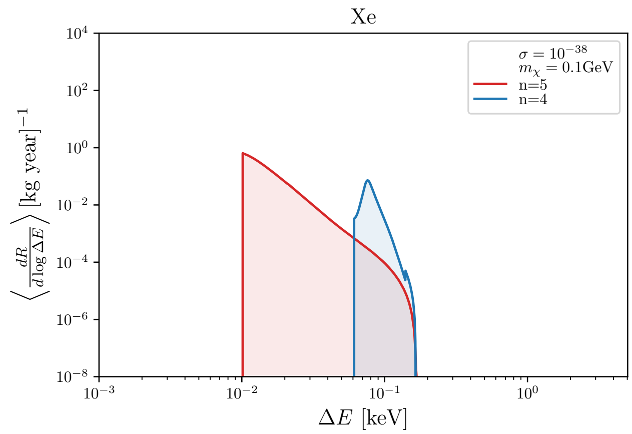
Xe
$\sigma = 10^{-38}$
$m_\chi = 0.1$GeV
n=5
n=4
$\left\langle \frac{dR}{d\log \Delta E} \right\rangle$ [kg year]$^{-1}$
ΔE [keV]

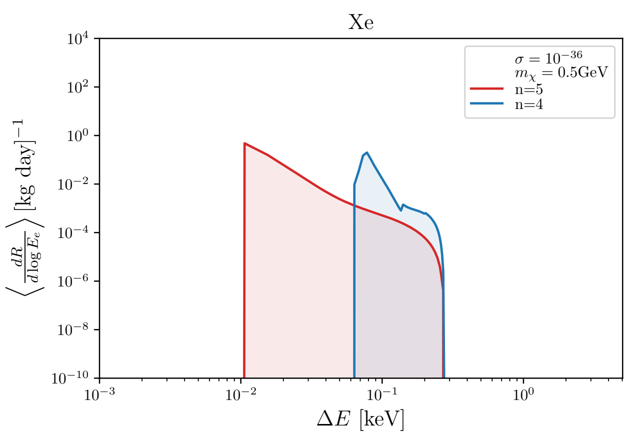
Xe
$\sigma = 10^{-36}$
$m_\chi = 0.5$GeV
n=5
n=4
$\left\langle \frac{dR}{d\log E_e} \right\rangle$ [kg day]$^{-1}$
ΔE [keV]

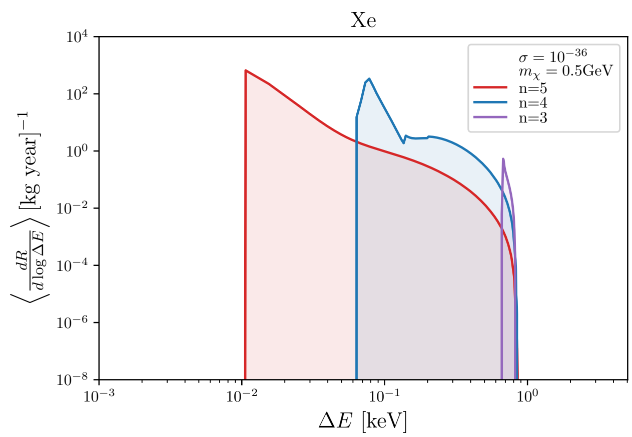
Xe
$\sigma = 10^{-36}$
$m_\chi = 0.5$GeV
n=5
n=4
n=3
$\left\langle \frac{dR}{d\log \Delta E} \right\rangle$ [kg year]$^{-1}$
ΔE [keV]

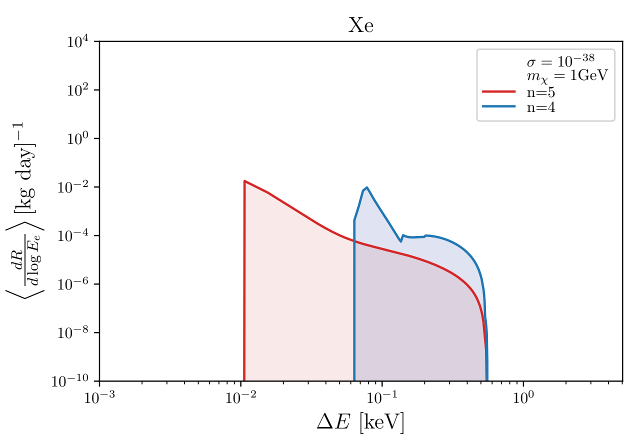
Xe
$\sigma = 10^{-38}$
$m_\chi = 1$GeV
n=5
n=4
$\left\langle \frac{dR}{d\log E_e} \right\rangle$ [kg day]$^{-1}$
ΔE [keV]

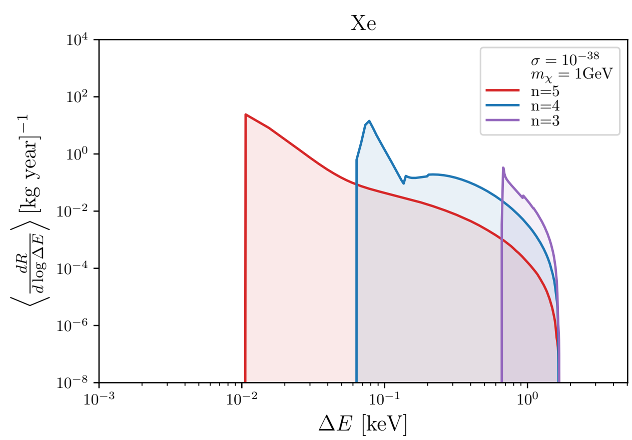
Xe
$\sigma = 10^{-38}$
$m_\chi = 1$GeV
n=5
n=4
n=3
$\left\langle \frac{dR}{d\log \Delta E} \right\rangle$ [kg year]$^{-1}$
ΔE [keV]

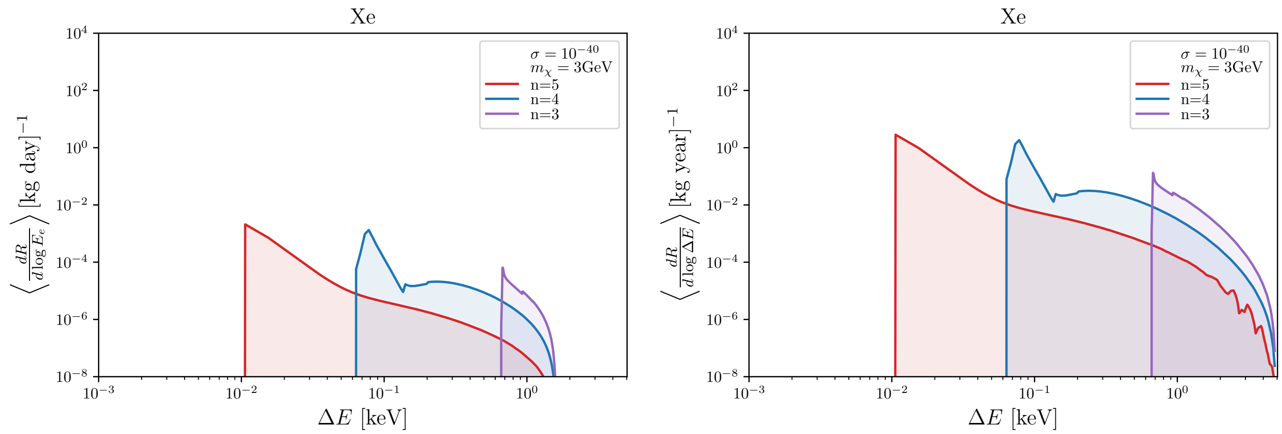

Figure 6.1: The plots are arranged as follows: The results were calculated with the radial wave functions obtained from the flexible atomic code. Every row belongs to a fixed nucleon cross section σ_n and dark matter mass m_χ. The left panel shows the differential event rate per day^{-1} kg^{-1} with respect to the energy deposit $\Delta E = E_{nl} + \epsilon$. The right panel shows the differential event rate per year^{-1} kg^{-1} with annual modulation.

6.1.2 Spherical waves with definite l/Fourier transformation

As we have already seen, the spherical wave approach and the Fourier transformation yield the same ionization probabilities. Therefore, it is sufficient to calculate the event rates for one of the two approaches. The plots show the differential event rates with respect to the energy of the ionized electron.

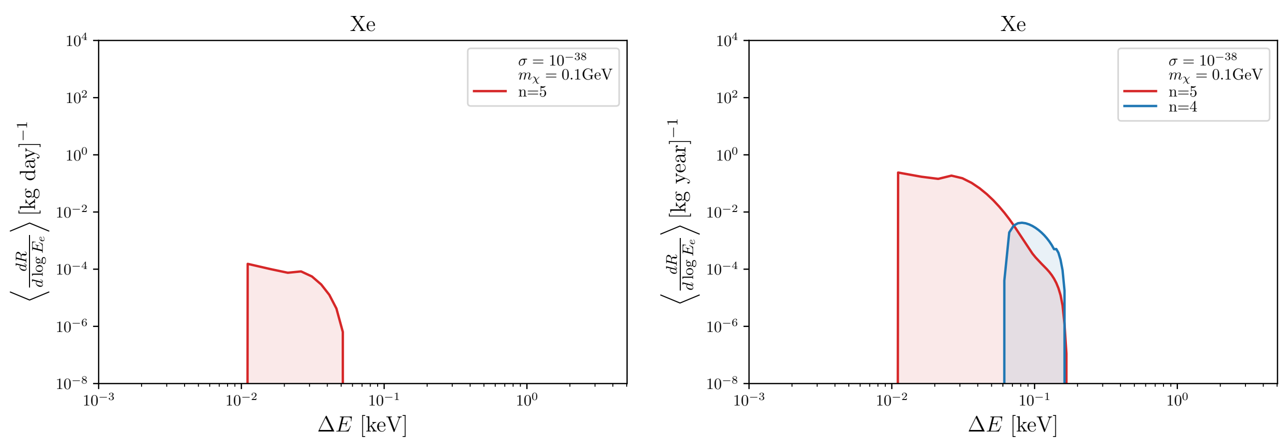

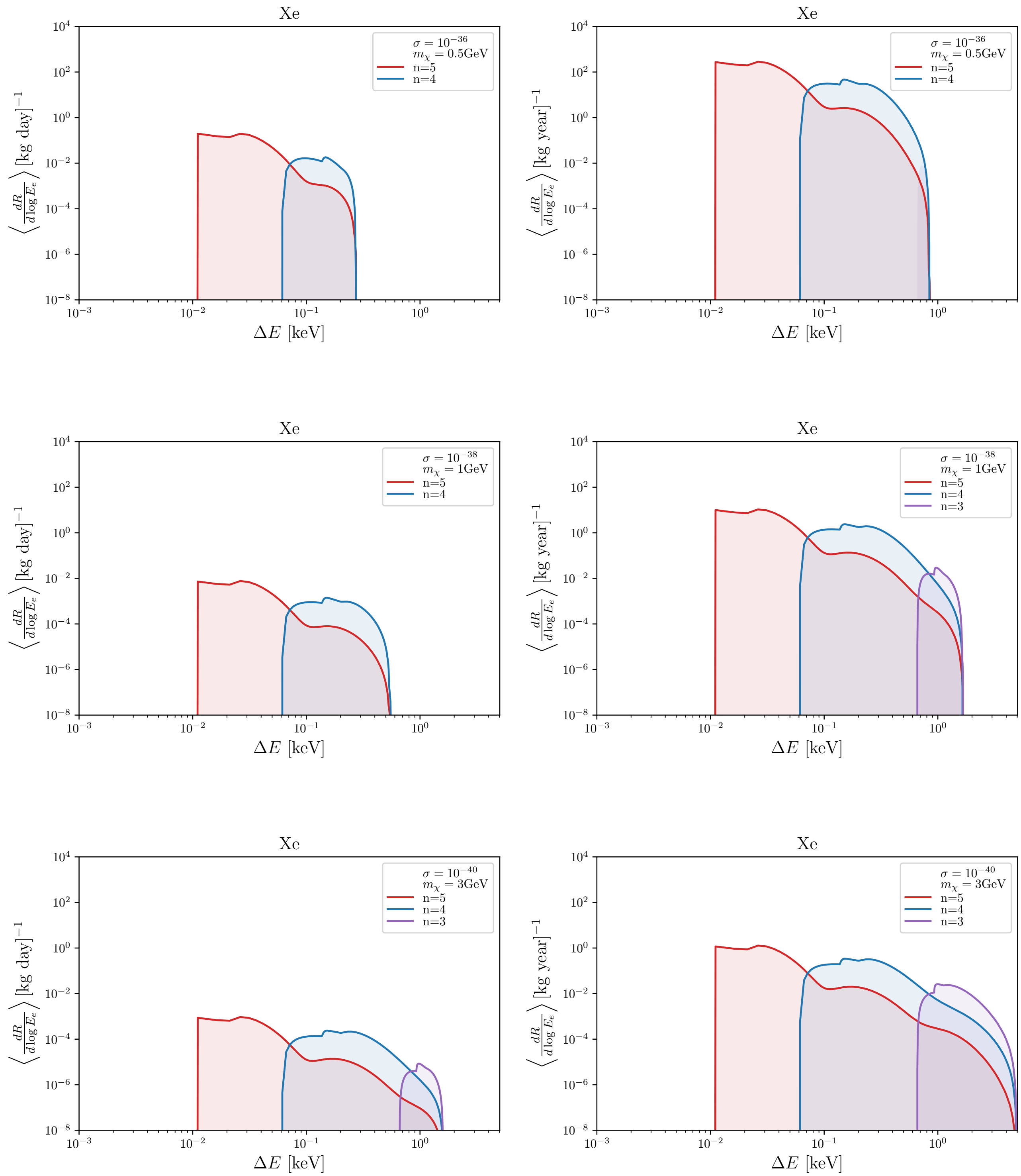

Figure 6.2: The plots are arranged as follows: Every row belongs to a fixed nucleon cross section σ_n and dark matter mass m_χ. The left panel shows the differential event rate per day^{-1} kg^{-1} with respect to the energy deposit $\Delta E = E_{nl} + \epsilon$. The right panel shows the differential event rate per year^{-1} kg^{-1} with annual modulation.

6.1.3 Coulomb wave functions

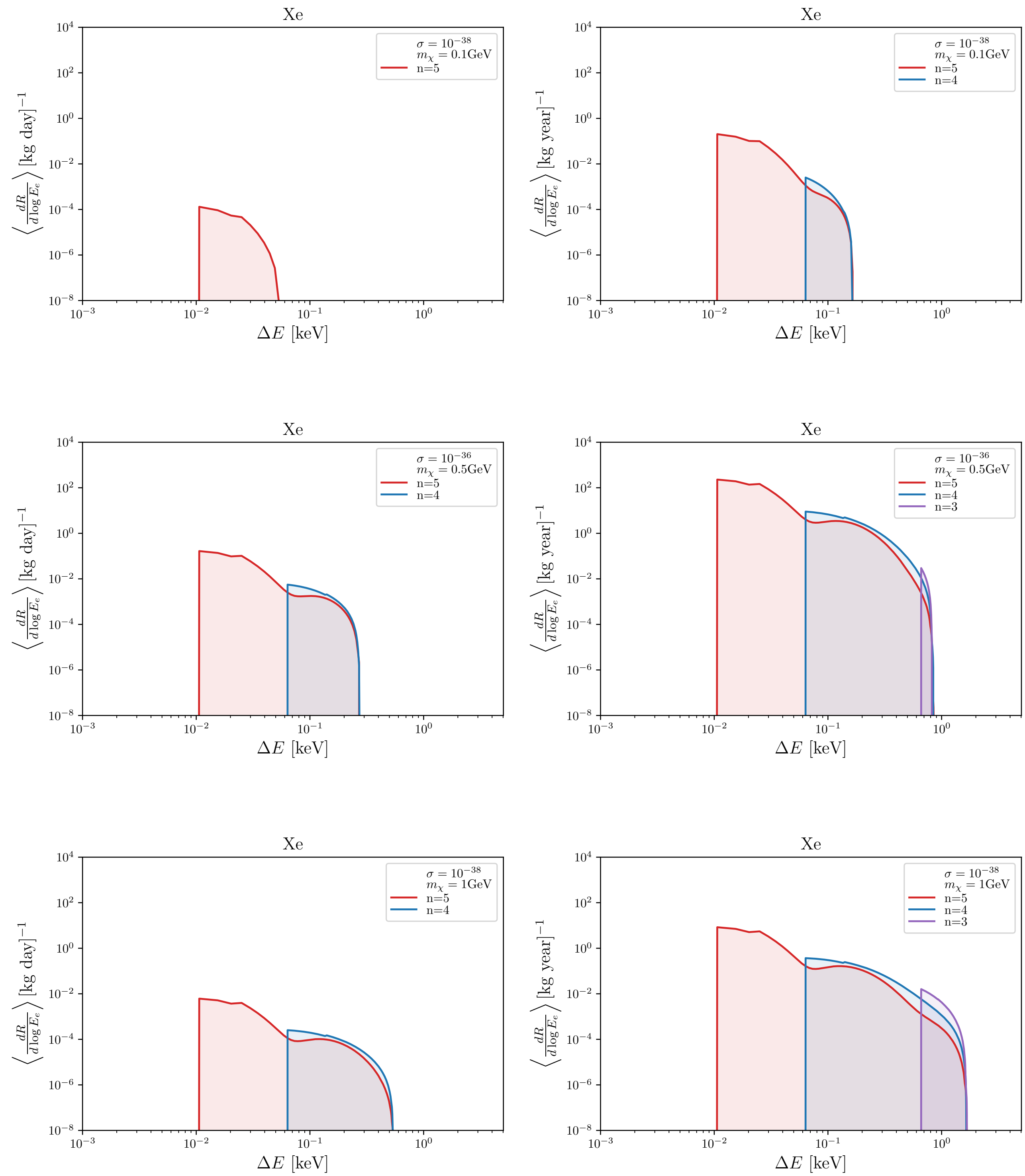

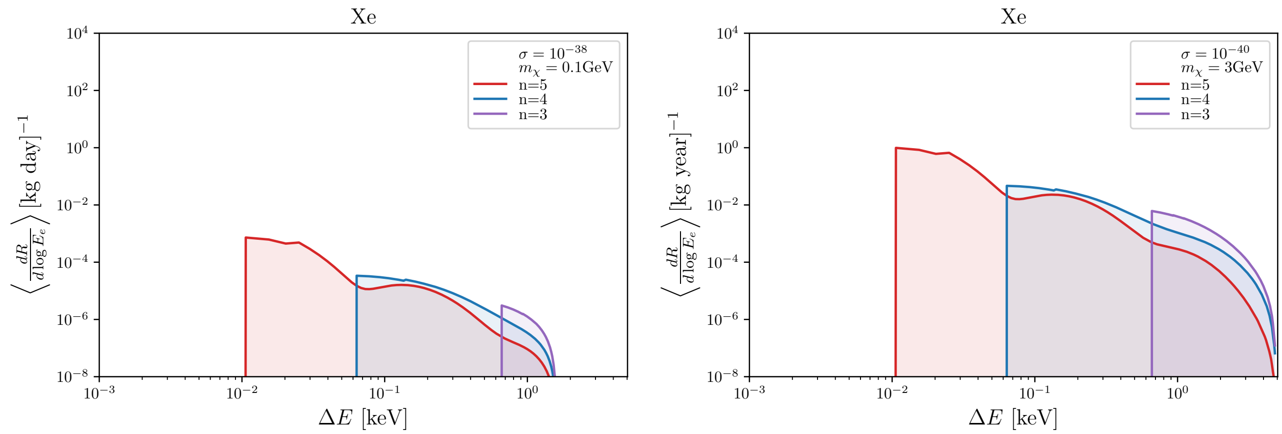

Figure 6.3: The plots are arranged as follows: Every row belongs to a fixed nucleon cross section σ_n and dark matter mass m_χ. The left panel shows the differential event rate per day^{-1} kg^{-1} with respect to the energy deposit $\Delta E = E_{nl} + \epsilon$. The right panel shows the differential event rate per year^{-1} kg^{-1} with annual modulation.

6.2 Conclusions and Outlook

The Migdal effect can be used to detect recoil signatures of dark matter through the prompt ionization or excitation of electrons. The calculation of the desired transition probabilities in this work is based on the realization of the electron cloud as a Slater determinant. Within this framework, we have shown that the main contribution to the ionization spectrum lies in the dipole approximation. For higher order transitions a general formula in the case of noble gases has been found with the use of the Wigner-Eckart theorem for a nonrelativistic as well as for a relativistic treatment of the electron cloud.

The ionization probabilities calculated with the numerical wave functions from the flexible atomic code [40] are in accordance with [35]. A purely numerical approach leads to tedious calculations with numerous data sets of continuum wave functions. However, a framework has been found to simplify the calculations of the Migdal effects with a method highly comparable to these results. The analytic solution of the free Schrödinger equation agrees very well with the numeric continuum wave functions from the numerical evaluation. These continuum wave functions obtained from the free Schrödinger equation in combination with the tabulated wave functions from Bunge et al [41] led to an analytic formula for the calculation of ionization probabilities and agrees well with the results of [35].

In general, the ionization potential for valence electrons in isolated atoms is of order of the binding energy $\mathcal{O}(10\text{eV})$. The theoretical formulation of the Migdal effects can be generalized to more complex materials such as crystals and semiconductors, e.g [49] [50]. The advantage of using semiconductors as a detector medium is that the ionization potential is of order $\mathcal{O}(1\text{eV})$. For Dirac materials the ionization potential is even of order $\mathcal{O}(10\text{meV})$ [51].

The nature of dark matter remains still unknown and sub GeV dark matter received more and more interest within the last years. In current dark matter experiments the maximum sensitivity is bound to background sources, such as the neutrino floor, where recoil events caused by neutrinos cannot be distinguished from dark matter recoil events anymore. As already mentioned there are numerous experimental approaches to reach a lower energy threshold for detectors. [52].

Appendices

A Nonrelativistic kinematics

For further calculations of the cross section of the spin independent interactions we will need some nonrelativistic kinematics.

Considering the scattering process $N + \chi \to N + \chi$ in the COM- frame, we have

$$p_1 = \begin{pmatrix} E_{\mathbf{p_1}} \\ \mathbf{p_1} \end{pmatrix} = \begin{pmatrix} \sqrt{m_\chi^2 + \mathbf{p}_1^2} \\ \mathbf{p_1} \end{pmatrix}, \qquad p_2 = \begin{pmatrix} E_{\mathbf{p_2}} \\ \mathbf{p_2} \end{pmatrix} = \begin{pmatrix} \sqrt{m_N^2 + \mathbf{p}_2^2} \\ \mathbf{p_2} \end{pmatrix}$$
$$k_1 = \begin{pmatrix} E_{\mathbf{k_1}} \\ \mathbf{k_1} \end{pmatrix} = \begin{pmatrix} \sqrt{m_\chi^2 + \mathbf{k}_1^2} \\ \mathbf{k_1} \end{pmatrix}, \qquad k_2 = \begin{pmatrix} E_{\mathbf{k_2}} \\ \mathbf{k_2} \end{pmatrix} = \begin{pmatrix} \sqrt{m_N^2 + \mathbf{k}_2^2} \\ \mathbf{k_2} \end{pmatrix}. \tag{A.1}$$

where $\mathbf{p}_1 = -\mathbf{p}_2 = \mathbf{p}_i$ and $\mathbf{k}_1 = -\mathbf{k}_2 = \mathbf{p}_f$.

The cross section in COM frame is

$$\begin{aligned}
\sigma =& \frac{1}{4E_{\mathbf{p}_1}E_{\mathbf{p}_2}|\mathbf{v}_1 - \mathbf{v}_2|}\int \frac{d^3k_1}{(2\pi)^3}\frac{d^3k_2}{(2\pi)^3}\frac{1}{2E_{\mathbf{k}_1}}\frac{1}{2E_{\mathbf{k}_2}}|\mathcal{M}|^2(2\pi)^4\delta^{(4)}(p_1 + p_2 - k_1 - k_2) \\
=& \frac{1}{16\pi^2 E_{\mathbf{p}_1}E_{\mathbf{p}_2}|\mathbf{v}_1 - \mathbf{v}_2|}\int \frac{d^3k_1}{2E_{\mathbf{k}_1}}\frac{d^3k_2}{2E_{\mathbf{k}_{f2}}}|\mathcal{M}|^2\delta(E_{\mathbf{p}_1} + E_{\mathbf{p}_2} - E_{\mathbf{k}_1} - E_{\mathbf{k}_2})\delta^{(3)}(\mathbf{k}_1 + \mathbf{k}_2) \\
=& \frac{1}{16\pi^2 E_{\mathbf{p}_1}E_{\mathbf{p}_2}|\mathbf{v}_1 - \mathbf{v}_2|}\int \frac{d^3p_f}{2E_{\mathbf{p}_f}}\frac{1}{2E_{-\mathbf{p}_f}}|\mathcal{M}|^2\delta(\underbrace{E_{\mathbf{p}_1} + E_{\mathbf{p}_2}}_{E_{CM}} - E_{\mathbf{p}_f} - E_{-\mathbf{p}_f}) \\
=& \frac{1}{16\pi E_{\mathbf{p}_1}E_{\mathbf{p}_2}|\mathbf{v}_1 - \mathbf{v}_2|}\int \frac{dp_f}{E_{\mathbf{p}_f}}\frac{p_f^2}{E_{-\mathbf{p}_f}}|\mathcal{M}|^2\delta(E_{\mathbf{p}_f} + E_{-\mathbf{p}_f} - E_{CM}).
\end{aligned} \tag{A.2}$$

Performing a change of variables from k to $x(p_f) = (E_{\mathbf{p}_f} + E_{-\mathbf{p}_f} - E_{CM})$, the Jacobian is

$$\frac{dx}{dp_f} = \frac{p_f}{E_{\mathbf{p}_f}} + \frac{p_f}{E_{-\mathbf{p}_f}} = \frac{E_{-\mathbf{p}_f} + E_{\mathbf{p}_f}}{E_{\mathbf{p}_f}E_{-\mathbf{p}_f}} \cdot p_f = \frac{E_{CM}}{E_{\mathbf{p}_f}E_{-\mathbf{p}_f}} \cdot p_f. \tag{A.3}$$

After using the COM condition $|\mathbf{p}_1| = |\mathbf{p}_2|$, we can rewrite

$$|\mathbf{v}_1 - \mathbf{v}_2| = \left|\frac{|\mathbf{p}_1|}{E_{\mathbf{p}_1}} + \frac{|\mathbf{p}_2|}{E_{\mathbf{p}_2}}\right| = \frac{E_{CM}}{E_{\mathbf{p}_1}E_{\mathbf{p}_2}}|\mathbf{p}\,|_i. \tag{A.4}$$

The final integral is now

$$\begin{aligned}\sigma =& \frac{1}{16\pi E_{CM}^2}\frac{1}{|\mathbf{p}_i|}\int_{m_N+m_\chi-E_{CM}}^{\infty} dx\,|\mathbf{p}_f|\,|\mathcal{M}|^2\,\delta(x)\\ =& \frac{|\mathcal{M}|^2}{16\pi E_{CM}^2}\frac{|\mathbf{p}_f|}{|\mathbf{p}_i|}\theta(E_{CM}-m_N-m_\chi). \end{aligned}\tag{A.5}$$

We conclude

$$\frac{d\sigma}{d\Omega} = \frac{|\mathcal{M}|^2}{64\pi^2 E_{CM}^2}\frac{|\mathbf{p}_f|}{|\mathbf{p}_i|}\theta(E_{CM}-m_N-m_\chi), \tag{A.6}$$

$$\frac{d\sigma}{d\cos\theta} = \frac{|\mathcal{M}|^2}{32\pi E_{CM}^2}\frac{|\mathbf{p}_f|}{|\mathbf{p}_i|}\theta(E_{CM}-m_N-m_\chi). \tag{A.7}$$

Due to Energy-momentum conservation for the scattering process $N+\chi \to N+\chi$ we have

$$E_{\mathbf{p}_1} + E_{\mathbf{p}_2} = E_{\mathbf{k}_1} + E_{\mathbf{k}_2} \tag{A.8}$$

$$\sqrt{m_\chi^2+\mathbf{p}_i^2} + \sqrt{m_N^2+\mathbf{p}_i^2} = \sqrt{m_\chi^2+\mathbf{p}_f^2} + \sqrt{m_N^2+\mathbf{p}_f^2} \tag{A.9}$$

$$\mathbf{p}_i = \mathbf{p}_f = \mathbf{p}. \tag{A.10}$$

The momentum transfer q_A is defined through the Mandelstam variable

$$\begin{aligned} q_A &= -t = -(p_2-k_2)^2 = -2m_N^2 + 2p_2\cdot k_2\\ &= -2m_N^2 + 2(m_N^2 + \mathbf{p}^2 - \mathbf{p}^2\cos\theta_{CM}) = 2|\mathbf{p}|^2(1-\cos\theta_{CM}). \end{aligned}\tag{A.11}$$

Since t is a Lorentz invariant quantity, we calculate it in the LAB frame with

$$\begin{aligned} p_1 &= \begin{pmatrix}\sqrt{m_\chi^2+\mathbf{p}_1^2}\\ \mathbf{p}_1\end{pmatrix}, \qquad p_2 = \begin{pmatrix} m_N\\ \mathbf{0}\end{pmatrix},\\ k_1 &= \begin{pmatrix}\sqrt{m_\chi^2+\mathbf{k}_1^2}\\ \mathbf{k}_1\end{pmatrix}, \qquad k_2 = \begin{pmatrix}\sqrt{m_N^2+\mathbf{k}_2^2}\\ \mathbf{k}_2\end{pmatrix}, \end{aligned}\tag{A.12}$$

so that we can express the momentum transfer q_A in terms of the recoil energy $E_R = \sqrt{m_N^2+\mathbf{k}^2} - m_N$

$$q_A = -t = -(p_2-k_2)^2 \simeq 2m_N E_R. \tag{A.13}$$

We can estimate the total momentum of the atomic system by $\mathbf{p} = \mu\mathbf{v}$, where $\mu = \frac{m_\chi m_N}{m_\chi + m_N}$ is the reduced mass and $\mathbf{v}$ is the velocity of the atom after the recoil. Combining Eq. (A.11) & (A.13) yields

$$E_R = \frac{\mathbf{p}^2}{m_N}(1 - \cos\theta_{CM}) \simeq \frac{\mu^2\mathbf{v}^2}{m_N}(1 - \cos\theta_{CM}) \tag{A.14}$$

We can use $dt = -2m_N E_R$ to rewrite Eq. (A.7) in terms of

$$\frac{d\sigma}{d\cos\theta} = \frac{d\sigma}{dt}\underbrace{\frac{dt}{d\cos\theta}}_{=2|\mathbf{p}|^2} = \frac{d\sigma}{dt}2|\mathbf{p}|^2, \tag{A.15}$$

so that we can express $\frac{d\sigma}{dt}$ with the use of $|\mathbf{p}_i| = |\mathbf{p}_f| = |\mathbf{p}|$ as

$$\frac{d\sigma}{dt} = \frac{|\mathcal{M}|^2}{64\pi E_{CM}^2|\mathbf{p}|^2}\theta(E_{CM} - m_N - m_\chi), \tag{A.16}$$

The differential cross section with respect to the nuclear recoil energy is

$$\frac{d\sigma}{dE_R} = \frac{d\sigma}{dt}\frac{dt}{dE_R} = \frac{m_N|\mathcal{M}|^2}{32\pi E_{CM}^2|\mathbf{p}|^2}\theta(E_{CM} - m_N - m_\chi) \tag{A.17}$$

B Hartree-Fock method

For the description of the electron cloud, the Hartree Fock method is an appropriate theory for numerical calculations. It provides a theoretical description of an approximate wave function for an N electron atom. Each electron in the atom is assumed to move independently in the nuclear Coulomb field and the Coloumb field of the remaining N-1 electrons [53].

For a system of N electrons the Hamiltonian can be approximated by

$$H(\mathbf{r}_1, \ldots, \mathbf{r}_N) = -\sum_{i=1}^{N}\frac{1}{2m_e}\nabla_i^2 - \sum_{i=1}^{N}\frac{Ze}{|\mathbf{r}_i - \mathbf{r}_N|} + \frac{1}{2}\sum_{i\neq j}\frac{e^2}{\mathbf{r}_{ij}}, \tag{B.1}$$

where $\mathbf{r}_{ij} = |\mathbf{r}_i - \mathbf{r}_j|$.

Let $\psi(\mathbf{r}_1, \ldots, \mathbf{r}_N)$ be a solution to the N-electron Schrödinger equation, then

$$H(\mathbf{r}_1, \ldots, \mathbf{r}_N)\psi(\mathbf{r}_1, \ldots, \mathbf{r}_N) = E\psi(\mathbf{r}_1, \ldots, \mathbf{r}_N) \tag{B.2}$$

and the wave function corresponding to the electrons is completely antisymmetric with respect to the interchange of two coordinates

$$\psi(\mathbf{r}_1, \ldots, \mathbf{r}_i, \ldots, \mathbf{r}_j, \ldots, \mathbf{r}_N) = -\psi(\mathbf{r}_1, \ldots, \mathbf{r}_j, \ldots, \mathbf{r}_i, \ldots, \mathbf{r}_N) \qquad \forall i, j. \tag{B.3}$$

To proceed further we want to introduce a single particle approximation, where we have to make the physically reasonable assumption that the electrostatic repulsion of the electrons can be treated as a central potential. The closed subshells have a spherical charge distribution, so that the interactions between the different shells and the valence electron are approximately spherically symmetric, such that we can start with an independent particle approximation. We can write $H = H_0 + H_{int}$ with

$$\begin{aligned} H_0(\mathbf{r}_1, \ldots, \mathbf{r}_N) &= \sum_{i=1}^{N} \left(-\frac{1}{2m_e} \nabla_i^2 - \frac{Ze^2}{|\mathbf{r}_i - \mathbf{r}_N|} + U(|\mathbf{r}_i - \mathbf{r}_N|) \right) \\ &= \sum_{i=1}^{N} h(|\mathbf{r}_i - \mathbf{r}_N|), \end{aligned} \tag{B.4}$$

$$H_{int} = \frac{1}{2} \sum_{i \neq j} \frac{e^2}{|\mathbf{r}_i - \mathbf{r}_j|} - \sum_{i=1}^{N} U(|\mathbf{r}_i - \mathbf{r}_N|), \tag{B.5}$$

where $U(|\mathbf{r}_i - \mathbf{r}_N|)$ is an appropriate approximation to the electron interaction potential.It is possible to seperate the N_e electron wave function $\psi(\mathbf{r}_1, \ldots, \mathbf{r}_{N_e})$ into single electron wave functions

$$\psi(\mathbf{r}_1, \ldots, \mathbf{r}_N) = \psi_a(\mathbf{r}_1)\psi_b(\mathbf{r}_2)\ldots\psi_n(\mathbf{r}_{N_e}). \tag{B.6}$$

The wave function is an eigenfunction of H_0 with eigenvalue

$$E^0_{ab\ldots n} = \epsilon_a + \epsilon_b + \cdots + \epsilon_n. \tag{B.7}$$

From (B.3) we get by permutation of the indices, $N_e!$ product functions that are degenerate in energy with that wave function. Since we need a completely antisymmetric wave function, we can use a Slater determinant to define such a wave function

$$\begin{aligned} \psi_{ab\ldots n}(\mathbf{r}_1, \mathbf{r}_2, \ldots, \mathbf{r}_{N_e}) &= \frac{1}{\sqrt{N_e!}} \begin{vmatrix} \phi_a(\mathbf{r}_1) & \phi_b(\mathbf{r}_1) & \ldots & \phi_n(\mathbf{r}_1) \\ \phi_a(\mathbf{r}_2) & \phi_b(\mathbf{r}_2) & \ldots & \phi_n(\mathbf{r}_2) \\ \vdots & & & \\ \phi_a(\mathbf{r}_{N_e}) & \phi_b(\mathbf{r}_{N_e}) & \ldots & \phi_n(\mathbf{r}_{N_e}) \end{vmatrix} \\ &= \frac{1}{\sqrt{N_e!}} \sum_{\sigma \in S_n} \operatorname{sgn}(\sigma) \prod_{i=1}^{N_e} \phi_{o_{\sigma(i)}}(r_i). \end{aligned} \tag{B.8}$$

The one electron orbitals states are normalized such that

$$\int d^3x \phi_o^*(\mathbf{r})\phi_{o'}(\mathbf{r})^\alpha = \begin{cases} \delta_{oo'} & \text{(bounded)} \\ 2\pi\delta(\epsilon - \epsilon')\delta_{\kappa\kappa'}\delta_{oo'} & \text{(continuum)} \end{cases} \tag{B.9}$$

Since the determinant vanishes, if two columns are identical, the Pauli exclusion principal is automatically fullfilled, since the quantum numbers $a, b, \ldots, n$ have to be distinct. Each of the quantum numbers $\{a, b, \ldots, n\}$ represents a set of three quantum numbers $\{n_a, \kappa_a, m_a\}$, such that the $N!$ wave functions are obtained by permuting the indices $\mathbf{r}_1, \mathbf{r}_2, \ldots, \mathbf{r}_N$. The wave function has to change sign upon interchange of two spatial or spin coordinates. It is obvious that 2 electrons can't have the same spatial and spin quantum numbers. Every of the spin orbitals $\phi_k(r_j)$ has parity $(-1)^l$, such that the Slater determinant hast the required parity $(-1)^{\sum_i l_i}$ [53].

The common procedure for calculations of the Hartree Fock method is to solve the eigenvalueproblem of the N_e electron wave functions, but therefore a convenient Hamiltonian has to be constructed. An appropriate Hamiltonian of the N-body problem can now only be constructed with foreknowledge of the eigensolutions of the coupled equations. The coupled equations are nonlinear and their solution can be approximated by iteration techniques, which will be repeated until certain precision is reached [54].

B.1 FAC

The Flexible Atomic Code is a fully relativistic program for the calculation of atomic radiative and collisional processes, where the standard jj-coupling scheme is used [40]. Each electron in the atom is assumed to move independently in the nuclear Coulomb field and the Coloumb field of the remaining N-1 electrons. The bound electrons of the atoms are now described by one electron Dirac orbitals $\phi(\mathbf{r})$, which satisfy the single particle Dirac equation

$$H_D \phi(\mathbf{r}) = \epsilon \phi(\mathbf{r}), \tag{B.10}$$

where ϵ is the energy of the atomic system and H_D is the relativistic Hamiltonian of the form

$$H_D = c\boldsymbol{\alpha} \cdot \mathbf{p} + \beta c^2 + V(\mathbf{r}), \tag{B.11}$$

where c is the speed of light, which is in atomic units $c = \frac{1}{\alpha} = 137.03599\ldots$ and $\boldsymbol{\alpha}$ and $\boldsymbol{\beta}$ are 4×4 Dirac matrices

$$\boldsymbol{\alpha} = \begin{pmatrix} 0 & \boldsymbol{\sigma} \\ \boldsymbol{\sigma} & 0 \end{pmatrix}, \qquad \boldsymbol{\beta} = \begin{pmatrix} \mathbb{1}_2 & 0 \\ 0 & -\mathbb{1}_2 \end{pmatrix}, \tag{B.12}$$

where $\boldsymbol{\sigma}$ refers to the 2×2 representation of the Pauli matrices.

The total angular momentum is given by $J = L + S$, where L is the orbital angular momentum and S is the 4×4 orbital spin angular momentum matrix defined by

$$S = \frac{1}{2}\begin{pmatrix} \boldsymbol{\sigma} & 0 \\ 0 & \boldsymbol{\sigma} \end{pmatrix}. \tag{B.13}$$

Since J commutes with the Dirac Hamiltonian H_D, we can classify the simulaneous eigenstates of H_D according to the values of energy J^2 and J_z. With the two component representation of S, the eigenstates of J^2 and J_z are spherical spinors $\Omega_{\kappa m}(\hat{\mathbf{r}})$.

The solution of the Dirac equation is

$$\begin{aligned} \phi_{o_i}(r) &= \frac{1}{r}\begin{pmatrix} P(r)\Omega_{\kappa m}(\theta,\phi) \\ iQ(r)\Omega_{-\kappa m}(\theta,\phi) \end{pmatrix}, \\ o_i &= \{\epsilon_i, \kappa_i, m_i\} \end{aligned} \tag{B.14}$$

where $\epsilon_i < 0$ defines a bound state, such that the state is characterized by the principal quantum number n_i, κ_i, m_i and $\epsilon_i > 0$ defines a continuum state. The spherical spinors satisfy the angular part of the Dirac equation. The radial part of the Dirac equation $\frac{1}{r}P(r)$ and $\frac{1}{r}Q(r)$ have to satisfy the coupled differential equations:

$$(V+1)P_\kappa(r) + \left(\frac{d}{dr} - \frac{\kappa}{r}\right)Q_\kappa(r) = \epsilon P_\kappa(r), \tag{B.15}$$

$$-\left(\frac{d}{dr} + \frac{\kappa}{r}\right)P_\kappa(r) + (V-1)Q_\kappa(r) = \epsilon Q_\kappa(r). \tag{B.16}$$

The one electron orbitals states are normalized such that

$$\sum_{\alpha=1}^{4}\int d^3x \phi_o(\mathbf{r})^{\alpha *}\phi_{o'}(\mathbf{r})^{\alpha} = \begin{cases} \delta_{nn'}\delta_{\kappa\kappa'}\delta_{mm'} & \text{(bounded)} \\ 2\pi\delta(\epsilon-\epsilon')\delta_{\kappa\kappa'}\delta_{mm'} & \text{(continuum)} \end{cases} \tag{B.17}$$

The one electron wave functions are calculated within a local central potential in self consistent field theory. In the standard Dirac-Fock-Slater method, the electron electron interaction includes the spherically averaged classical potential, due to the bound electrons and a local approximation to the exchange interaction. Since this potential includes the undesirable effect of self interaction and has an incorrect asymptotic behavior, the program uses a slightly different potential for the electron electron interaction, namely

$$\begin{aligned} V^{ee}(r) =& \frac{1}{r\sum_a \omega_a\rho_a(r)}\Big[\sum_{ab}\omega_a(\omega_b - \delta_{ab})Y^0_{bb}(r)\rho_a(r) \\ &+ \sum_a \omega_a(\omega_a - 1)\sum_{k>0} f_k(a,a)Y^k_{aa}(r)\rho_a(r) \\ &+ \sum_{a\neq b}\sum_k \omega_a\omega_b g_k(a,b)Y^k_{ab}(r)\rho_{ab}(r)\Big], \end{aligned} \tag{B.18}$$

where $a = n\kappa$ and $b = n'\kappa'$ denoting the subshells and ω_a is the fractional occupation number of the subshell $n\kappa$ and

$$\rho_{ab}(r) = P_a(r)P_b(r) + Q_a(r)Q_b(r), \tag{B.19}$$

$$Y^k_{ab}(r) = r \int \frac{r^k_<}{r^{k+1}_>}\rho_{ab}(r')dr', \tag{B.20}$$

$$r_< = \min(r, r'),$$

$$r_> = \max(r, r').$$

The direct and exchange coefficient are defined as

$$f_k(a, b) = -\left(1 + \frac{1}{2j_a}\right)\begin{pmatrix} j_a & k & j_b \\ -\frac{1}{2} & 0 & \frac{1}{2} \end{pmatrix}^2, \tag{B.21}$$

$$g_k(a, b) = -\begin{pmatrix} j_a & k & j_b \\ -\frac{1}{2} & 0 & \frac{1}{2} \end{pmatrix}^2. \tag{B.22}$$

In the Dirac Hartree Fock approximation is a single electron state is given by a one electron Dirac orbital

$$\phi_o(x) = \frac{1}{r}\begin{pmatrix} P_o(r)\Omega_{\kappa m}(\vartheta, \varphi) \\ iQ_o(r)\Omega_{-\kappa m}(\vartheta, \varphi) \end{pmatrix}, \tag{B.23}$$

where o determines the atomic orbital

$$o_i = \begin{cases} (\epsilon_i, \kappa_i, m_i) & \text{(continuum states)} \\ (n_i, \kappa_i, m_i) & \text{(bound states)} \end{cases} \tag{B.24}$$

C Spherical spinors

For the description of atomic energy levels it is necessary to find eigenstates, which govern the angular orbital momentum L as well as the spin angular momentum S. The eigenstates of the orbital angular momentum L_z and the associated Casimir operator L^2 are the spherical harmonics $Y_{l,m}(\theta, \phi)$ and the eigenstates of the spin angular momentum S and it's associated Casimir operator S^2 is a spinor χ_μ. Spherical spinors are eigenfunctions of the operator

$$\mathbf{K} = -\mathbb{1} - \boldsymbol{\sigma} \cdot \mathbf{L}. \tag{C.1}$$

with an eigenvalue equation of the form

$$\mathbf{K}\Omega_{jlm} = \kappa\Omega_{jlm}, \tag{C.2}$$

where κ is the relativistic angular momentum quantum number and is defined as

$$\kappa = \begin{cases} -l-1 & \text{for} \quad j = l + \frac{1}{2} \\ l & \text{for} \quad j = l - \frac{1}{2} \end{cases} \tag{C.3}$$

The spherical spinors can be brought to the form [55]

$$\Omega_{\kappa m} = \begin{pmatrix} \mathrm{sgn}(-\kappa) & \sqrt{\frac{\kappa+\frac{1}{2}-m}{2\kappa+1}} Y_{l,m-\frac{1}{2}} \\ & \sqrt{\frac{\kappa+\frac{1}{2}+m}{2\kappa+1}} Y_{l,m+\frac{1}{2}} \end{pmatrix}, \tag{C.4}$$

with $\kappa \in \{\pm1, \pm2, \pm3, \dots\}$ and $m \in \{-|\kappa| + \frac{1}{2}, -|\kappa| + \frac{3}{2}, \dots, |\kappa| - \frac{1}{2}\}$.

It is also possible to define spherical spinors in terms of Clebsch Gordan coefficients by

$$\Omega_{jlm} = \sum_{\mu} C(l, \frac{1}{2}, j; m-\mu, \mu, m) Y_{l,m-\mu}(\theta, \phi) \chi_{\mu}. \tag{C.5}$$

D Normalization of continuum wavefunctions

In the non relativistic case, the state of an ionized electron is characterized by the angular momentum quantum number l, the magnetic quantum number m and the energy ϵ. In contrast, to the bound state wave functions, where the energy spectrum is characterized by discrete values, the energy ϵ of the ionized electron can now take all values $\epsilon > 0$ in the continuum. For a wave function $\psi(\mathbf{x})$ with a continuous spectrum it is not possible to fullfill the usual normalization condition

$$\int d^n x \, \psi(\mathbf{x})^* \psi(\mathbf{x}) = 1. \tag{D.1}$$

Let f be an observable with a continuous spectrum and ψ_f an eigenfunction of with eigenvalue f. In general an arbitrary state ψ can be represented in the form of

$$\psi = \sum\!\!\!\!\!\!\int a_f \psi_f, \tag{D.2}$$

where the wave functions ψ_f form a complete set of eigenfunctions with eigenvalue f. In the case of a continuous wave function the expansion is expressed by an integral

$$\psi(\mathbf{x}) = \int dx \; a_f \; \psi_f(\mathbf{x}). \tag{D.3}$$

The wave function ψ_f can now be normalized in such a way that $|a_f|^2 df$ is the probability that the observable in the state ψ has a value between f and $f + df$. The completeness relation claims that the coefficients a_f have to fulfill

$$\int |a_f|^2 df = 1, \tag{D.4}$$

where the integration takes place over the space of all possible values f can take. In the case of continuum wave functions, we require a normalization condition such that the quantity $|a_f|^2 df$ is the probability that the state under consideration has a value between $f + df$[42]. The coefficients a_f of the eigenfunctions ψ_f are determined by

$$a_f = \int dx\ \psi_f^*(\mathbf{x})\psi(\mathbf{x}). \tag{D.5}$$

Substituting Eq. (D.3) into Eq. (D.5), we arrive at

$$a_f = \int a_{f'} \left(\int \psi_f^*(\mathbf{x})\psi_{f'}(\mathbf{x})dx \right) df'. \tag{D.6}$$

Since this relation has to be fulfilled for arbitrary a_f, the coefficient $a_{f'}$ is zero for $f \neq f'$. For $f = f'$, the coefficient becomes infinite, otherwise the integral over f would vanish. Thus,

$$\int dx\ \psi_f^*(\mathbf{x})\psi_{f'}(\mathbf{x}) = \delta(f' - f), \tag{D.7}$$

where $\delta(f' - f)$ is the Dirac delta function. For similar arguments, we obtain that

$$\int \psi_f^*(\mathbf{x})\psi_f(\mathbf{y})df = \delta(\mathbf{x} - \mathbf{y}). \tag{D.8}$$

From our previous analysis we can see that the function $a(f)$, as well as the function $\psi_f(\mathbf{x})$, completely determines the state of the system and is sometimes called the wave function in the f representation. The quantity $|\psi(\mathbf{x})|^2$ determines the probability to have a state in an interval dx, whereas the quantity $|a(f)|^2$ determines the probability of a quantity f to lie in an interval df. The wavefunctions $\psi_f(\mathbf{x})$ are eigenfunctions of f in the $x - representation$ [42][54].

D.1 Plane wave

In this appendix, we want to normalize a plane wave

$$\phi_{\mathbf{k}}(\mathbf{r}) = \mathcal{N} e^{i\mathbf{k}\cdot\mathbf{r}}, \tag{D.9}$$

with the normalization condition

$$\int d^3r \phi_{\mathbf{k'}}^*(\mathbf{r})\phi_{\mathbf{k}}(\mathbf{r}) = \frac{\pi}{2}\delta(\epsilon - \epsilon'). \tag{D.10}$$

First, we normalize it on the "k-scale" by the normalization condition

$$\int d^3r \phi^*_{\mathbf{k'}}(\mathbf{r})\phi_{\mathbf{k}}(\mathbf{r}) = \frac{\pi}{2}\frac{1}{k^2}\delta(k-k'). \tag{D.11}$$

Therefore

$$\begin{aligned}\int d^3r \phi^*_{\mathbf{k'}}(\mathbf{r})\phi_{\mathbf{k}}(\mathbf{r}) =& \mathcal{N}^2 \int dr\, r^2 \int_0^{2\pi} d\varphi \int d\cos\vartheta e^{i(\mathbf{k}-\mathbf{k'})\mathbf{r}} \\ =& \mathcal{N}^2 \int dr\, r^2 \int_0^{2\pi} d\varphi \int d\cos\vartheta \sum_{l=0}^{\infty}\sum_{l'=0}^{\infty}(-i)^{l'} i^l (2l'+1)(2l+1) \\ & \times P_{l'}(\cos\vartheta')P_l(\cos\vartheta) j_{l'}(k'r) j_l(kr)\end{aligned} \tag{D.12}$$

Now ϑ and ϑ' are the angles of $(\mathbf{k},\mathbf{r})$ and $(\mathbf{k'},\mathbf{r})$ respectively. Let α be angle between $\mathbf{k}$ and $\mathbf{k'}$, then

$$\cos\vartheta' = \cos\vartheta\cos\alpha + \sin\vartheta\sin\alpha\cos\varphi, \tag{D.13}$$

such that we can rewrite

$$\begin{aligned}P_{l'}(\cos\vartheta')P_l(\cos\vartheta) =& P_{l'}(\cos\vartheta)P_l(\cos\vartheta)P_{l'}(\cos\alpha) \\ & + 2P_l(\cos\vartheta)\sum_{m'=1}^{\infty}\frac{(l'-m')!}{(l'+m')!}P_{l'}^{m'}(\cos\vartheta')P_l(\cos\alpha)\cos(m'\varphi).\end{aligned} \tag{D.14}$$

The integration over $d\varphi$ gives zero for the second term and the first term is only nonzero for $l = l'$, because of the orthogonality relation of the Legendre polynomials

$$\int_{-1}^{1} d\cos\vartheta P_{l'}(\cos\vartheta)P_l(\cos\vartheta) = \delta_{ll'}\frac{2}{2l+1}, \tag{D.15}$$

Hence,

$$\int d^3r \phi^*_{\mathbf{k'}}(\mathbf{r})\phi_{\mathbf{k}}(\mathbf{r}) = 4\pi\mathcal{N}^2 \int dr\, r^2 \sum_{l=0}^{\infty}(2l+1)P_l(\cos\alpha) j_{l'}(k'r) j_l(kr) \tag{D.16}$$

Now we can make use of Eq. (**??**)

$$\begin{aligned}\int d^3r \phi^*_{\mathbf{k'}}(\mathbf{r})\phi_{\mathbf{k}}(\mathbf{r}) =& \frac{4\pi\mathcal{N}^2}{kk'} \int dr\, r^2 \sum_{l=0}^{\infty}(2l+1)P_l(\cos\alpha) R_{k'l}(r) R_{kl}(r) \\ =& \frac{4\pi\mathcal{N}^2}{k^2}\sum_{l=0}^{\infty}(2l+1)P_l(\cos\alpha)\frac{\pi}{2}\delta(k-k') \\ =& \frac{4\pi^2\mathcal{N}^2}{k^2}\delta(k-k')\sum_{l=0}^{\infty}\frac{2l+1}{2}P_l(\cos\alpha).\end{aligned} \tag{D.17}$$

Now we can make use of $1 = P_l(1)$ and the summation formula for Legendre polynomials to obtain

$$\sum_{l=0}^{\infty} \frac{2l+1}{2} P_l(\cos\alpha) P_l(1) = \delta(1-\cos\alpha), \tag{D.18}$$

such that we arrive at

$$\int d^3 r \phi^*_{\mathbf{k'}}(\mathbf{r}) \phi_{\mathbf{k}}(\mathbf{r}) = \frac{4\pi^2 \mathcal{N}^2}{k^2} \delta(k-k')\delta(1-\cos\alpha). \tag{D.19}$$

Now we multiply this expression by $2\pi k^2 \sin\alpha \, dk \, d\alpha$ to integrate it over the whole "k-space" and normalize it to one, which yields

$$1 = 8\pi^3 \mathcal{N}^2 = \mathcal{N}^2 16\pi^2 \frac{\pi}{2}. \tag{D.20}$$

The normalization according to Eq. (D.11) is therfore $\mathcal{N} = \frac{k}{4\pi}$. Since $\phi_\epsilon(\mathbf{r}) = \sqrt{\frac{m_e}{k}} \phi_{\mathbf{k}}(\mathbf{r})$, such that the continuum wave function on the energy-scale is given by

$$\phi_\epsilon(\mathbf{r}) = \frac{1}{4\pi} \sqrt{m_e k} e^{i\mathbf{k}\cdot\mathbf{r}}. \tag{D.21}$$

E Radial part of the Fourier transformation

the electron transition amplitude is of the form

$$\tilde{\phi}_{nlm}(\mathbf{p}) = \int \phi_{nlm}(x) e^{-i\mathbf{p}\cdot\mathbf{r}} d^3 r = \chi_{nl}(p) Y_{lm}(\vartheta_p, \varphi_p). \tag{E.1}$$

We can write

$$Z^{nlm}_{\epsilon l' m'}(\mathbf{q}_e) = \frac{1}{4\pi} \sqrt{k m_e} \int d^3 r e^{-i\mathbf{p}\cdot\mathbf{r}} \phi_{nlm}(\mathbf{r}) = \frac{1}{4\pi} \sqrt{k m_e} \chi_{nl}(p) Y_{lm}(\vartheta_p, \phi_p). \tag{E.2}$$

The angular part of $\tilde{\phi}(p)_{nlm}$ contains a spherical harmonic $Y_{lm}(\vartheta_r, \varphi_r)$, such that we can make use of the formula

$$\sum_{m=-l}^{l} Y^*_{lm}(\vartheta_r, \varphi_r) Y_{lm}(\vartheta_p, \varphi_p) = \frac{2l+1}{4\pi} P_l(\cos\vartheta), \tag{E.3}$$

where ϑ is the angle between $\mathbf{r}$ and $\mathbf{p}$. The radial part $\chi_{nl}(p)$ can now be calculated by

$$\chi_{nl}(p) = \frac{4\pi}{2l+1} \sum_{m=-l}^{l} \tilde{\phi}(p)_{nlm} Y^*_{lm}(\vartheta_p, \phi_p). \tag{E.4}$$

Thus, the radial part reduces to

$$\chi_{nl}(p) = \int_0^{2\pi} d\varphi \int drr^2 R_{nl}(r) \int_0^{\pi} d\vartheta \sin\vartheta e^{-i\mathbf{p}\cdot\mathbf{r}} P_l(\cos\vartheta). \tag{E.5}$$

The operator $e^{-i\mathbf{p}\cdot\mathbf{r}}$ can now be expanded according to [38]

$$e^{-i\mathbf{p}\cdot\mathbf{r}} = \sum_{L=0}^{\infty} (-i)^L (2L+1) j_L(pr) P_L(\cos\vartheta). \tag{E.6}$$

Integrating over the azimuthal angle and making use of Eq. (E.6) yields

$$\chi_{nl}(p) = 2\pi \sum_{L=0}^{\infty} (2L+1)(-i)^L \int drr^2 R_{nl}(r) j_L(pr) \int_{-1}^{1} d\cos\vartheta P_L(\cos\vartheta) P_l(\cos\vartheta), \tag{E.7}$$

where $j_L(qr)$ is the spherical Bessel function. The orthogonality relation of the Legendre polynomials is

$$\int_0^{\pi} d\vartheta \sin\vartheta P_L(\cos\vartheta) P_l(\cos\vartheta) = \delta_{Ll} \frac{2}{2l+1}, \tag{E.8}$$

such that Eq. (E.7) reduces to

$$\chi_{nl}(p) = 4\pi(-i)^l \int drr^2 R_{nl}(r) j_l(pr), \tag{E.9}$$

where $j_l(r)$ is the spherical Bessel function.

Bibliography

[1] G. Bertone, D. Hooper, and J. Silk, "Particle dark matter: Evidence, candidates and constraints," 2005.

[2] C. Kouvaris and J. Pradler, "Probing sub-GeV Dark Matter with conventional detectors," arXiv:1607.01789v2.

[3] J. Bovy and S. Tremaine, "On the local dark matter density," *Astrophysical Journal* **756** no. 1, (2012) 1–16, arXiv:1205.4033.

[4] L. Bergström, "Non-baryonic dark matter: Observational evidence and detection methods," *Reports on Progress in Physics* (2000) .

[5] Planck Collaboration, "Planck 2018 results. VI. Cosmological parameters," arXiv:1807.06209.

[6] A. G. Riess, S. Casertano, W. Yuan, L. Macri, J. Anderson, J. W. MacKenty, J. B. Bowers, K. I. Clubb, A. V. Filippenko, D. O. Jones, and B. E. Tucker, "New Parallaxes of Galactic Cepheids from Spatially Scanning the Hubble Space Telescope : Implications for the Hubble Constant," *The Astrophysical Journal* (2018) , arXiv:1801.01120.

[7] "Astrophysical Constants and Parameters," *Particle Data Group* (2017) . http://pdg.lbl.gov/.

[8] D. Baumann, "Cosmology Lecture Notes -Part III Mathematical Tripos,".

[9] F. Zwicky, "On a new type of reasoning and some of its possible consequences [2]," 1933.

[10] V. C. Rubin and J. Ford, W. Kent, "Rotation of the Andromeda Nebula from a Spectroscopic Survey of Emission Regions," *The Astrophysical Journal* (1970) .

[11] J. F. Navarro, "The Structure of Cold Dark Matter Halos," *Symposium - International Astronomical Union* (1996) .

[12] D. J. Fixsen, E. S. Cheng, J. M. Gales, J. C. Mather, R. A. Shafer, and E. L. Wright, "

The Cosmic Microwave Background Spectrum from the Full COBE FIRAS Data Set ," *The Astrophysical Journal* (1996) .

[13] A. Natarajan, "Closer look at CMB constraints on WIMP dark matter," *Physical Review D - Particles, Fields, Gravitation and Cosmology* (2012) , `arXiv:1201.3939`.

[14] G. Gelmini and P. Gondolo, "DM production mechanisms," *Particle Dark Matter: Observations, Models and Searches* (2010) 121–141, `arXiv:1009.3690`.

[15] E. W. Kolb and M. S. Turner, *The early universe*. 1990.

[16] M. Hindmarsh and O. Philipsen, "WIMP dark matter and the QCD equation of state," *Physical Review D* (2005) .

[17] F. A. Liam, W. Haxton, E. Katz, N. Lubbers, and Y. Xu, "The effective field theory of dark matter direct detection," *Journal of Cosmology and Astroparticle Physics* (2013) .

[18] J. D. Lewin and P. F. Smith, "Review of mathematics, numerical factors, and corrections for dark matter experiments based on elastic nuclear recoil," 1996.

[19] J. Engel, S. Pittel, and P. Vogel, "Nuclear Physics of Dark Matter Detection," *International Journal of Modern Physics E* (1992) .

[20] R. H. Helm, "Inelastic and elastic scattering of 187-Mev electrons from selected even-even nuclei," *Physical Review* (1956) .

[21] G. Fricke, C. Bernhardt, K. Heilig, L. A. Schaller, L. Schellenberg, E. B. Shera, and C. W. De Jager, "Nuclear ground state charge radii from electromagnetic interactions," *Atomic Data and Nuclear Data Tables* (1995) .

[22] K. Freese, M. Lisanti, and C. Savage, "Colloquium: Annual modulation of dark matter," *Reviews of Modern Physics* (2013) .

[23] A. K. Drukier, K. Freese, and D. N. Spergel, "Detecting cold dark-matter candidates," *Physical Review D* (1986) .

[24] R. Schoenrich, J. Binney, and W. Dehnen, "Local Kinematics and the Local Standard of Rest arXiv : 0912 . 3693v1 [astro-ph . GA] 18 Dec 2009," *Monthly Notices of the Royal Astronomical Society* (2009) , `arXiv:0912.3693v1`.

[25] F. Mignard, "Local galactic kinematics from Hipparcos proper motions," *Astronomy and Astrophysics* **354** no. 2, (2000) 522–536.

[26] A. M. Green, "Effect of realistic astrophysical inputs on the phase and shape of the

weakly interacting massive particles annual modulation signal," *Physical Review D* (2003) , `arXiv:0304446 [astro-ph]`.

[27] M. Schumann, "Direct detection of WIMP dark matter: concepts and status," *Journal of Physics G: Nuclear and Particle Physics* (2019) .

[28] D. G. Cerdeño and A. M. Green, "Direct detection of WIMPs," in *Particle Dark Matter: Observations, Models and Searches*. 2010.

[29] L. Tvrznikova, "Sub-GeV Dark Matter Searches and Electric Field Studies for the LUX and LZ Experiments," `arXiv:1904.08979`. `http://arxiv.org/abs/1904.08979`.

[30] E. Aprile and T. Doke, "Liquid xenon detectors for particle physics and astrophysics," *Reviews of Modern Physics* (2010) , `arXiv:0910.4956`.

[31] Xenon Collaboration, "Light Dark Matter Search with Ionization Signals in XENON1T," `arXiv:1907.11485`. `http://arxiv.org/abs/1907.11485`.

[32] M. Schumann, "Dual-phase liquid xenon detectors for dark matter searches," in *Journal of Instrumentation*. 2014.

[33] J. Lindhard, V. Nielsen, M. Scharff, and P. V. Thomsen, "Integral equations governing radiation effects," *Mat. Fys. Medd. Dan. Vid. Selsk* (1963) .

[34] C. E. Dahl, "The physics of background discrimination in liquid xenon, and first results from Xenon10 in the hunt for WIMP dark matter.,".

[35] M. Ibe, W. Nakano, Y. Shoji, and K. Suzuki, "Migdal effect in dark matter direct detection experiments," *Journal of High Energy Physics* **2018** no. 3, (2018) , `arXiv:1707.07258v2`.

[36] E. Aprile, J. Aalbers, F. Agostini, M. Alfonsi, L. Althueser, F. D. Amaro, V. C. Antochi, E. Angelino, F. Arneodo, D. Barge, L. Baudis, B. Bauermeister, L. Bellagamba, M. L. Benabderrahmane, T. Berger, P. A. Breur, A. Brown, E. Brown, S. Bruenner, G. Bruno, R. Budnik, C. Capelli, J. M. R. Cardoso, D. Cichon, D. Coderre, A. P. Colijn, J. Conrad, J. P. Cussonneau, M. P. Decowski, P. de Perio, A. Depoian, P. Di Gangi, A. Di Giovanni, S. Diglio, A. Elykov, G. Eurin, J. Fei, A. D. Ferella, A. Fieguth, W. Fulgione, P. Gaemers, A. G. Rosso, M. Galloway, F. Gao, M. Garbini, L. Grandi, Z. Greene, C. Hasterok, C. Hils, E. Hogenbirk, J. Howlett, M. Iacovacci, R. Itay, F. Joerg, S. Kazama, A. Kish, M. Kobayashi, G. Koltman, A. Kopec, H. Landsman, R. F. Lang, L. Levinson, Q. Lin, S. Lindemann, M. Lindner, F. Lombardi, J. A. M. Lopes, E. L. Fune, C. Macolino, J. Mahlstedt, L. Manenti, A. Manfredini, F. Marignetti, T. M. Undagoitia,

J. Masbou, S. Mastroianni, M. Messina, K. Micheneau, K. Miller, A. Molinario, K. Morå, Y. Mosbacher, M. Murra, J. Naganoma, K. Ni, U. Oberlack, K. Odgers, J. Palacio, B. Pelssers, R. Peres, J. Pienaar, V. Pizzella, G. Plante, R. Podviianiuk, J. Qin, H. Qiu, D. R. García, S. Reichard, B. Riedel, A. Rocchetti, N. Rupp, J. M. F. dos Santos, G. Sartorelli, N. Šarčević, M. Scheibelhut, S. Schindler, J. Schreiner, D. Schulte, M. Schumann, L. S. Lavina, M. Selvi, P. Shagin, E. Shockley, M. Silva, H. Simgen, C. Therreau, D. Thers, F. Toschi, G. Trinchero, C. Tunnell, N. Upole, M. Vargas, G. Volta, O. Wack, H. Wang, Y. Wei, C. Weinheimer, D. Wenz, C. Wittweg, J. Wulf, J. Ye, Y. Zhang, T. Zhu, and J. P. Zopounidis, "A Search for Light Dark Matter Interactions Enhanced by the Migdal effect or Bremsstrahlung in XENON1T," `arXiv:1907.12771`. `http://arxiv.org/abs/1907.12771`.

[37] W. J. Herre, *A Guide to Molecular Mechanics and Quantum Chemical Calculations*. 2003.

[38] D. A. Varshalovich, A. N. Moskalev, and V. K. Khersonskii, "Angular momentum operators," in *Quantum Theory of Angular Momentum*. 1988.

[39] J. I. Read, "The local dark matter density," *Proceedings of Science* **161** (2014) 1–62, `arXiv:1404.1938`.

[40] M. F. Gu, "The flexible atomic code," *Canadian Journal of Physics* **86** no. 5, (2008) 675–689.

[41] C. F. Bunge, J. A. Barrientos, and A. V. Bunge, "Roothaan-Hartree-Fock ground-state atomic wave functions: Slater-type orbital expansions and expectation values for Z = 2-54," *Atomic Data and Nuclear Data Tables* (1993) .

[42] L. Landau and E. M. Lifshitz, *Quantum Mechanics, Non-relativistic Theory*. second ed., 1965.

[43] V. B. Berestetskii and E. M. Lifshitz, *Quantum electrodynamics*. Elsevier, second edi ed., 1982.

[44] H. A. Bethe and E. E. Salpeter, *Quantum Mechanics of One- and Two-Electron Atoms*. 1957.

[45] P. Agnes, I. F. Albuquerque, and T. Alexander, "Constraints on Sub-GeV Dark-Matter-Electron Scattering from the DarkSide-50 Experiment," *Physical Review Letters* (2018) , `arXiv:1802.06998`.

[46] Lawrence Berkeley National Laboratory, "X-Ray Data Booklet,". `https://xdb.lbl.gov/`.

[47] R. Essig, J. Mardon, and T. Volansky, "Direct detection of sub-GeV dark matter," *Physical Review D - Particles, Fields, Gravitation and Cosmology* **85** no. 7, (2012) 1–9, `arXiv:1108.5383v3`.

[48] J. Kopp, V. Niro, T. Schwetz, and J. Zupan, "DAMA/LIBRA data and leptonically interacting dark matter," *Physical Review D - Particles, Fields, Gravitation and Cosmology* (2009) .

[49] R. Essig, J. Pradler, M. Sholapurkar, and T.-t. Yu, "On the relation between Migdal effect and dark matter-electron scattering in isolated atoms and semiconductors," `arXiv:1908.10881v2`.

[50] Z.-l. Liang, L. Zhang, F. Zheng, and P. Zhang, "Describing Migdal effects in diamond crystal with atom-centered localized Wannier functions," `arXiv:1912.13484v2`.

[51] R. M. Geilhufe, F. Kahlhoefer, and M. W. Winkler, "Dirac Materials for Sub-MeV Dark Matter Detection: New Targets and Improved Formalism," `arXiv:1910.02091`. `http://arxiv.org/abs/1910.02091`.

[52] E. Aprile, J. Aalbers, F. Agostini, M. Alfonsi, L. Althueser, F. D. Amaro, V. C. Antochi, E. Angelino, F. Arneodo, D. Barge, L. Baudis, B. Bauermeister, L. Bellagamba, M. L. Benabderrahmane, T. Berger, P. A. Breur, A. Brown, E. Brown, S. Bruenner, G. Bruno, R. Budnik, C. Capelli, J. M. Cardoso, D. Cichon, D. Coderre, A. P. Colijn, J. Conrad, J. P. Cussonneau, M. P. Decowski, P. De Perio, A. Depoian, P. Di Gangi, A. Di Giovanni, S. Diglio, A. Elykov, G. Eurin, J. Fei, A. D. Ferella, A. Fieguth, W. Fulgione, P. Gaemers, A. Gallo Rosso, M. Galloway, F. Gao, M. Garbini, L. Grandi, Z. Greene, C. Hasterok, C. Hils, E. Hogenbirk, J. Howlett, M. Iacovacci, R. Itay, F. Joerg, S. Kazama, A. Kish, M. Kobayashi, G. Koltman, A. Kopec, H. Landsman, R. F. Lang, L. Levinson, Q. Lin, S. Lindemann, M. Lindner, F. Lombardi, J. A. Lopes, E. López Fune, C. MacOlino, J. Mahlstedt, M. Manenti, A. Manfredini, F. Marignetti, T. Marrodán Undagoitia, J. Masbou, S. Mastroianni, M. Messina, K. Micheneau, K. Miller, A. Molinario, K. Morå, Y. Mosbacher, M. Murra, J. Naganoma, K. Ni, U. Oberlack, K. Odgers, J. Palacio, B. Pelssers, R. Peres, J. Pienaar, V. Pizzella, G. Plante, R. Podviianiuk, J. Qin, H. Qiu, D. Ramírez Garciá, S. Reichard, B. Riedel, A. Rocchetti, N. Rupp, J. M. Dos Santos, G. Sartorelli, N. Šarčević, M. Scheibelhut, S. Schindler, J. Schreiner, D. Schulte, M. Schumann, L. Scotto Lavina, M. Selvi, P. Shagin, E. Shockley, M. Silva, H. Simgen, C. Therreau, D. Thers, F. Toschi, G. Trinchero, C. Tunnell, N. Upole, M. Vargas, G. Volta, O. Wack, H. Wang, Y. Wei, C. Weinheimer, D. Wenz, C. Wittweg, J. Wulf, J. Ye, Y. Zhang, T. Zhu, and J. P. Zopounidis, "Search for Light Dark Matter

Interactions Enhanced by the Migdal Effect or Bremsstrahlung in XENON1T," *Physical Review Letters* **123** no. 24, (2019) 1–7, arXiv:1907.12771.

[53] W. R. Johnson, *Atomic structure theory: Lectures on atomic physics.* 2007.

[54] J. Ross, "Quantum Mechanics (Merzbacher, Eugen)," *Journal of Chemical Education* (1962) .

[55] R. Szmytkowski, "Recurrence and differential relations for spherical spinors," arXiv:1011.3433v1.